INFORMATION TO USERS

This manuscript has been reproduced from the microfilm master. UMI films the text directly from the original or copy submitted. Thus, some thesis and dissertation copies are in typewriter face, while others may be from any type of computer printer.

The quality of this reproduction is dependent upon the quality of the copy submitted. Broken or indistinct print, colored or poor quality illustrations and photographs, print bleedthrough, substandard margins, and improper alignment can adversely affect reproduction.

In the unlikely event that the author did not send UMI a complete manuscript and there are missing pages, these will be noted. Also, if unauthorized copyright material had to be removed, a note will indicate the deletion.

Oversize materials (e.g., maps, drawings, charts) are reproduced by sectioning the original, beginning at the upper left-hand corner and continuing from left to right in equal sections with small overlaps. Each original is also photographed in one exposure and is included in reduced form at the back of the book.

Photographs included in the original manuscript have been reproduced xerographically in this copy. Higher quality 6" x 9" black and white photographic prints are available for any photographs or illustrations appearing in this copy for an additional charge. Contact UMI directly to order.

U·M·I

University Microfilms International
A Bell & Howell Information Company
300 North Zeeb Road, Ann Arbor, MI 48106-1346 USA
313/761-4700 800/521-0600

Order Number 9207079

Modulation spectroscopy of semiconductors and semiconductor microstructures

Hang, Zhijiang, Ph.D.

City University of New York, 1991

Copyright ©1991 by Hang, Zhijiang. All rights reserved.

U·M·I
300 N. Zeeb Rd.
Ann Arbor, MI 48106

Modulation Spectroscopy of Semiconductors and Semiconductor Microstructures.

by

Zhijiang Hang

A dissertation submitted to the Graduate Faculty in Physics in partial fulfillment of the requirements for the degree of Doctor of Philosophy, The City University of New York.

1991

© 1991

ZHIJIANG HANG

All Rights Reserved

This Manuscript has been read and accepted for the Graduate Faculty in Physics in satisfaction of the dissertation requirement for the degree of Doctor of Philosophy.

6/7/91
date

Fred Pollak
Chairman of Examining Committee

6/19/91
date

Executive Officer

F. H. Pollak
P. Montano
H. Homma
M. Den Boer
M. Dutta

Supervisory Committee

The City University of New York

Abstract

MODULATION SPECTROSCOPY OF SEMICONDUCTORS AND SEMICONDUCTOR MICROSTRUCTURES

by

Zhijiang Hang

Advisor: Professor Fred H. Pollak

The electronic properties of semiconductors and semiconductor microstructures have been studied by electromodulation spectroscopy. We have evaluated the parameters which describe the dependency of the energy gap E_o and broadening parameters of E_o on temperature. We have concluded that both electron-optic and electron-acoustic phonon interactions as well as the thermal expansion contribute to the energy shifts of the band gap (E_o) of InP and $In_xGa_{1-x}As$ (x=0.06 and 0.15). It is mainly electron-optical phonon interaction which contributes to the broadening (E_o) of the energy gaps.

We have made considerable progress in developing PR as an in-situ monitoring/control method for semiconductor growth. Measurements have been performed in an actual metalorganic chemical vapor deposition (MOCVD) reactor. We found a systematic difference between the temperature of the GaAs substrate and a thermocouple not in contact with the sample. Also, it is now possible to evaluate Aluminum composition in GaAlAs during actual growth. A major step forward has been a substantial reduction in data acquisition time to 30 seconds so that real-time measurements are now feasible.

Photoreflectance also has been used to study alternating composition layers of multiple quantum wells (MQW) both lattice-matched ($Ga_{1-x}Al_xAs$/GaAs MQW) and lattice-mismatched or strained ($In_xGa_{1-x}As$/GaAs and GaSb/AlSb MQW) systems. The rich spectra were observed at room temperature, and they consisted of both symmetry allowed and forbidden confined (CT) and unconfined (UT) transitions. Both the CT and UT exhibited coupling effects between wells(miniband dispersion). With this

information we can examine existing theories, such as Bastard Model theory [31,32], and also experimentally determine the following: 1) the band alignment of the heterostructure (band offset); 2) the alloy composition of $Ga_{1-x}Al_xAs$ or $In_xGa_{1-x}As$ epilayers; and the thickness of wells and barriers. In addition, an investigation of the strained-layer systems enables us to determine the strain distribution. We also use Franz-Keldysh Oscillation (FKO) to study the effects of various conditions (UHV, air, temperature, light intensity) on surface photovoltage (V_S) effects on the determination of Fermi level pining (V_S) on (100) GaAs.

Acknowledgements

I wish to express my great appreciation to my advisor, Distinguished Professor Fred H. Pollak. Without his guidance, support, and encouragement this work would never have seen the light of day. His enthusiasm and creativity in exploring and understanding physics was an inspiration. His kind assistance and constant interest in my progress has given me more than one could hope for in a mentor.

To other members of the committee, Professor Pedro Montana and Hiroshi Homma of Brooklyn College, Professor H. Den Boer of Hunter College and Dr. Mitra Dutta, they have my sincere thanks for agreeing to serve on my committee and for their careful reading of my thesis manuscript and for their helpful advice. I particularly want to thank Dr. Jerry Woodall and Mr. Dave Pettit for providing samples for this study.

I am deeply indebted to Dr. Hong-en Shen for his valuable help and encouragement. I have been most fortunate to have had

the opportunity to work closely with him. I also appreciate the help of the other colleagues in the Semiconductor Institute; Dr. Dong Yan, Mr. X. Yin and Mr. Y. Yin stand out in this regard.

Special thanks to Mr. Martin Berman and Louis Tundis of Machine Shop for their excellent service and assistance in designing and making the experiment setup. I wish to express my gratitude to Mr. Montford Naylor, Director of Administration of Semiconductor Institute for his encouragement, kind help and assistance.

I also wish to give thanks to Dr. Peter Norris and Ken Capuder of EMCORE Co. for offering the facility and for their cooperation and efforts in the successful completion of the PR in-situ project. I wish to acknowledge with gratitude the department of physics of Brooklyn College for providing me with this opportunity, the Research Foundation of CUNY and Brooklyn College Foundation for financial support during the course of this work.

I also wish to give my thanks to Professor Herman

Cummins of City College for providing assistance and encouragement. Special thanks professor B. Ruth for his carefully reading my manuscripts and giving corrections.

Words can not express my appreciation and admiration for my wife Jing Xu for her support and sacrifice during my difficult time. This work is as much a reflection of that support and sacrifice as of my efforts.

Contents

FIGURES

Tables

Chapter I

INTRODUCTION

There are a considerable number of electronic and optical techniques to study the electronic properties of semiconductor materials, such as the Hall effect[1], cyclotron resonance [2], transmission electron microscopy (TEM) [3], absorption spectroscopy [4], Photoluminescence (PL) [4, 5], PL excitation spectroscopy(PLE) [6], Resonant Raman Scattering (RRS) [7], scanning ellipsometry [8,9] and modulation spectroscopy[10,11,12], etc. However each of these techniques provides only specific information about the material, structure or interface of interest. For example, carrier concentrations and mobilities of the semiconductors can be measured by the Hall effect. The band mass can be evaluated by using cyclotron resonance. The layer thickness and interfacial quality of semiconductor microstructure can be determined from TEM. The energy band structure of the materials can be obtained from

absorption or PLE as well as from modulation spectroscopy. Many of the methods discussed above are very specialized and sometimes difficult to employ, or require cryogenic temperatures. For example, PL requires cryogenic temperatures. Electromodulation spectroscopy [10,11,12] is a simple and informative tool used to characterize semiconductors and semiconductor structures, in which a simple measurement can provide a large amount of qualitative and quantitative information about the materials studied. Since the electromodulation signal is not only proportional to the derivatives of the dielectric function but is inversely proportional to the reduced interband mass (μ), this technique provides maximum sensitivity to interband transitions and thus to the band structure of the material being studied. It is also possible to perform lineshape analysis, and thereby to obtain more information about the transition of interest as well as about the optoelectronic processes responsible for the modulation of the optical functions. In addition, many modulation measurements

can be performed at room temperature and still provide valuable information.

The modulation spectroscopy is a branch of optical spectroscopy that deals with the measurement and interpretation of changes in optical spectra of a sample which are caused by modifying in some way the measurement conditions. The optical properties of the material may be modified directly by applying a repetitive perturbation such as an electric, or magnetic field, a heat pulse, a uniaxial stress, etc. This process is termed "external" perturbation. Alternatively, in processes termed "internal" modulation, the change may occur in the measurement conditions themselves, for example, the measuring wavelength may be modulated. There are several advantages to using of modulation spectroscopy in the study and characterization of semiconductors: 1) the derivative nature of modulation spectra suppresses uninteresting background effects and emphasizes structures localized in the energy region of interband transitions. Weak features that may not have been seen in the absolute spectra are greatly

enhanced; 2) the lineshape of a spectrum can be fit, and from the fitting process information about the nature of the transitions can be obtained; 3) it can be performed in a wide temperature range from 18K to 873K, and 4) since modulation spectroscopy is an ac method, there is also information in variables such as phase [13], modulation frequency [14,15], modulation amplitude [13], pump wavelength(PR) [14], as well as in others, which are related to the properties of materials studied.

The optical properties may be modulated directly by applying a perturbation such as an electric or magnetic field, a heat pulse, or a uniaxial stress. In this study we focus on electromodulation spectroscopy, where an electric field is applied to the sample. Electromodulation is a particular useful form of modulation spectroscopy since it often yields the sharpest structure [16, 17] and is sensitive to the surface/ interface electric field [18, 19, 20, 21 14, 13, 22]. It is an excellent tool to detect the surface electric field and related quantities such as Fermi level

pining and carrier concentrations [23,24,25]. In EM, mainly those of electroreflectance (ER) and photoreflectance (PR), the dielectric function is modulated through an application of an electric field; either directly as in ER or indirectly as in PR. For ER, the modulated electric field is obtained directly from an applied external field. In PR, the field is modulated through changes in the surface photovoltage induced by the absorption of the above band gap photons. Since perturbations are usually small, the spectra are closely related to the derivative of the unperturbed spectra with respect to the photon energy.

The first task of this thesis is to study the temperature dependence of the direct gaps of semiconductor materials such as GaAs [26], InP [27], $Ga_{1-x}Al_xAs$ [26], and $In_xGa_{1-x}As$ [28,29] in a wide temperature range, up to 600°C by using PR. The study of the temperature behavior of band gap and lifetime broadening can provide us with fruitful information about electron-phonon interactions [8,9,29,30,31,32,33,34,35] and excitonic effects

[26,27]. From an applied point of view, the ability to perform the measurement of the band gap at elevated temperatures (600°), which corresponds to growth conditions of molecular beam epitaxy (MBE), metal-organic chemical vapor deposition (MOCVD) or gas phase molecular beam epitaxy (GPMBE), opens up many new possibilities for applications. For example, the temperature of substrate materials such as GaAs or InP, the alloy composition of $Ga_{1-x}Al_xAs$ or $In_xGa_{1-x}As$ could be monitored in-situ during actual film growth process [28,36].

Photoreflectance is an extremely suitable technique for investigation of the optical properties of fundamental band gap of semiconductors. The PR yields maximum sensitivity to interband electronic transitions. By using PR, the optical feature of the energy band gap can be measured up to 600°C. In comparison, by using scanning ellipsometry, the energy band gaps of the GaAs and InP were measured only up to 500K. This probably is due to the fact that the electromodulation spectrum is not only proportional

to the third derivative of the dielectric function for band-to-band transition but is inversely proportional to the reduced interband mass (μ), while the ellipsometry signal is proportional to $\mu^{3/2}$. Some of the advantages of using PR to measure the band gap at elevated temperature are the following: 1) derivative nature of PR yields maximum sensitivity to interband electronic transition even up to high temperatures; 2) the contactless nature of PR enables us to perform an experiment in transparent ambient and does not require a special holder or contact on the samples. Thus it can be used as an in-situ or ex-situ monitoring tool in fabrication processes such as in MBE or MOCVD.

The second task of this thesis is to study alternating composition layers of multiple quantum wells (MQW) [37, 38, 39, 40, 41] of both lattice matched (such as $Ga_{1-x}Al_xAs/GaAs$ MQW [42, 43]) and lattice-mismatched or strained ($In_xGa_{1-x}As/GaAs$ [44] and GaSb/AlSb MQW [45]) systems by using PR. In the past, the $Ga_{1-x}Al_xAs/GaAs$ structures have served as a model system to understand the electronic and

optical properties of alternating layer structures. Rich spectra of the MQW were observed at room temperature, and they consisted of both symmetry allowed and forbidden confined (CT) and unconfined (UT) transitions. Both the CT and UT exhibited coupling effects between wells(miniband dispersion). With this information we can examine existing theories, such as Bastard Model theory [31,32], and also experimentally determine the following: 1) the band alignment of the heterostructure (band offset); 2) the alloy composition of $Ga_{1-x}Al_xAs$ or $In_xGa_{1-x}As$ epliayers; and the thickness of the wells and barriers of quantum wells. In addition, an investigation of the strained layers system enables us to determine the strain distribution.

This thesis is divided into five chapters.

Chapter II deals with electromodulation spectroscopy. The necessary theoretical background for understanding the experimental results is given in this chapter as well as a discussion of the low field and generalized Franz-Keldysh Oscillations (FKO) theories.

In Chapter III, we discuss the PR measurements of the direct (E_o) gaps of technologically important semiconductors such as GaAs, GaAlAs, InP and $In_xGa_{1-x}As$ (x=0.06 and 0.15) to 600°C. The electron-phonon interaction can be qualitatively understood by analyzing the temperature dependence of the energy gap $E_o(T)$ and the broadening parameter $\Gamma(E_o(T))$. It was found that mainly electron-optical phonon interactions contribute to the broadening parameter $\Gamma(E_o)$ of $In_xGa_{1-x}As$ (x=0.06 and 0.15). By taking into account the effects of thermal expansion in the temperature shifts of band gaps of $In_xGa_{1-x}As$ (x=0.06 and 0.15), we are able to obtain parameters which are directly related to the electron-phonon interaction.

We also present experimental results in which the spectra were obtained in an actual MOCVD reactor , through a diffuser plate including a rotating substrate (500 rev/min) and flowing gas. We will show a real time measurement from which we obtained the spectra of E_o of GaAs at 650°C in 30 seconds.

Chapter IV contains the theoretical background

of semiconductors and semiconductor microstructures, including lattice matched and lattice mismatched (strained layer systems), and the experimental results obtained by modulation spectroscopy for both lattice matched and lattice mismatched MQWs. In the study of a series of GaAs/$Ga_{1-x}Al_xAs$ MQW grown by MBE with different barrier widths, the evidence for coupling between multiple wells (miniband dispersion in several confined transitions above the fundamental one) was observed. In Section 3.2.2 and 3.2.3, we present a study of $In_xGa_{1-x}As$/GaAs and GaSb/AlSb strained layer systems which provides extensive information about the band offset parameter, strain distribution, and widths of wells and barriers, etc.

In Chapter V, using photoreflectance, we have studied how various changes in UHV, air, temperature and light intensity, through their influence on the surface built-in potential in determining the Fermi level pinning on (100) GaAs.

Finally, in Chapter VI, we summarize the results and conclusions of our investigations.

Chapter II

DISCUSSION OF MODULATION SPECTROSCOPY

The idea of modulation spectroscopy [11,12, 51,52] is a very general principle of experimental physics. Instead of directly measuring an optical spectrum, the derivative of the spectrum with respect to some parameter is measured. This can be achieved by applying the parameter as a small perturbation in a periodic fashion and measuring the corresponding change in the optical properties with a phase sensitive detector (or Lock-in amplifier). Structure in the conventional optical spectrum is considerably enhanced in the derivative spectrum, and structureless background is eliminated.

There are two categories of modulation techniques: internal and external. In the internal modulation method, the parameter of the optical beam, such as the wavelength or the degree of polarization, is modulated. In the external method, an independent modulation parameter (e. g. a stress, an electric field, etc) is applied to the sample.

The external modulation methods can be further subdivided into two aspects according to the nature of the perturbation. The first and more simple aspect of external modulation method is that the optical properties are modulated by the perturbation, such as stress and temperature, in which the translation symmetry of crystal is preserved under this kind of perturbation. This external modulation usually gives the first derivative lineshape spectra (see Fig 1a).

The second type of method is more complicated, in which the free electrons and holes inside the crystal are accelerated by the perturbing electric field, thus breaking the translational invariance of the crystal. The lineshape for low field modulation corresponds to high order derivative-like spectra (see Fig. 1b), while for high field modulation, the lineshape contains Franz-keldshy Oscillation (FKO). In contrast, for bound state such as exciton, impurities and quantum levels in isolated quantum wells, the lineshape is the first-derivative like, since the electric field does not accelerate the particles.

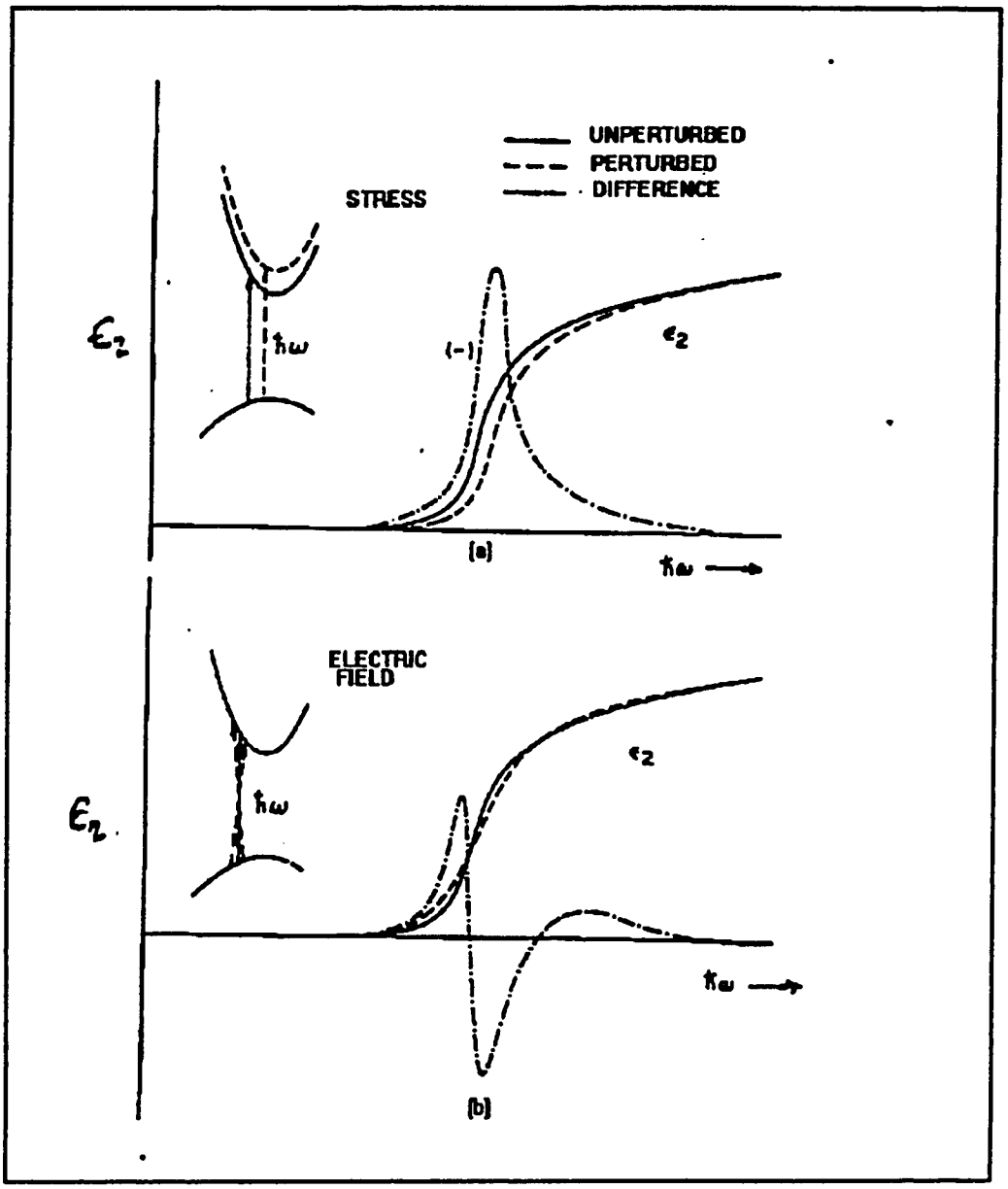

Figure 1. Two categories of modulation mechanism . a)First derivative modulation process where lattice periodicity is preserved. b) electric field modulation where lattice periodicity is not preserved.

2.1 Dielectric Function and Modulation Spectra

In order to understand the mechanism of the modulation spectroscopy, we present here the derivation of the basic physical quantities from fundamental quantum mechanics. We discuss the relationship between the electronic band structure and optical transition. Finally, we show the changes in the dielectric function under different kinds of perturbations [11].

2.1.1 Transition Probability

The effect of a radiation field on the crystal electronic states can be studied using the standard quantum mechanical method. We know that the kinetic energy of electron in the presence of an electromagnetic field can written as:

$$(1/2m)(P+eA/c)^2 \qquad (1)$$

where m is the mass of an electron, P is the momentum, e is the electron charge, and A is the

vector potential of the electromagnetic field. Furthermore we can neglect non-linear effects by disregarding the term in A^2. The interaction Hamiltonian of an electron in a radiation field is given by:

$$H_{eR}=(e/mc)A\cdot P \qquad (2)$$

The effect of a radiation field on the crystal can be studied by treating H_{eR} as a time dependent perturbation term on the electronic states of the crystal. This time dependent term will cause electrons to make transitions between occupied bands to empty bands. Also from the transition probability rate, the relationship between the electronic structure and the optical constants can be derived.

The probability of transition per unit time between initial $|i\rangle$ and final $|f\rangle$ states is:

$$P_{i\to f}=(2\pi/\hbar)|\langle f|H_{eR}|i\rangle|^2\delta(E_f-E_i\mp\hbar\omega) \qquad (3)$$

where E_i and E_f are the energies of the initial and

final states, respectively. This relationship has the interpretation that the perturbation H_{eR} induces transitions with either absorption of a photon (minus sign) or emission of a photon (plus sign). The transition between valence band $\psi_{v,ki}$ and conduction band $\psi_{c,kf}$ induced by the radiation $A_o e e^{i(kr-\omega t)}$+cc photon, $P_{i\to f}$ can be expressed as:

$$P_{i\to f}=(2\pi/\hbar)[(eA_o)/(mc)]^2|\langle\psi_{c,kf}|e^{ikr}e\cdot p|\psi_{v,ki}\rangle|^2 x \delta(E_f-E_i-\hbar\omega)+cc \qquad (4)$$

where e is the polarization in the direction of electric field, k is wave vector and cc indicates the complex conjugate of the previous term. The matrix $\langle\psi_{c,kf}|e^{ikr}e\cdot p|\psi_{v,ki}\rangle$ will equal zero unless:

$$k_f=k_i+k \qquad (5)$$

The range of variation of k_i (and $k_{f)}$) is π/a_1 with a_1 of the order of a few angstroms. For typical photon energy, the wavelength is of the order of 10^4 Å, and $k=2\pi/10^4$. Therefore $k \ll k_i$ (or k_f). We thus obtain

the "vertical" transition rule:

$$k_i = k_f \tag{6}$$

Equation (4) can be simplified as:

$$P_{i\to f} = (2\pi/\hbar)[(eA_o)/(mc)]^2 |e \cdot M_{cv}(k)|^2 \delta(E_c - E_v - \hbar\omega) \tag{7}$$

$$\begin{aligned} e \cdot M_{cv}(k) &= \langle \psi_{c,k} | e \cdot p | \psi_{v,k} \rangle \\ &= e \int_{\text{crystal volume}} \psi_c^*(k,r)(-i\hbar\nabla)\psi_v(k,r)dr \end{aligned} \tag{8}$$

To obtain the number of transitions W(hω) per unit time per unit volume induced by light of frequency ω, we must sum Eq.(7) over all possible states in the unit volume, i. e. we must sum over k, the spin variable s, and over the band indices v (occupied) and c (empty). Therefore:

$$W(h\omega) = 2\pi/\hbar[(eA_o)/(mc)]^2 \Sigma \int 2dk/(2\pi)^3 |e \cdot M_{cv}(k)|^2 x$$
$$\delta(E_c - E_v - \hbar\omega) \tag{9}$$

2.1.2 Connection With The Optical Constants

The optical properties can be described in terms of the complex dielectric function $\epsilon=\epsilon_1+i\epsilon_2$ or the complex refraction index $N=n+i\kappa$, where n is the ordinary refraction index and κ is known as the extinction coefficient. The optical constants ϵ and N are connected by the relation $\epsilon = N^2$, and the absorption coefficient α depends on the above optical constants via:

$$\alpha=2\kappa\omega/c=(\omega\epsilon_2)/(nc) \qquad (10)$$

The average energy density, u, in a medium of a radiation field, described by the vector potential, A is related to the optical constants through the relationship:

$$u=(nA_0\omega)^2/(2\pi c^2) \qquad (11)$$

The absorption coefficient is, by definition, the energy absorbed per unit time per unit volume divided by the energy flux:

$$\alpha(\omega)=(\hbar\omega W(\omega))/u(c/n) \qquad (12)$$

Thus we obtain for the absorption coefficient for a vertical transition:

$$\alpha(\omega)=(4\pi^2e^2)/(ncm^2\omega)\Sigma\int 2dk/(2\pi)^3|e\cdot M_{cv}(k)|^2x$$
$$\delta(E_c-E_v-\hbar\omega) \qquad (13)$$

Using Eq.(10):

$$\epsilon_2(\omega)= (4\pi^2e^2)/(m^2\omega^2)\Sigma\int 2dk/(2\pi)^3|e\cdot M_{cv}(k)|^2x$$
$$\delta(E_c-E_v-\hbar\omega) \qquad (14)$$

The matrix elements $|e\cdot M_{cv}(k)|^2$ are smooth functions of k. By taking $e\cdot M_{cv}(k)$ as a constant, then:

$$\epsilon_2(\omega)= (4\pi^2e^2)/(m^2\omega^2)\Sigma|e\cdot M_{cv}(k)|^2\int 2dk/(2\pi)^3x$$
$$\delta(E_c-E_v-\hbar\omega) \qquad (15)$$

The quantum expression for ϵ_1 can be obtained by the Kramers-Kronig relationship:

$$\epsilon_1=1+2/\pi\ P\int \omega'\epsilon_2(\omega')/(\omega'^2-\omega^2)\ d\omega' \qquad (16)$$

where P indicates the principlal part.

By direct substitution of Eq.(15) into Eq. (16)

$$\epsilon_1(\omega)=1+(8\pi e^2)/m^2\Sigma|e\cdot M_{cv}(k)|^2\int 2dk/(2\pi)^3 x$$
$$\hbar/[E_c-E_v]x1/\{[E_c-E_v]^2/\hbar^2-\omega^2\} \qquad (17)$$

Define the joint density of states for interband transitions:

$$J_{cv}(\omega)=\int 2dk/(2\pi)^3\delta(E_c-E_v-\hbar\omega)^2 \qquad (18)$$

and $\epsilon_2(\omega)$ can be written as:

$$\epsilon_2(\omega)=(4\pi^2e^2)/(m^2\omega^2)\Sigma|e\cdot M_{cv}(k)|^2\ J_{cv} \qquad (19)$$

J_{cv} can be rewritten as:

$$J_{cv}(E)=2/(2\pi)^3\int dS/|(\nabla_k[E_c(k)-E_v(k)]| \qquad (20)$$

where dS represents an element of surface in k space

on the surface defined by the equation

$$E_c(k)-E_v(k)=E \tag{21}$$

From Eq. (20), singularities in the joint density of states are expected when

$$\nabla_k[E_c(k)-E_v(k)] =0 \quad \text{or} \tag{22a}$$

$$\nabla_k E_c(k)=\nabla_k E_v(k) =0 \tag{22b}$$

These are called Van-Hove singularities, and are responsible for the structure in the optical and modulated optical spectra of semiconductors. The transitions giving rise to the structure are usually localized in the BZ. Because these structures are associated with the critical point defined by Eq. (22), it is usually entirely adequate to replace the actual complicated variation $E_{cv}(k)$ with a series of parabolic expansions:

$$E_{cv}(k)=E_{cv}(k_{jcv})+1/2\hbar^2[(k_x-k_{jx}^{cv})^2/\mu_{xx}^{cv}+$$

$$(k_y-k_{jy}^{cv})^2/\mu_{yy}^{cv}+(k_z-k_{jz}^{cv})^2/\mu_{zz}^{cv}] \qquad (23)$$

These are centered about each critical point k_j^{cv} for a given band pair c and v, where the reciprocal mass tensor is defined as:

$$\mu_{cv}^{-1}=1/\hbar^2\nabla_k\nabla_k(E_c(k)-E_v(k)). \qquad (24)$$

If we take any single critical point, suppress all indices and take $(k-k_j^{cv})$ as the variable relative to the local coordinate system that diagonalized the mass tensor μ^{-1} then Eq.(23) can be written in the simplified form:

$$E_{cv}(k)=E_g+1/2\hbar^2(k_x^2/\mu_{xx}+k_y^2/\mu_{yy}+k_z^2/\mu_{zz}) \qquad (25)$$

Thus the band structure is represented locally by only 4 parameters: the threshold energy $E_g=E_c(k_j)-E_v(k_j)$ and the three components of the mass tensor. Introducing the broadening parameter Γ, the joint density J_{cv} for one, two and three dimension can be calculated. Therefore the ϵ_2 can be written as:

$$\epsilon_2(E,\Gamma)\sim\begin{cases}|e\cdot M_{cv}(k)|^2/E^2(E_g-E+i\Gamma)^{-1/2} & \text{1D critical point}\\ |e\cdot M_{cv}(k)|^2/E^2\ln(E_g-E+i\Gamma) & \text{2D critical point}\\ |e\cdot M_{cv}(k)|^2/E^2(E_g-E+i\Gamma)^{1/2} & \text{3D critical point}\end{cases} \tag{26}$$

This is for M_o critical point in which μ_{xx}, μ_{yy}, and μ_{zz} are positive.

In modulation experiments, the perturbation changes the dielectric function ϵ. Let us assume that the real and imaginary parts of the dielectric function are changed by the amount $\Delta\epsilon_1$ and $\Delta\epsilon_2$, respectively. Then it can be shown:

$$\Delta R/R=\alpha\Delta\epsilon_1+\beta\Delta\epsilon_2 \tag{27}$$

where R is the reflectivity, and α and β are the Seraphin coefficients, which have a characteristic energy dependence for most semiconductors. In the event that perturbation ξ such as temperature, pressure, uniaxial stress, etc, does not destroy the translation symmetry of the crystal, the situation

is fairly simple: $\Delta\epsilon=(\partial\epsilon/\partial\xi)\Delta\xi$. This gives rise to the first derivative of lineshape spectra.

The most complicated form of modulation is electromodulation since in certain cases (bulk material and superlattices), it can change the periodicity of the sample. In the non-excitonic case, the free electron-hole pairs experience a position-dependent potential, which destroys the translation symmetry of the crystal, i. e. charged particle can be accelerated. There are three different kinds of cases: 1) The exciton or bound states of quantum well modulated by a low electric field 2) the low field limit and 3) the high field.

2.2 Modulation Spectroscopy

2.2.1 The bound states under low electric field.

For bound states or excitons, since the electric field does not accelerate the particle (charge are zero), the translational symmetry of thr crystal is preserved. The binding energy and life

time of states are modulated by the electric field, the situation is also simple: $\Delta\epsilon=(\partial\epsilon/\partial\xi)\Delta\xi$. This gives rise to the first derivative of lineshape spectra. A more sophisticated derivation is shown in Section 4.1.5.

2.2.2 The Low field limit

The time dependent Schrödinger equation for an electron in a crystal in the presence of an electric field F can be written as [11]:

$$H\psi=i\hbar\partial\psi/\partial t \tag{28}$$

$$H=H_o+eF\cdot r \tag{29}$$

where H_o is the crystal Hamiltonian. The time evolution of the wave function, which at the time t=0 is the Bloch function $\psi_n(k_o,r)$ is given by:

$$\psi(r,t)=\exp(-i(Ht/\hbar)\psi_n(k_o,r) \tag{30}$$

The main effect of the electric field on a periodic system is to change the wave vector from k to k-eFt/h. The effect is to mix states with the k vector along the field direction. The solution of the time dependent Schrödinger equation can be approximately written as:

$$\psi_n(k,r,t)=\exp\left[-i/\hbar \int E_n(k)dt \right] \psi_n(k,r,) \qquad (31)$$

with k given by:

$$k(t)=k_o-eFt/\hbar \qquad (32)$$

I can now determine the optical constant of a crystal in the presence of an electric field, using procedures similar to the previous section. By taking into account the time dependence of the solution (32), and the broadening parameter Γ, we obtain for the imaginary part of the dielectric function in the presence of the electric field F:

$$\epsilon_2(\omega)= (4\pi^2e^2)/(m^2\omega^2)\Sigma\int 2dk/(2\pi)^3 \left| e\cdot M_{cv}(k) \right|^2 x$$

$$\delta(E_{cv}(k-teF/\hbar)+i\Gamma-\hbar\omega) \qquad (33)$$

Eq.(33) can be expressed as the Fourier time transformation:

$$\epsilon_2(\omega)= (e^2)/(\pi^2m^2\omega^2)\Sigma\int dk/(\pi)^2|e\cdot M_{cv}(k)|^2x \int dt\ \exp\{-i[(E_{cv}(k-teF/\hbar)-i\Gamma+\hbar\omega]t\} \qquad (34)$$

The exponent in Eq.(34) satisfies time-reversal invariance:

$$-i[(E_{cv}(k-teF/\hbar)-i\Gamma+\hbar\omega]t \longrightarrow -i\int dt'X [(E_{cv}(k-teF/\hbar)-i\Gamma+\hbar\omega]$$

Expanding $E_{cv}(k)$ and retaining terms only to second-order ('weak field approximation'), Eq. (34) can be written as:

$$\epsilon_2(\omega)= (e^2)/(\pi^2m^2\omega^2)\Sigma\int dk/(\pi)^2|e\cdot M_{cv}(k)|^2x \int dt\ \exp\{-i[(E_{cv}(k)-i\Gamma+\hbar\omega]t-i(\Omega t')^3/3)\} \qquad (35)$$

where $(\hbar\Omega)^3=e^2F^2\hbar^2/8\mu$, μ is the interband effective

reduced mass in the field direction. If the field is small or the broadening Γ large, such that $\Gamma >> \hbar\Omega$, we can expand the exponent containing Ω to get $\exp[-i(\Omega t')^3/3\hbar] \approx 1-i(\Omega t')^3/3\hbar$. With this we obtain the ϵ_2 in Aspen's low field limit:

$$\epsilon_2(E,F,\Gamma)=\epsilon_2(\omega,0,\Gamma)+(\hbar\Omega)^3/3E^2\partial^3[E^2\epsilon_2(E,0,\Gamma)+\cdots \quad (36)$$

noting that t'^3 is operationally equivalent in Eq.(36) to $[i\hbar(\partial/\partial E)]^3$ in quantum mechanics.

By the Kramers-Kronig relation, we are able to obtain ϵ_1 in the presence of an electric field F:

$$\epsilon_1(E,F,\Gamma)=\epsilon_1(\omega,0,\Gamma)+(\hbar\Omega)^3/3E^2\partial^3[E^2\epsilon_1(E,0,\Gamma)+\cdots \quad (37)$$

Therefore we have a change in the dielectric function in the presence of a small electric field,

$$\Delta\epsilon=(1/3)(\hbar\Omega)^3(\partial^3/\partial E^3)[E^2\epsilon(E,\Gamma)] \quad (38)$$

where $\hbar\Omega=(e^2F^2\hbar^2/8\mu)^{1/3}$ is the characteristic electro-optic energy of the system. It is obvious that the

electric field-induced change is related to the third derivative with respect to energy of the unperturbed dielectric function. This is in contrast to the first derivative nature of modulation techniques which preserved translational symmetry. From Eq.(38), we found that the lineshape of $\Delta\epsilon$ is independent of the field and its amplitude simply increases as the square of the field and inversely as the interband effective mass in the field direction.

Since the low-field electroreflectance (ER) structure of a single critical point is well localized within an energy range not exceeding several broadening parameters, the unperturbed dielectric function can be replaced with the local dielectric function discussed in the last section. Thus the relative change in reflectivity can be written as:

$$\Delta R/R=\mathrm{Re}\{[Ce^{i\Theta}(E-E_g+i\Gamma)]^{-n}\} \qquad (39)$$

where C and Θ are the amplitude and phase factor

which vary slowly with E. These can essentially be considered to be independent of small changes in E. The parameter C determines the amplitude of the lineshape while the asymmetry of the lineshape is determined by the parameter Θ. Energy gap (E_g) and and broadening (Γ) determine the location and width of the structure. The parameter n determines the nature of critical points. n=2.5 is for three dimensional critical points , n=3.0 for two dimensional critical points, and n=3.5 is for one dimensional critical points. In the case of an exciton, the electric field modulates the exciton binding energy as well as broadening and amplitude. It gives rise to the first derivative of lineshape function and thus yields n=2. (A detailed discussion will be presented in Section 4. 1. 5).

2.2.3 Franz-Keldysh Oscillations.

If the low field limit is not valid, then full quantum mechanics must be used. Several different but equivalent methods have been reported in the

literature to calculate the dielectric function in the presence of the electric field [49, 50, 51, 52, 53, 54, 55]. We outline only the simplest, i. e., the stationary state approach in the effective mass approximation [49].

The calculation begins with the center of mass problem of the electron and hole:

$$[(\hbar^2/2\mu)\nabla^2+eFz+W_i]\ \phi_i(z)=0 \qquad (40)$$

The solution of Eq.(40) is given by:

$$\phi_i(z)=(eF/\hbar\Theta)\ Ai[(eFz-W_i)/\hbar\Theta] \qquad (41)$$

with eigenvalue W_i with the z-axis parallel to F and where

$$\hbar\Theta=(e^2F^2\hbar^2/2\mu)^{1/3} \qquad (42)$$

and Ai is the Airy function. The imaginary part of the dielectric function in the zero broadening limit is:

$$\epsilon_2(E)=(\Xi/E^2)\ \Sigma\ |\ \phi(0)|^2\delta(W_1-E) \qquad (43)$$

where $\Xi=(2e^2\hbar^2/m^2)|e\cdot M_{cv}|^2(2\mu/\hbar)^{3/2}$. By substituting $\phi(0)$ from Eq.(41) into Eq.(43), the result is given by:

$$\epsilon_2(E,F)=(\Xi/E^2)(\hbar\Theta)^{1/2}\pi[Ai'^2(\eta)-\eta Ai(\eta)] \qquad (45a)$$

$$\epsilon_2(E,0)=(\Xi/E^2)(\hbar\Theta)^{1/2}(E-E_g)^{1/2}H(E-E_g) \qquad (45b)$$

where $H(x)$ is the step function and $\eta=(E_g-E)/\hbar\Theta$. This result and its Kramer-Kronig transform are usually expressed as the difference $\Delta\epsilon$ between finite-field and zero field limits given in terms of two functions, $F(\eta)$ and $G(\eta)$:

$$\Delta\epsilon(E,F)=(\Xi/E^2)(\hbar\Theta)^{1/2}[G(\eta)+iF(\eta)] \qquad (46)$$

where

$$F(\eta)=\pi[Ai'^2(\eta)-\eta Ai^2(\eta)]-(-\eta)^{1/2}H(-\eta) \qquad (47)$$

$$G(\eta)=\pi[Ai'(\eta)Bi'(\eta)-\eta Ai(\eta)Bi(\eta)]+\eta^{1/2}H(\eta) \qquad (48)$$

The lineshape factor G and F, plotted as field induced changes in real and imaginary parts of dielectric function are shown in Fig.2. The optical features for $\eta<0$ was called Franz-Keldysh oscillations (FKO).

The Physical picture of FKO is photo-assisted indirect interband transitions in real space. It is also sometimes called photo-assisted tunneling. Transitions between the valence and conduction bands are now possible for an energy smaller than E_g through the quantum effect, which corresponds to the exponential tail for $\eta>0$. Transitions above the energy gap ($\eta<0$) show resonance effects whenever the distance the electron travels equals an integer number of de Broglie wavelengths, which corresponds to the periodic peaks in Fig 2.

Using the asymptotic expression of the Airy function [11]:

$$Ai(\eta)=\pi^{1/2}(-\eta)^{-1/4}\sin[(2/3)(-\eta)^{3/2}+\pi/4] \qquad (49)$$

$$v\pi=\phi+(4/3)[(E_v-E_g)/\hbar\Theta]^{3/2} \qquad (50)$$

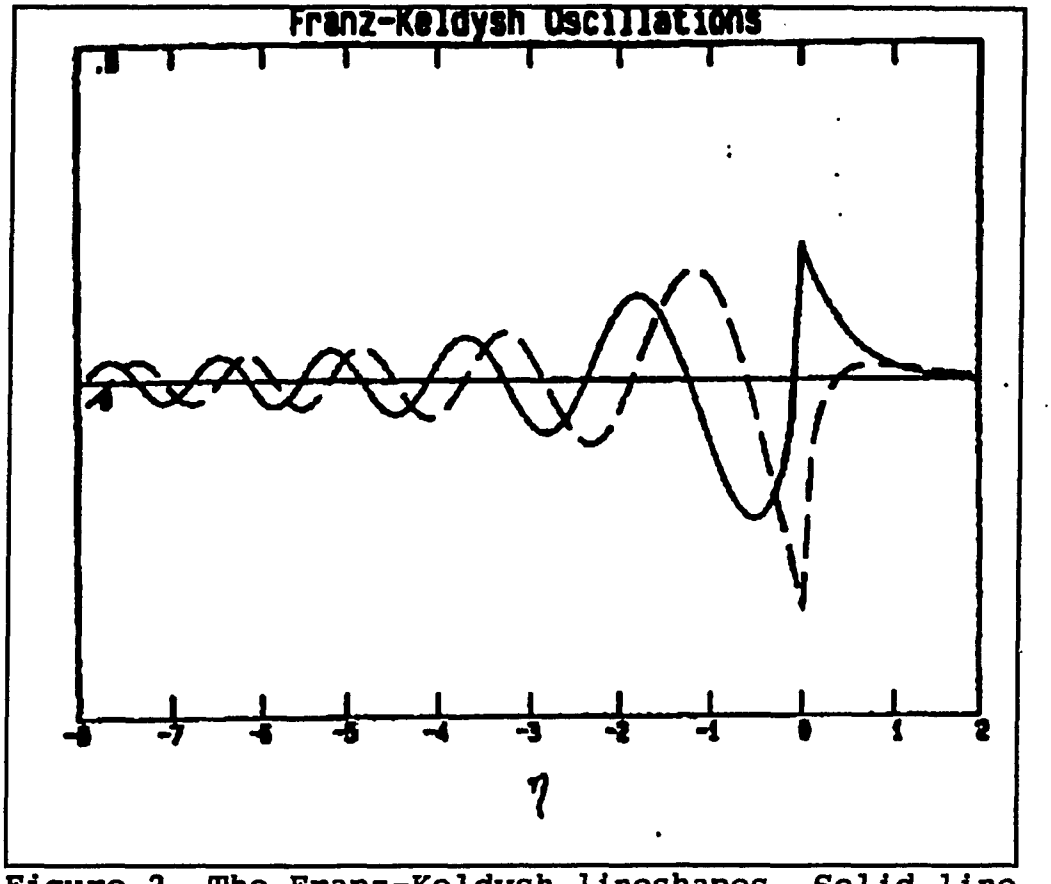

Figure 2. The Franz-Keldysh lineshapes. Solid line G dashed line F.

Thus, a plot of extreme number ν versus $4/3(E_\nu-E_g)^{3/2}$ yields a slope of $(\hbar\Theta)^{-3/2}$, where ϕ is an arbitrary phase factor, E_ν is the photon energy of the νth oscillation and E_g is the band gap. The electric field F can be evaluated via equation (42). In many situations, for example, in the space charge layer of semiconductor or semiconductor structure, F is not uniform. However, if F varies linearly with

distance from the surface/interface then it has been shown that the period of the FKO is a direct measure of the maximum electric field in this region [20, 54] and not the average electric field. [55, 21].

2.3 Experiment Setup

Shown in Fig. 3 is a schematic representation of a PR experiment. Light from an appropriate lamp source passes through a monochromator (probe beam). The exit intensity at wavelength λ is focused onto the sample by means of a lens (or mirror), where $I_o(\lambda)$ is the intensity of light striking the sample. Electromodulation of the sample is produced by the photoexcitation of electron-hole pairs created by a laser or other secondary (pump) beam. [12,13,10]. This pump beam is chopped at frequency Ω_s. The reflected beam is collected by a second lens (mirrors) and is focused onto an appropriate detector such as silicon-photodiode. In the figure, we have not shown the two lenses (mirrors). The light striking the detector contains two signals

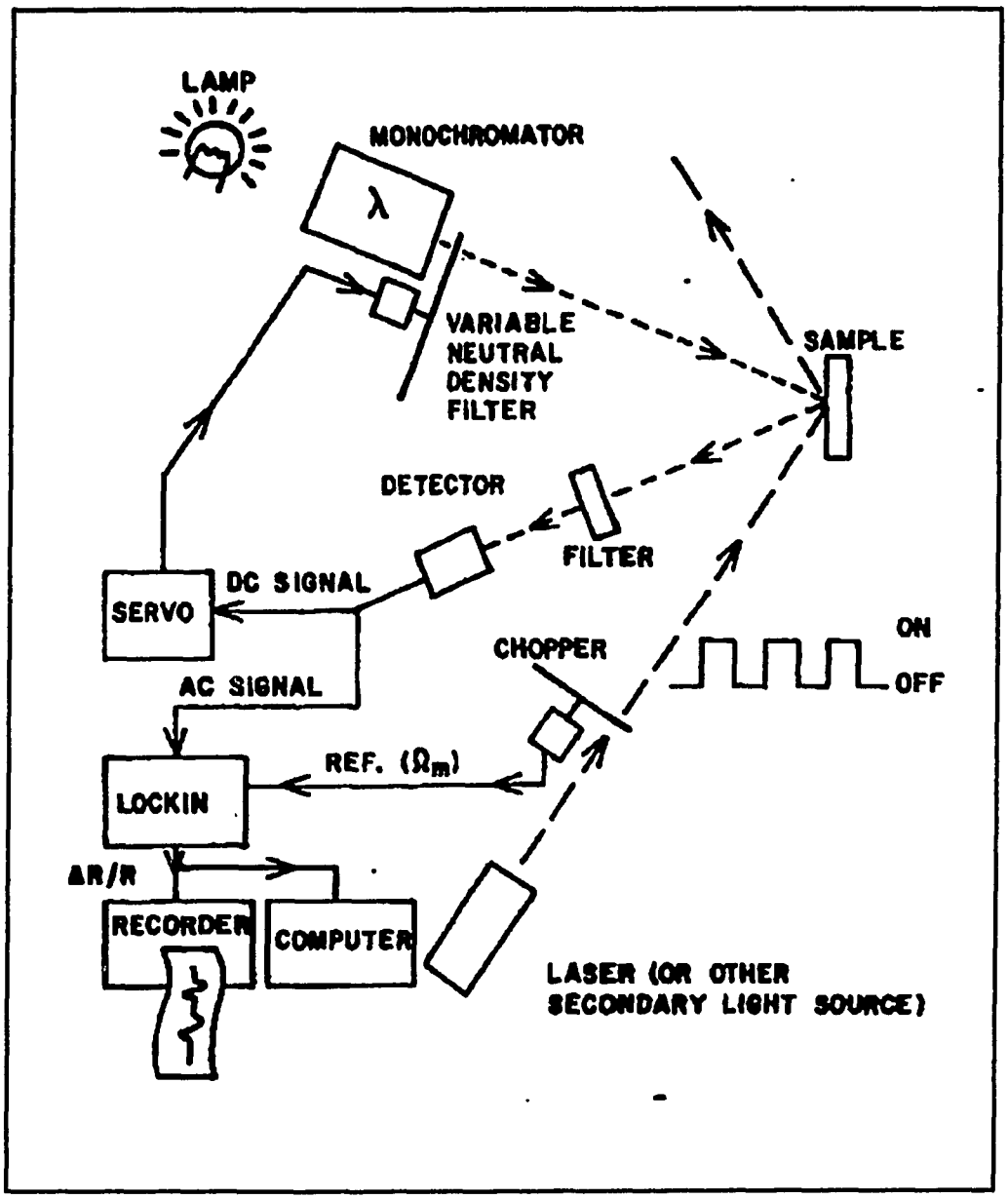

Figure 3 Schematic of photoreflectance apparatus setup

the dc (or average value) is given by $I_o(\lambda)R(\lambda)$, where $R(\lambda)$ is the dc reflectance of the material,

while the modulated value (at frequency Ω_m) is $I_o(\lambda)\Delta R(\lambda)$, where $\Delta R(\lambda)$ is the modulated reflectance. The ac signal from the detector, proportional to $I_o\ \Delta R$ is measured by a lock-in amplifier. In order to evaluate the quantity of interest $\Delta R(\lambda)/R(\lambda)$ a normalization procedure was used to eliminate the uninteresting common feature I_o. [10]. The normalization is achieved by a variable neutral density filter (VNDF) connected to a servomotor which is placed in the optical path between the probe monochromator and the sample. The dc signal from the detector is used as input to the servo motor which varies the VNDF, and, hence, $I_o(\lambda)$, in order to keep V_{dc} constant. In this procedure the operating conditions of experiment such as the detector amplification, and instrumental resolution, etc., are kept constant.

2.4 Mechanism of Photoreflectance

At the surface of a semiconductor such as GaAs

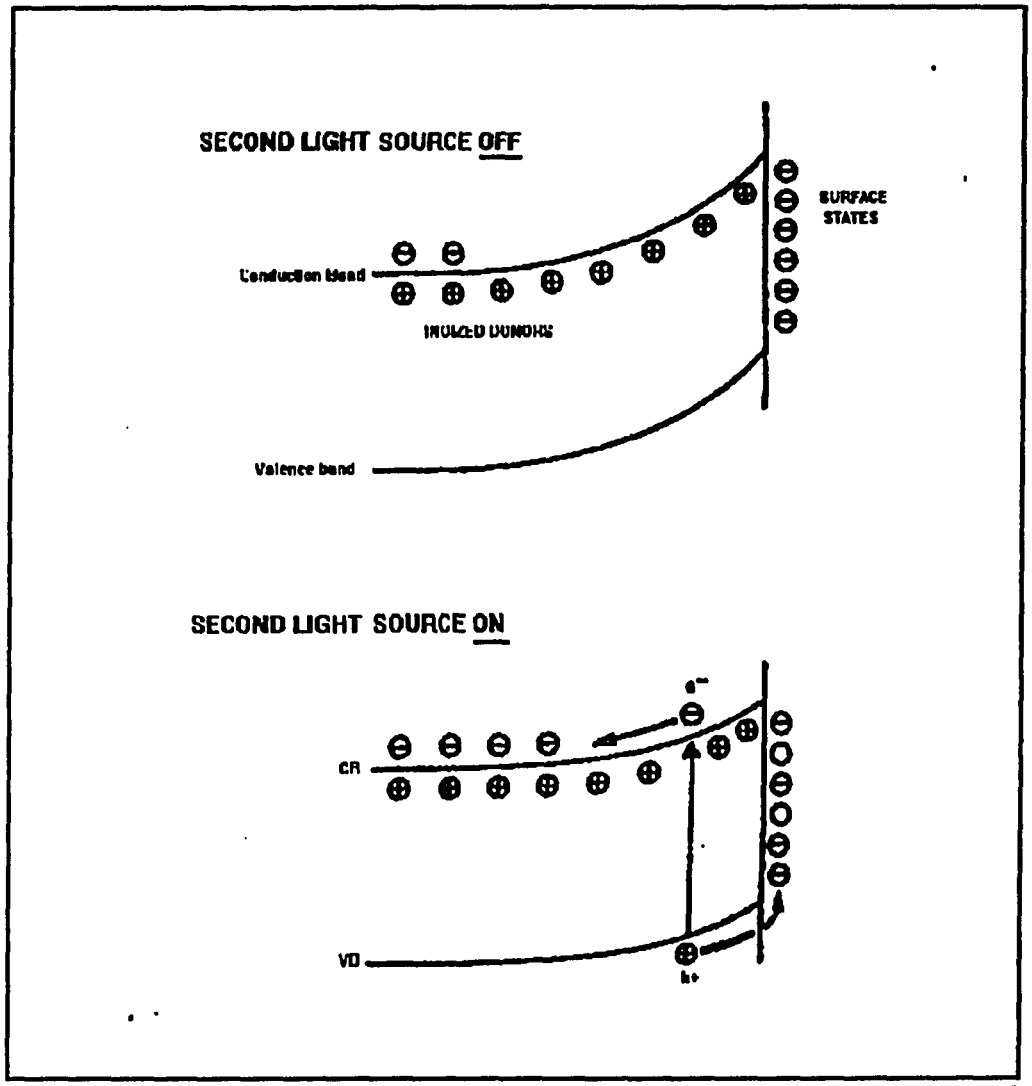

Figure 4 Schematic representation of band bending of n-type GaAs influence by the light.

the fermi level (V_f) is pinned in the energy gap by the surface states. The equilibrium of the fermi level in the bulk and at its surface is established through the formation of a depletion layer and

through the bending of the electronic bands within this layer. When the light is on, the incident photons produce electron-hole pairs within the semiconductor surface space charge region which separate in the electric field of the depletion region, resulting in a reduction of the band bending, and hence the surface electric field is decreased.

The modulation of the optical constants for PR is achieved by creation of electron-hole pairs by a secondary (or pump) light beam. The main effect is a reduction of built-in surface (or interface) field through a recombination of minority species with charges in the surface (or interface) states. The reduction of built-in surface is shown schematically in Fig 4 for an n-type semiconductor. In the upper portion (second light off) of the diagram, band bending and the population of the surface (interface) states are maximum. In the lower portion, with the secondary light on, there are photo-excited electron-hole pairs. These photo-excited holes move toward the surface and

recombine with electrons in the surface states, and, hence, reduce the band bending. This causes a modulation of the space-charge region electric field. The lineshape of PR in this case is identical to the electroreflectance lineshape.

2.5 Lineshape Fit Techniques

In modulation spectroscopy, one of the objectives is to determine the parameters in Eq.(39) and to relate them to the model band structure by Eq. (17). Given an experimental lineshape, E_g and Γ are determined by the energy location and broadening parameter of the structure, respectively. The exponent n is determined by the number of oscillations and the overall sharpness of structure. n is related to the effective dimensionality of the critical point in the Brillouin zone and order of differentiation. The fitting function yields information about the nature of transitions. For bound states, such as exciton and quantum levels in isolated wells, the spectrum is described by the

first derivative of the lineshape function, since the electric field does not accelerate the particles and translational symmetry of the crystal are preserved. (Further discussion will be presented in Chapter 4). As in the case of unbound states, such as band-to-band transition, the low field lineshape is well represented by the third derivative of the Lorentzian function. The lineshape of spectra is also important to obtain the built-in electric field of semiconductor surface and interface by equation (50).

Chapter III

TEMPERATURE DEPENDENCE OF SEMICONDUCTORS

Recently there has been a growing interest in studies of the temperature dependence of the energy gaps and the broadening parameters of semiconductors such as GaAs, InP, $Ga_{1-x}Al_xAs$ and $In_xGa_{1-x}As$ by optical techniques including ellipsometry [8,9] or photoreflectance (PR) [56,27,28,36]. The investigation of a shift in the energy of band gaps and an increasing lifetime broadening with increasing temperature can provide us with fruitful information about electron-phonon interactions [44,45], and excitonic effects [29,56], etc. Using PR, it has been possible to observed energy gap (E_o) of semiconductors such as GaAs, InP, $Ga_{1-x}Al_xAs$ and $In_xGa_{1-x}As$ up to 600°C. This temperature is a factor of two higher than the temperature in recently reported spectral ellipsometry results. This is probably due to the fact that the electromodulation spectrum [11] is not only proportional to the third derivative of the dielectric function, but is inversely proportional to the reduced interband mass

(μ), while the ellipsometry signal is proportional to $\mu^{3/2}$. (μ<1). From an applied point of view, the ability to measure band gaps at elevated temperatures (~600°C) corresponding to growth conditions of molecular beam epitaxy (MBE), metal-organic chemical vapor deposition (MOCVD) or gas phase molecular beam epitaxy (GPMBE) opens up many new possibilities. For example, (a) the temperature of a substrate material (GaAs or InP) or (b) the alloy composition of GaAlAs or InGaAs could be monitored in-situ during actual growth procedures [28,36].

3.1 Theoretical Background

It is well known that the electron-phonon interaction contributes to both the temperature shift of the energy gap and the increase of the lifetime broadening. Cardona et al. have made extensive microscopic analyses of these temperature-dependent shifts and broadening for semiconductors such as Ge[31,33,34], Si[31,33,34] and GaAs[32] based on the renormalization of the band energies by

the electron-phonon coupling. We illustrate here the same treatment as presented by Cardona, etc [31, 32]. We only outline the basic equations and physical meaning.

In deriving the relevant relations for the phonon induced energy shift and broadening, we follow the theory of Ref 31, and 32. Consider a crystal with atoms of species κ which occupy sites $R(k,\kappa)$ and have displacements $u(l,\kappa)$ from equilibrium, where l labels the unit cells. In order to describe the renormalization of the semiconductor band structure by the electron-phonon interaction, the electron-atom interaction $V(r-R(l,\kappa)-u(l,\kappa))$ is Taylor expanded about the position $u(l,\kappa)=0$. The zero-order Hamiltonia H_o gives the one-electron states $|k,n\rangle$ and band energies ϵ_{kn} where k, n are wave-vector and band index. The first two terms of the expansion of $V(r-R(l,\kappa)-u(l,\kappa))$ in powers of $u(l,\kappa)$ are

$$H_1= \Sigma\ (\partial V/\partial R_\alpha(l,\kappa))u_\alpha(l,\kappa) \qquad (51)$$

$$H_2=1/2\ \Sigma(\partial^2 V/[\partial R_\alpha(l,\kappa)\partial R_\beta(l',\kappa')]u_\alpha(l,\kappa)u_\beta(l',\kappa') \qquad (52)$$

H_1 represents the electron-phonon interaction involved absorption or emission of one phonon, while H_2 represents the electron-phonon interaction involved absorption or emission of two phonon.The subscripts α, β denote Cartesian components which are summed when repeated. The adiabatic approximation allows the neglect of the time dependence of $u(l,\kappa)$. Using standard perturbation theory, we have:

$$E_{kn}(\{u(l,\kappa)\}=\epsilon_{kn}+\langle k,n|H_2|k,n\rangle+\Sigma'|\langle k',n'|H_1|k,n\rangle|^2/(\epsilon_{kn}-\epsilon_{k'n'}+i\Gamma) \qquad (53)$$

The first and second correction terms to the unperturbed energy of the initial state ϵ_{kn} are called "Debye-Waller", and "Fan" terms, respectively. The Feynman diagram is shown in Fig. 5. The Debye-Waller term is purely real. This term will not make a contribution to life time broadening. In the Fan terms the scattering process involves that electron-phonon interaction which induces transitions from initial state $|k,n\rangle$ to intermediate state $|k'.n'\rangle$ and to initial state (see

Fig. 5b). This term not only makes a contribution to energy shift, but also to lifetime broadening. Equation (53) can be written as

$$E_{kn}(T)=\epsilon_{kn}+\Delta E_{kn}(T)+i\Gamma_{kn}(T) \qquad (54)$$

where

$$\Delta E_{kn}(T)=\Sigma\ E(Q_j,|k,n>)[n_{qj}(T)+1/2] \qquad (55)$$

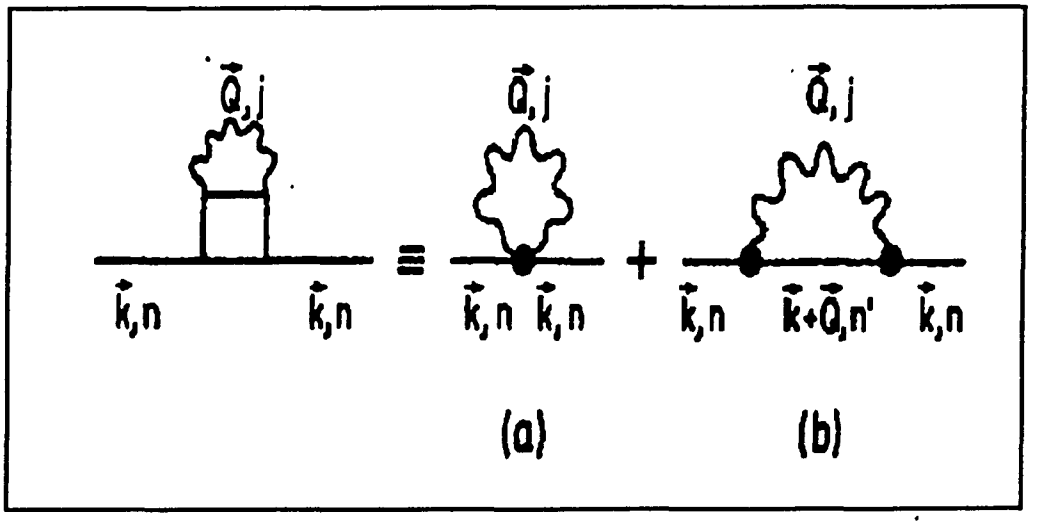

Figure 5 Self-energy graphs which give the temperature renormalization of the band energies to second order in atomic displacement a)represents the lowest-order Debye-Waller correction; and b) represents the Fan term.

and

$$\Gamma_{kn}(T)= \Sigma\ \Gamma(Q_j,|k,n>)[n_{qj}(T)+1/2]. \qquad (56)$$

where n_{qj} is the Bose-Einstein occupation factor $(e^{\beta\omega Qj}-1)^{-1}$ with $\beta=1/k_BT$.

$$E(Q_j,|k,n>)=\hbar/N\cdot \Sigma \frac{<kn|\partial V/\partial R_\alpha(\kappa)|k+Qn'><k+Qn'|\partial V/\partial R_\beta(\kappa')|kn>}{\epsilon_{kn}-\epsilon_{k+Qn'}} \cdot$$

$$\exp(-iQ(\tau_\kappa-\tau_{\kappa'})(M_\kappa M_{\kappa'}\omega^2_{Qj})^{-1/2}\epsilon_\alpha(-Q_{j\kappa})\epsilon_\beta(Q_{j\kappa'})$$

$$-\hbar/2N\cdot \Sigma \frac{<kn|\partial V/\partial R_\alpha(\kappa)|kn'><kn'|\partial V/\partial R_\beta(\kappa')|kn>}{\epsilon_{kn}-\epsilon_{kn'}} \cdot$$

$$[(M_\kappa\omega_{Qj})^{-1}\epsilon_\alpha(-Q_{j\kappa})\epsilon_\beta(Q_{j\kappa})+(M_{\kappa'}\omega_{Qj})^{-1}\epsilon_\alpha(-Q_{j\kappa'})\epsilon_\beta(Q_{j\kappa'})], \qquad (57)$$

and

$$\Gamma(Q_j,|k,n>)= \pi\hbar/N\ \Sigma <kn|\partial V/\partial R_\alpha(\kappa)|k+Qn'>$$

$$<k+Qn'|\partial V/\partial R_\beta(\kappa')|kn>\ X\ \exp(-iQ(\tau_\kappa-\tau_{\kappa'})(M_\kappa M_{\kappa'}\omega^2_{Qj})^{-1/2}\epsilon_\alpha(-$$

$$Q_{j\kappa})\epsilon_\beta(Q_{j\kappa'})\ \delta\ (\epsilon_{kn}-\epsilon_{k+Qn}) \qquad (58)$$

where M_κ is the mass of the atom κ located in the unit cell at position τ_κ, N is the number of unit cell in the crystal, $\epsilon(Q_{j\kappa})$ is the polarization

vector for the phonon Q_j of the atom κ.
From the expression of $E(Q_j,|k,n>)$, it was found that all wave vectors of phonons (acoustic as well as optical phonons) make a contribution to the temperature shift of the band gap.

In this model, phonon energies were neglected since they are very small compared with the energy of the electronic states. In Equation (56) there is a $\delta(\epsilon_{kn}-\epsilon_{k+Q,n})$ function in the term $\Gamma(Q_j,|k,n>)$. This δ function means that only Q=0 phonons can make contributions to the broadening, due to the conservation of the energy. The maximum value of the phonon momenta Q_{max} is π/a_1 with a_1 of the order of a few angstroms. Since the wavelength of a typical photon is of the order of 10^4 Å and $k=2\pi/10^4$, the photon momentum $k<<Q_{max}$. It is obvious that in the process of interband transition induced by an absorption of photons, only small values (near Q=0) of phonon momenta are gained by electrons. From the phonon dispersion curves, at near Q=0, the density of the optical phonon modes are at a maximum, while the density states of the acoustic phonon are very small. Therefore, mainly the optical phonons

contribute to the broadening of the energy gap.

With this theoretical treatment, if a group of phonons of frequencies close to $k_B\theta_B/\hbar$ [or $k_B\theta/\hbar$] yields the dominant contribution to $\Delta E_{kn}(T)$,[or $\Gamma_{kn}(T)$], respectively, then we have:

$$\Delta E_{kn}(T)=a_B'[1+2/(e^{\theta_B'/T}-1)] \qquad (59)$$

and

$$\Gamma_{kn}(T)=\Gamma_1'/[1+2/(e^{\theta/T}-1)] \qquad (60)$$

where $a_B'=1/2\Sigma\ E(Q_j,|k,n>)$

and $\Gamma_1'= 1/2\ \Sigma\ \Gamma(Q_j,|k,n>)$

To obtain the total shift and broadening at the critical point, the shift and broadening of the valence and conduction band states are added up, respectively. Therefore, we have the expressions for temperature dependence of energy gaps and broadening as followings, which are used to fit the experimental data:

$$E(T)-\Delta E_{th}=E_B(0)'-a_B'[1+2/(e^{\theta_B'/T}-1)] \qquad (61)$$

where ΔE_{th} represent the energy shift due to thermal expansion, which can be calculated by combining deformation potential (a) and thermal expansion coefficients α_{th}. $E_B'(0)-a_B$ corresponds to the energy gap at T=0, a_B represents the average value of the strength of electron-phonon coupling and θ_B corresponds to average phonon frequency. The temperature dependence of broadening can be written as:

$$\Gamma(T)=\Gamma_o+\Gamma_1/(e^{\theta/T}-1) \qquad (62)$$

where Γ_o corresponds to other broadening mechanisms due to the intrinsic lifetime, electron-electron interaction, impurities, dislocations and alloy scattering.

3.2 Temperature dependence of Semiconductors

In the past few years our group has been engaged in the systematic investigation of the

temperature dependence of the direct gaps of III-V semiconductors such as, GaAs, $Ga_{0.82}Al_{0.18}AS$ [56], InP [27] and $In_xGa_{1-x}As$ (x=0.06 and 0.15) [28,29] in a wide temperature range, up to 600°C. For these semiconductors E_o can be evaluated to ± 5 meV at these elevated temperatures. Thus the temperature of GaAs and InP substrate material could be determined to ±10°C. The aluminum composition of GaAlAs and In content of InGaAs could be monitored during actual growth procedures. We also performed PR measurements in an actual MOCVD reactor, through a diffuser plate, including rotating substrate (500 rev/min) and flowing gases. In addition, real time measurements were made, to demonstrate PR as a control/ monitoring method.

3.2.1 GaAs and $Ga_{0.82}Al_{0.18}As$

For both GaAs and $Ga_{0.82}Al_{0.18}As$, we have measured the temperature behavior of the energy gap up to 600°C. The temperature dependence of energy gap E_o has been analyzed in terms of the Varshni expression.

The <100> GaAs samples used in this experiment are undoped, semi-insulating (SI) material grown by the liquid-encapsulated Czochraski method. The $Ga_{0.82}Al_{0.18}As$ sample was fabricated in a Varian Gen II MBE system at the United Technology Center. It was grown on a GaAs buffer layer (not intentionally doped) of 0.8 μm thickness on a SI <100> GaAs substrate. The $Ga_{0.82}Al_{0.18}As$ epilayer was 1 μm thick. The Al composition was determined using the relation $E_o(Ga_{1-x}Al_xas)=E_o(GaAs)+1.45x$ for $x<0.4$ [57].

Shown by the dotted lines in Fig. 6 are the PR spectra for E_o(GaAs) at T=25°C, 250°C, and 610°C. The dotted lines in Fig. 7 are the experimental data for the $Ga_{0.82}Al_{0.18}As$ sample in the vicinity of $E_o(Ga_{0.82}Al_{0.18}As)$ at 25°C, 324°C, and 620°C. The highest temperature spectra for GaAs and $Ga_{0.82}Al_{0.18}As$ required scans of 20 and 15 min, respectively. Lineshape of all the spectra were independent of pump beam intensity, i. e., we have low-field modulation regime. The solid lines in Figs. 6 and 7 are least-squares fit to the third-derivative of a Lorentzian function form(TDFF) [11] since E_o of GaAs and GaAlAs are three dimensional interband

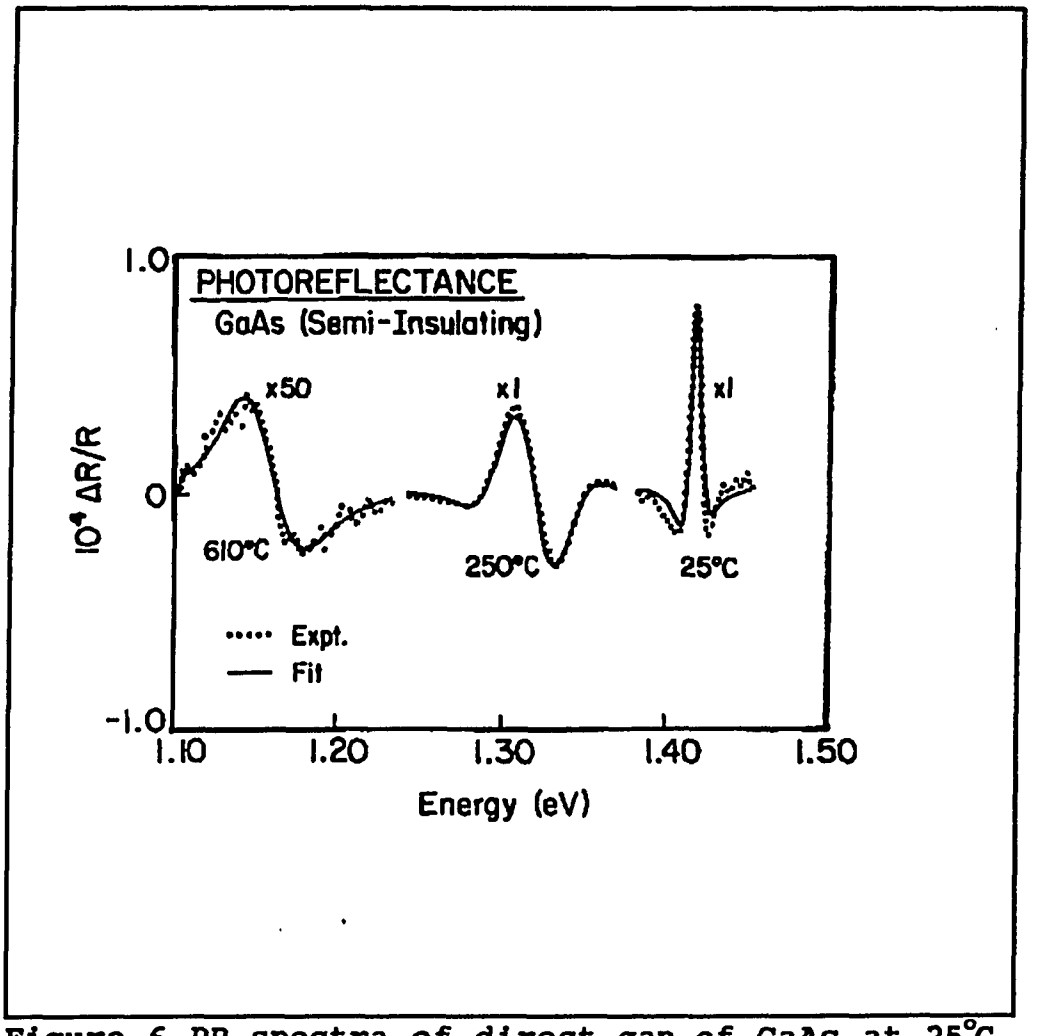

Figure 6 PR spectra of direct gap of GaAs at 25°C, 250°C, and 610°C. Solid line is a leaset squares fit to TDFF.

transitions. Even at 600°C it was possible to evaluate the energy of E_o to ± 5meV. For GaAs, the fit to the experimental data is quite good for all three temperatures while for $E_o(Ga_{0.82}Al_{0.18}As)$ at 25°C there is an oscillation on the high energy side which is probably due to a built-in dc field [54] or

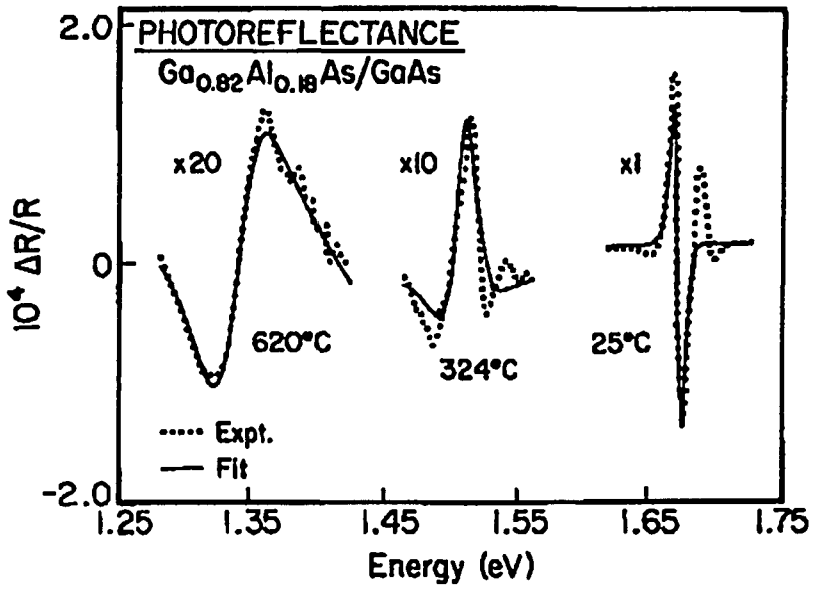

Figure 7 PR Spectra of the direct gap of $Ga_{0.82}Al_{0.18}As$ at 25°C, 324°C, and 620°C. The solid line is a least squares fit to TDFF.

to interference effects from the $Ga_{0.82}Al_{0.18}As$/GaAs interface. Further work is needed to understand the lineshape of $E_o(Ga_{0.82}Al_{0.18}As)$.

Table I. Values of the parameters which describe the temperature dependence of the energies of the E_o and $E_o+\Delta_o$ optical features of various materials.

Material	Spectral Feature	E(0) (eV)	α 10^{-4}eV/K	β (K)	E_B (eV)	a_B (meV)	Θ_B (K)
GaAs	E_o	1.512±0.005	5.1±0.5	190±82	1.571±0.023[a]	57±29[a]	240±102[a]
InP	E_o	1.432±0.007	4.1±0.3	136±60	1.474±0.010	51±2	259±10
InP	$E_o+\Delta_o$	1.544±0.010	4.3±0.6	120±80	1.584±0.016	49±4	248±20
$In_{0.06}Ga_{0.94}As$	E_o	1.420±0.005	4.8±0.4	200±50	1.466±0.014	44±9	203±45
$In_{0.15}Ga_{0.85}As$	E_o	1.285±0.005	5.0±0.4	231±40	1.339±0.015	53±10	238±50
$Al_{0.18}Ga_{0.82}As$	E_o	1.771±0.007	6.3±0.5	236±73			

a) Parameters E_B, a_B, and Θ_B are from Ref. 8.

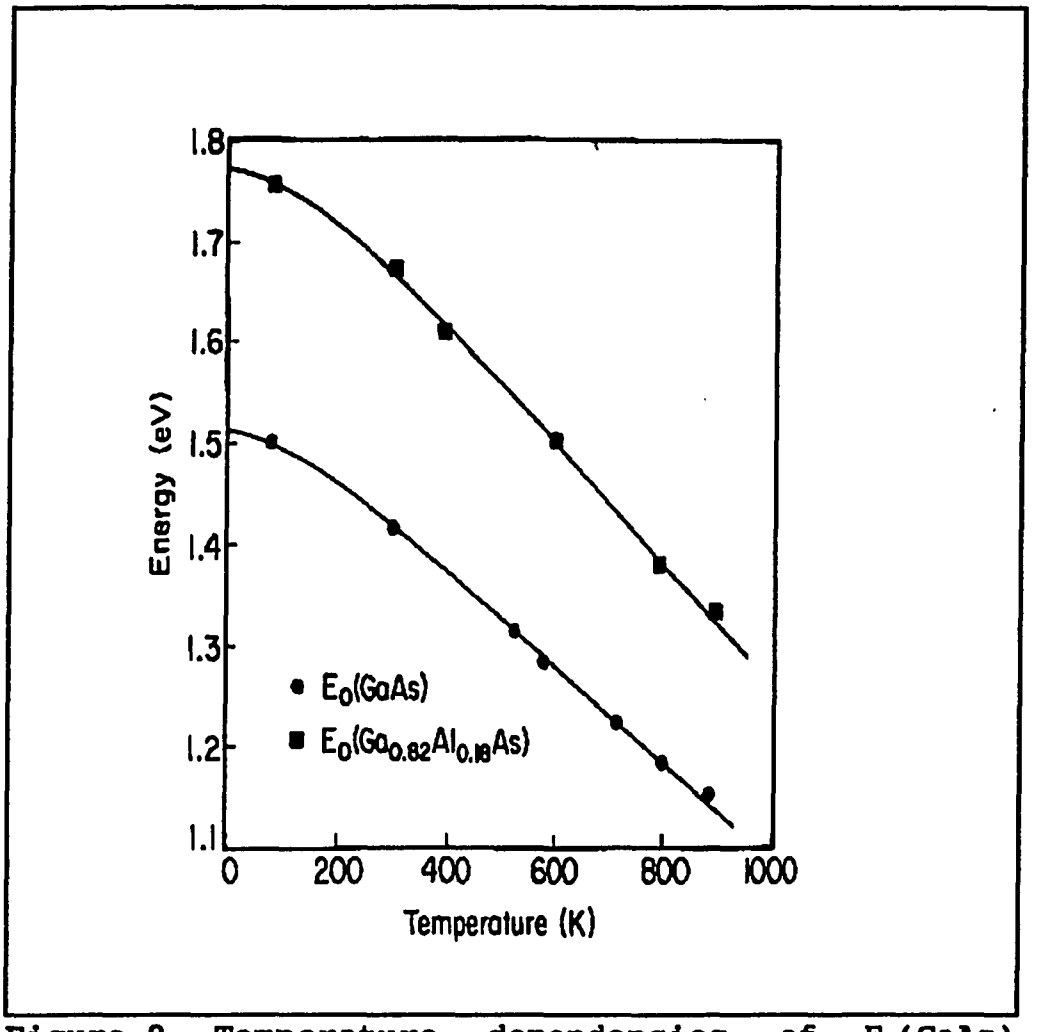

Figure 8 Temperature dependencies of E_o(GaAs) (circles) and $E_o(Ga_{0.82}Al_{0.18}As)$ (squares). Solid line is a least squares fit to Varshni expression.

In Fig. 8, we show the experimental values of E_o for GaAs (circles) and $Ga_{0.82}Al_{0.18}As$(squares) as a function of temperature including 77 K measurement. The solid lines are a least-square fit to Varshni's semi-empirical relation [58]:

$$E(T) = E(0) - \alpha T^2/(\beta+T) \qquad (63)$$

There E(0) is the value of the energy gap at T=0 and α and β are called Varshni coefficients [58]. This equation was commonly used to analyze temperature dependence of semiconductors [8,9,56,59]. The constant β was interpreted as being related to the Debye temperature, with $\beta \approx \theta_D$. The obtained values of $E_o(0)$, α and β for the two materials are listed in Table I. For $Ga_{0.82}Al_{0.18}As$ these are first values of Varshni coefficients.

3.2.2 InP.

For this sample, the temperature dependence of the band gap (E_o) has been analyzed in terms of the expressions given by the Varshni Eq.(63) and Bose-Einstein Eq.(64); the temperature behavior of the broadening parameter of E_o has been analyzed.

This <100> InP sample was also an undoped, Semi-insulating material fabricated by the liquid-encapsulated Czochralski method. The surface of the sample was polished using a procedure given

descriped in Ref [60]. The 6328 Å line of a 3 mW He-Ne laser chopped at 900Hz was used for the PR measurement up to 200°C. Above this temperature, 500 mW of the 5145 Å line of an Ar-ion laser was employed.

In Fig. 9, the dotted lines are the experimental PR spectra at 25°C, 305°C and 600°C in the region of the E_o and $E_o+\Delta_o$ optical features. Similar to cases of GaAs and GaAlAs, it was found that lineshapes also were independent of the pump beam intensity, i. e., we have low field electromodulation regime. By performing lineshape analysis, it is evident that the electron-hole interaction, or excitonic effect participated in band to band transition below 300°C, including 77K, since the lineshapes were best represented by the FDGF fit in this temperature range. Lautenschlaager et al [9] also found that the E_o and $E_o+\Delta_o$ optical features measured by ellipsometry were best represented by excitonic lineshapes up to 80K. Since the peaks were too weak and broad at above 80K, it is difficult to perform a lineshape analysis

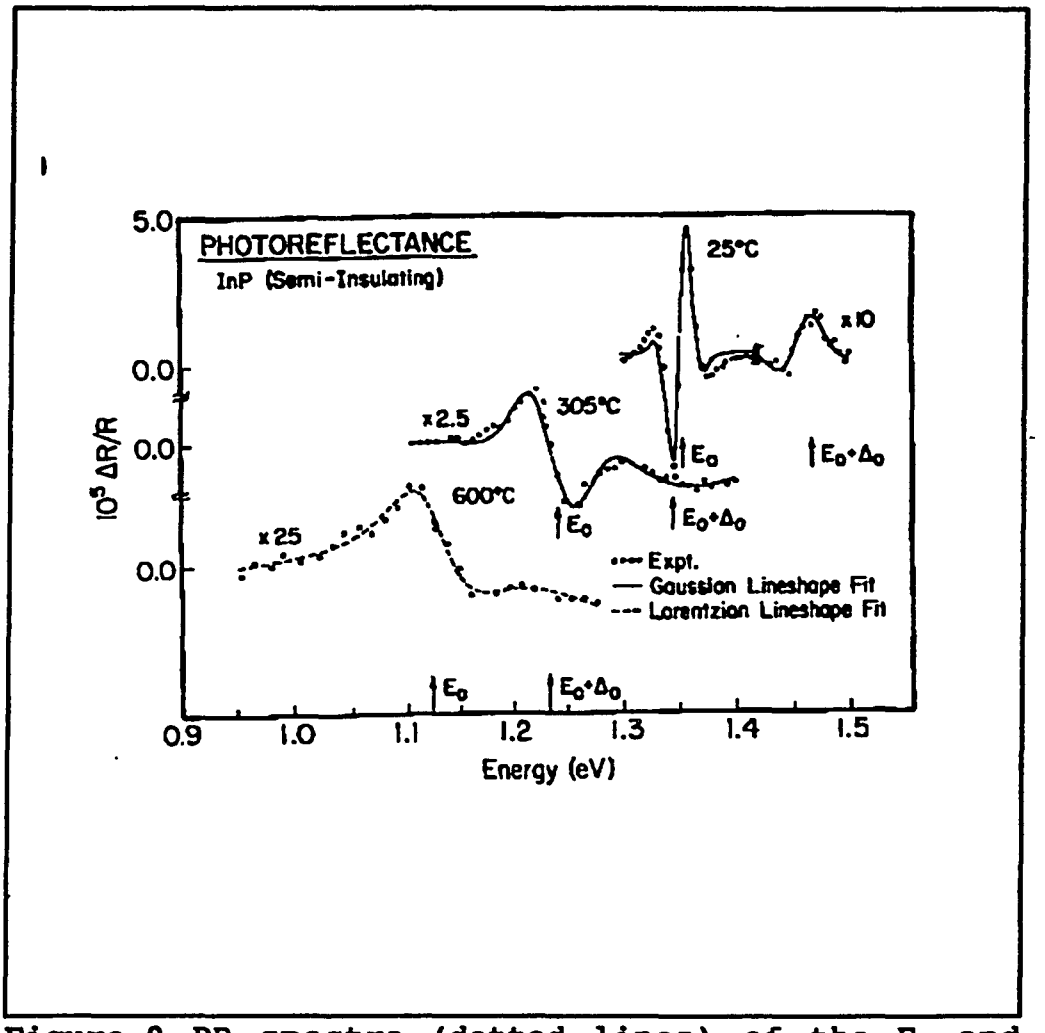

Figure 9 PR spectra (dotted lines) of the E_o and $E_o+\Delta_o$ optical features of InP at T=25°C, 305°C and 600°C.

Plotted in Fig. 10., are the temperature dependence of E_o (closed circles) and $E_o+\Delta_o$ (open circles). The solid lines are least-squares fit to the Varshni Eq. (63). The obtained parameters of $E_o(0)$, α and ß for E_o and $E_o+\Delta_o$ are listed in Table I. The data also has been fit to the Lautenschlager

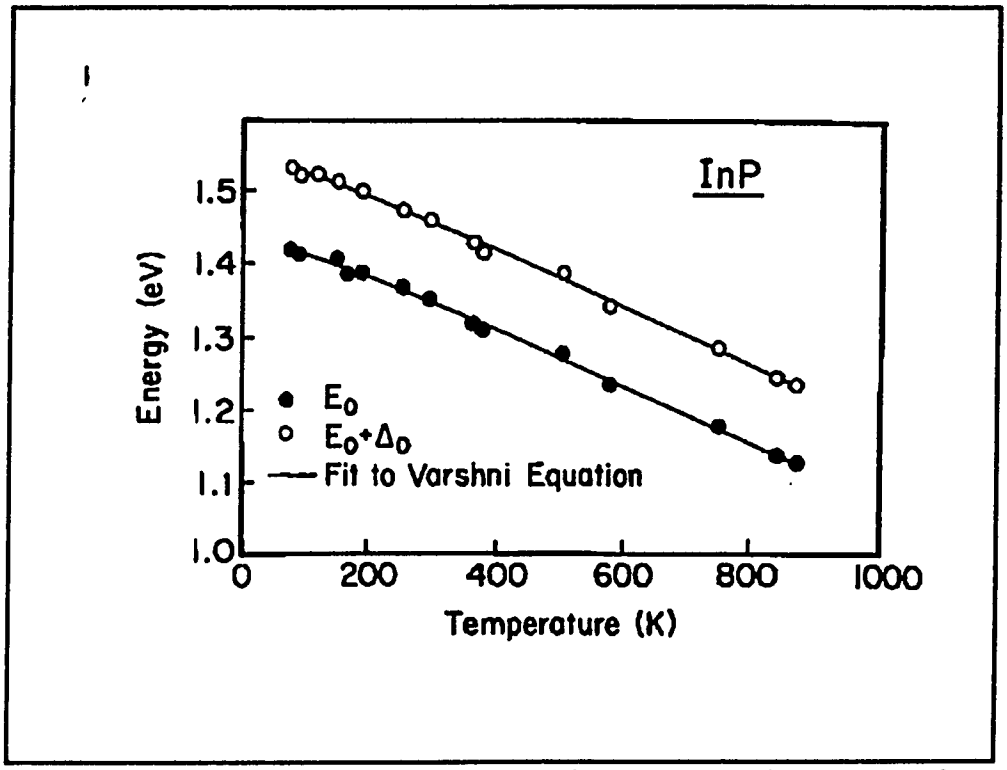

Figure 10 Temperature dependence of the energies of E_o (closed circles) and $E_o+\Delta_o$ (open circles). The solid line is a least-square fit to the Varshni expression.

equation [8]:

$$E(T)= E(0)-a_B(1+2/(e^{\theta_B/T}-1) \qquad (64)$$

where E_B, a_B and θ_B are parameters to be determined from experiments. Note that this expression is

Table II. Parameters involved in the temperature dependence of the broadening parameter of E_o of InP fitting to equation $\Gamma(T)=\Gamma_o+\Gamma_1/(e^{\theta/T}-1)$.

Material	Spectral Feature	Γ_o (meV)	Γ_1 (meV)	θ (K)	θ_{I_o} (K)
InP	$\Gamma(E_o)$	5±0.5	42±6	480±120	491

different from Eq.(61), the parameters a_B and Θ_B include the thermal expansion contributions. The numbers for E_B, a_B, and Θ_B were listed in Table I. Our values of E(0), α and ß are in reasonable agreement with those of Varshni [58], even though the latter were obtained from measurements only up to 300K. The numbers of E_B, a_B, and Θ_B for E_o are considerably different than those of Ref. 9. However, for $Eo+\Delta_o$ the values are in reasonable agreement. As shown in Fig. 10 and Table I, E_o and $E_o+\Delta_o$ have the same temperature dependence. Because of its atomic origin the spin-orbit splitting should be independent of temperature.

The temperature dependence of broadening parameter $\Gamma(E)$ is displayed in Fig. 11. Representative error bars are shown. The solid line is a least-squares fit to Eq.(62). The obtained values of Γ_o, Γ_1 and Θ corresponding to the broadening parameter of E_o (which have not reported previously) are listed in table II. We found that the temperature Θ obtained from the broadening equation (65) is the same as the optical phonon temperature. It is larger than the parameter Θ_B from

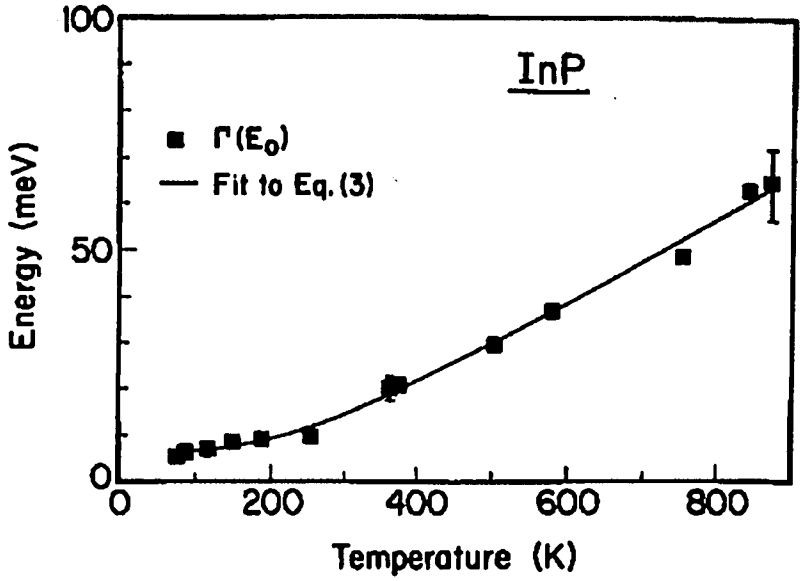

Figure 11 Temperature dependence of the broadening parameter of E_o. Representative error bar are shown. The solid line is a least squares fit to Eq.(65).

the energy dependence equation (64), since the energy shift due to the electron-phonon interaction the acoustical as well as the optical phonons

contribute while for the broadening parameter mainly optical phonons are responsible.

3.2.3 $In_xGa_{1-x}As$ (x=0.06 and 0.15) .

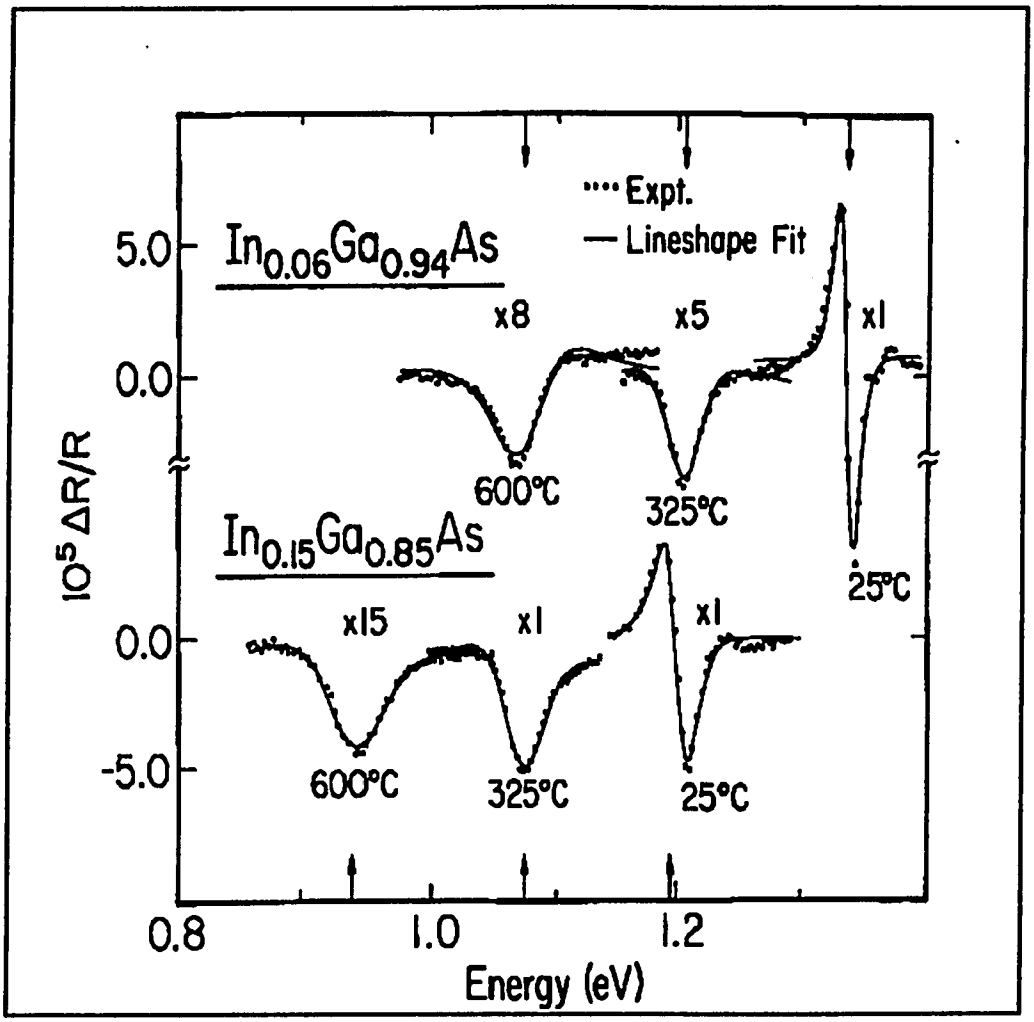

Figure 12. PR spectra of $E_0(In_{0.06}Ga_{0.94}As)$ and $E_0(In_{0.15}Ga_{0.85}As)$ at 25, 325 and 600°C. The solid lines are least squares fit to TDFF.

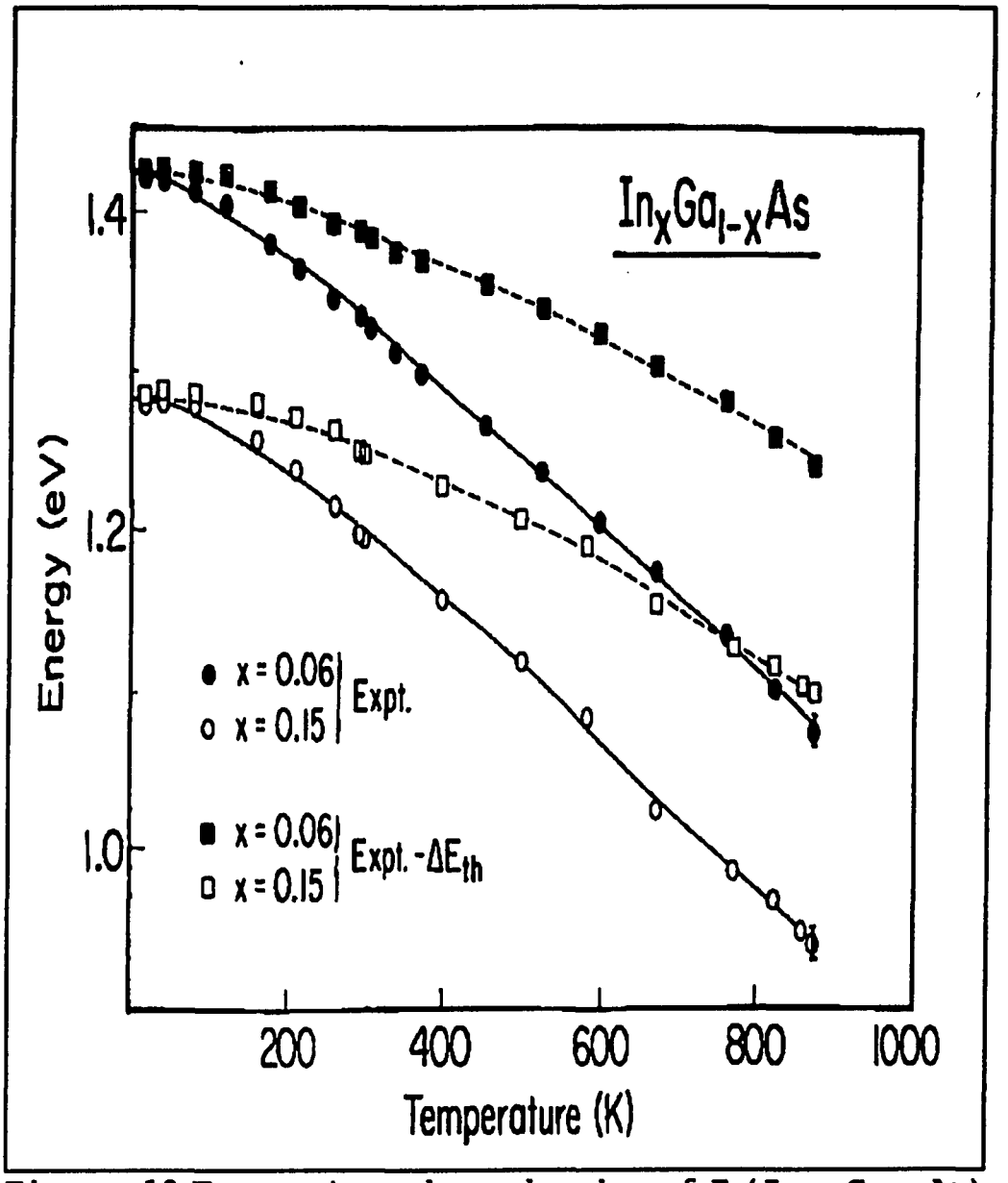

Figure 13 Temperature dependencies of $E_o(In_{0.06}Ga_{0.94}As)$ $E_o(In_{0.15}Ga_{0.85}As)$.

The semiconductor, $In_xGa_{1-x}As$, is an important material for both fundamental research and device applications. It is a model semiconductor for high

speed devices [61, 62] such as high electron mobility transistors and field-effect transistors, etc, because of its small electron effective mass and high electron mobility. It is also used to fabricate quantum confinement heterostructure lasers[62], in which the desired optical properties can be achieved by controlling the indium composition and the thickness of layers in the quantum wells.

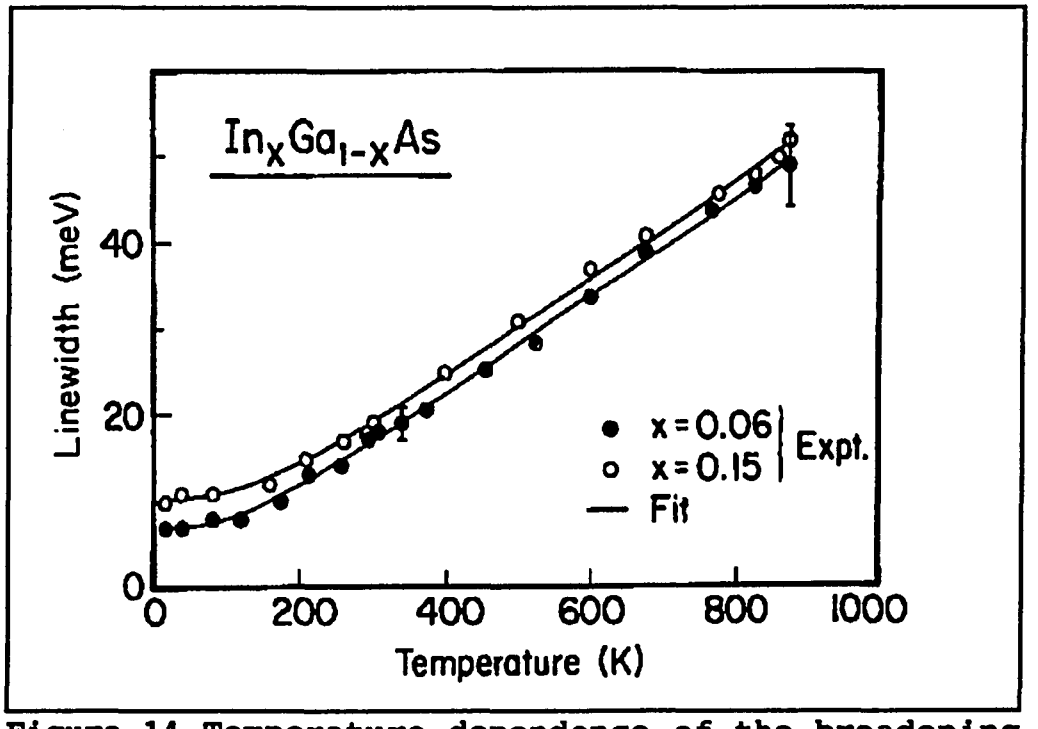

Figure 14 Temperature dependence of the broadening parameter of $In_xGa_{1-x}As$ (x=0.06 and 0.15)

In this section we report photoreflectance (PR)[16] measurements of the direct gap (E_o) of

undoped, strain-relieved $In_xGa_{1-x}As/GaAs$ (x=0.06 and 0.15) from 18 K to 600°C in the photon energy range from 0.9 to 1.5 eV. Photoreflectance is a contactless form of electromodulation[16]. We have analyzed the temperature dependence of E_o by both Varshni[58] and Bose-Einstein expressions [6,8,9,30,31,32]. Because of the relatively low indium composition of our samples these parameters are similar to those of GaAs [8]. By taking into account the component of the energy gap shift due to the thermal expansion coefficient we have obtained revised parameters which are directly related to the electron-phonon interaction [27]. The temperature variation of the broadening parameter $\Gamma(E_0)$ has been studied in terms of the Bose-Einstein expression. We find that while both acoustic and optical phonons participate in the energy shift only the electron-optical phonon interaction is responsible for the changes in linewidth.

The measurements were performed on two epitaxial layers of (100) $In_xGa_{1-x}As$ (undoped) of thickness 1.5 and 1.0 μm for x=0.06 and 0.15, respectively, grown on 0.5 μm of GaAs buffers

(undoped) on a GaAs (undoped) substrate. The growth procedure was molecular beam epitaxy. The indium compositions of 0.06 and 0.15 were determined from E_o at 300K using the relation [63] $E_o(In_xGa_{1-x}As)=E_o(GaAs)-1.53x+0.45x^2$. These values were close to those estimated from the growth conditions. For these thicknesses of the epitaxial layers the lattice-mismatched strain should be completely relaxed [64]. This relaxation was confirmed by X-ray measurements on both samples.

The PR apparatus [10] and heater arrangement [56,27] were similar to those already reported in the literature. The temperature was measured by a iron-constantan thermocouple in contacted with the sample surface. For measurements up to about 200°C the pump beam was the 6328 Å line of a 3 mW He-Ne laser chopped at 851 Hz. Above this temperature 300 mW of the 6471 Å line of a Kr-ion laser was employed.

Displayed by the dotted lines in the top and bottom of Fig. 12 are the PR spectra of the $In_{0.06}Ga_{0.94}As$ and $In_{0.15}Ga_{0.85}As$ samples, respectively, at 25°C, 325°C, and 600°C. The solid lines are

least-squares fits to the third derivative functional form (TDFF) [11] for a three-dimensional critical point. The obtained values of E_o are designated by arrows in the figure. The fit also yielded the broadening parameter.

We have observed that at 25°C and below, the spectra exhibited Franz-Keldysh Oscillation (FKO) above the band gap. [11, 54] For example, one FKO can be detected in the 25°C spectra of both samples in Fig. 12. The small number of FKO indicates that we are close to the low-field regime and hence the TDFF is applicable [11, 54]. At lower temperatures more FKO become evident because of the decrease in the linewidth. In this regime, the energy gap and broadening parameter were obtained from the three point method [11]. The origin of these FKO will be the subject of a future article [65].

We also attempted to fit the 25°C spectra for both samples with a first-derivative Gaussian functional form (FDGF) [54]. The TDFF, which is appropriate for unbound band-to-band transitions [64], yielded a better fit than the FDGF, a lineshape which represents transitions associated

with bound states such as excitons.[17] The lack of an excitonic contribution is not unreasonable since for these samples the linewidth at 25°C and above (≥15 meV) is greater than the exciton binding energy.[66] It is interesting to note that for bulk InP, excitonic contributions in the PR spectra were observed up to about 300°C.[27]

Plotted in Fig. 13 are the temperature dependence of E_o for the x=0.06 (closed circles) and 0.15 (open circles) samples. Representative error bars are shown. The solid lines are least-squares fit to the Varshni semi-empirical relationship equation (63). The obtained values of E(0), α and ß for both samples are listed in Table I. For comparison, we have also listed in Table I the values of these quantities for GaAs obtained by previous investigators [8, 56]. The values α and ß for the $In_xGa_{1-x}AS$ samples are found to be similar to those of GaAs because of the low In concentration of the layers.

The data also has been fitted to the Bose-Einstein expression of equation (64). Our numbers for E_B, a_B and Θ_B are given in Table I; also

listed are the corresponding values for GaAs [8].

The temperature dependence of $\Gamma(E_o)$ for both $In_{0.06}Ga_{0.94}As$ (closed circles) and $In_{0.15}Ga_{0.85}As$ (open circles) samples are displayed in Fig. 14. Representative error bars are shown. The solid line is a least-squares fit to the equation (62): The values of Γ_o, Γ_1, and θ corresponding to the broadening parameter of E_o are listed in Table III. Also given in Table III are the corresponding numbers for GaAs.[8] The first term of the Eq.(62) corresponds to broadening mechanisms due to intrinsic lifetime, electron-electron interaction, impurity, dislocation and alloy scattering effects. The obtained value of Γ_o for the x=0.15 sample is larger than that for the x=0.06 material and both are significantly greater than expected from alloy scattering (~2 meV) [67]. These results are probably related to the relatively high concentration of misfit locations associated with the strain-relieved. For example, the linear density of dislocations for the former sample is about a factor two greater in relation to the latter material [68].

The second term of Eq.(62) corresponds to

lifetime broadening due to the electron-phonon interaction. The quantity Γ_1 represents the strength of the electron-optic phonon coupling while Θ is the optical phonon temperature.

Due to the low In composition of our samples Γ_1 and Θ for InGaAs should be similar to those of GaAs [8]. However, because of the larger error margins of the data from Ref. 8 comparison is hard to make although there are no inconsistencies. Our value for these parameters are more accurate since our maximum temperature was about a factor of three greater than that of Ref. 8 for the determination of the temperature variation of Γ.

The temperature shift of E_o contains contributions from both thermal expansion and electron-phonon coupling effects [8, 26]. Therefore, in order to obtain parameters directly related to the latter influence, it is necessary to eliminate the contribution of the former. For example, the quantities α and β of Eq. (63) and a_B and Θ_B of Eq.(64) include the influence of the lattice dilation. The energy shift ΔE_{th} due to the thermal expansion can be written as:

$$\Delta E_{th} = -3a(\alpha_{th}T) \qquad (65)$$

where a is the hydrostatic deformation potential, and α_{th} is the linear expansion coefficient. For our samples we have obtained the values of a and α_{th} listed in Table IV by a linear interpolation between the corresponding coefficients of GaAs and InAs [70]. For the latter quantity we have used the average thermal expansion coefficient of the end point materials since the temperature dependence of α_{th}(InAs) in not known. Equations (63) can be rewritten as:

$$E(T)-\Delta E_{th} = E(0) - \alpha' T^2/(\beta'+T) \qquad (66)$$

The solid (x=0.06) and open (x=0.15) squares in Fig. 13 represent data which results from subtracting ΔE_{th} [Eq.(65)] from the experimental values of E(T). The dashed lines are least-squares fits to Eq. (66). These data also have been fitted to Eq.(61). The obtained values of α', β', a_B' and θ_B' $E_B'(0)$ are listed in Table IV.

From Tables III and IV, it can be seen that the

values of θ_B' are less than θ. Since both electron-optical and electron-acoustic phonon interactions contribute to the energy shift of the band gap [8,9,6,32], this leads to a low average phonon frequency θ_B'. Since θ for both samples is quite similar to the LO phonon temperatures (θ_{LO1} and θ_{LO2}) the temperature variation of Γ is due mainly to the interaction of the electron with optical phonons. These observation are in agreement with existing theory [31, 32].

The electron-phonon interaction also can be studied by Raman Scattering (RS) [71, 72, 73]. It has been known for many years that energetic electrons relax predominantly via electron-phonon interactions [71, 72]. By evaluating the relaxation time, we also can obtain the strength of electron-phonon coupling. Since RS has the advantage of being an instantaneous process and being able to probe both electron and phonon in the same experiment [71], it is also one of the powerful tools to probe the electron-phonon scattering times. By studying relaxation of the energetic electrons by RS, Kim and

Yu [71] have evaluated the time to emit one LO phonon for high doped (10^{18}) bulk GaAs by using the assumption that the dominant cooling mechanism of energetic electrons is responsible for the emission of LO phonons via the Frohlich interaction. The time they found to emit one LO phonon is about 200 fs. They predicted that the time will be short for low carrier concentration materials. From our values of Γ_1, the time for one LO phonon process is about 30 ±10 fs (from the uncertainty relation $\Delta t \cdot \Gamma_1 \approx \hbar$). Since our samples are undoped, the comparison between our experiments and those of Kim and Yu can not be made at this moment. But our values of the time of electron-phonon interaction are close to the values obtained by Tang, et al. [74]. They reported that the relaxation time for intrinsic GaAs was about 40 fs by using the equal-pulse correlation technique.

Woolley have suggested that after the thermal expansion term is removed the parameter ß' of Eq.(66) is directly proportional to the Debye temperature Θ_D by the relation $ß' = (3/8)\Theta_D$. Also

Table III. Parameters involved in the temperature dependence of the broadening parameter of E_o of $In_xGa_{1-x}As$ (x=0.06 and 0.15) using the fit $\Gamma(T) = \Gamma_0 + +\Gamma_1/(e^{\Theta/T}-1)$.

Materials	Γ_o (meV)	Γ_1 (meV)	Θ (K)	Θ_{LO1} (K)	Θ_{LO2} (K)
6%	7.5±0.5	23±6	380±122	410[a]	376[a]
15%	10.5±0.5	23±6	390±120	406[a]	375[a]

(a) Longitudinal optic phonon temperature for the "GaAs-like"(Θ_{LO1}) and "InAs like" (Θ_{LO2}) modes of $In_xGa_{1-x}As$ obtained from Raman measurements.

Table IV. Values of parameters which describe the temperature dependence of the direct energy gaps of $In_xGa_{1-x}As$ taking into account the effect of thermal expansion.

Materials	α_{th} (10^{-6}/K)	a (eV)	α' (10^{-4}eV/K)	β' (K)	$(3/8)\Theta_D$ (K)	a_B' (meV)	Θ_B' (K)	E_B' (eV)
6%	6.69[a]	-9.54[a]	2.5±0.4	140±40	127[a]	33±7	280±45	1.453±0.012
15%	6.48[a]	-9.24[a]	2.6±0.4	150±40	124[a]	39±8	300±50	1.323±0.013

(a) The parameters α_{th}, a, and Θ_D were estimated by using linear interpolation between the values of GaAs and InAs as listed in Ref. 70.

listed in Table IV are Θ_D for the two In compositions estimated by linear interpolation between the end point binary materials [70]. As can be seen there is good agreement between ß' and $(3/8)\Theta_D$.

The parameter α' of Eq. (66) can be related to a_B' and Θ_B' of Eq. (61) by taking the high temperature limit of both expressions. This yields $\alpha'=2a_B/\Theta_B$. Table III shows that this relation is indeed satisfied.

It can be seen from Fig. 13 that it is important to take into account the effect of the lattice-dilation when evaluating the electron-phonon parameter related to the energy gap red shift. At 600°C the thermal expansion term corresponds to about 45% of the total variation for both samples.

In conclusion we have measured the temperature dependence of the direct band gap and its broadening parameter for $In_xGa_{1-x}As$ (x=0.06 and 0.15) in the temperature range 18K to 600°C. We have analyzed $E_o(T)$ in terms of both Varshni and Bose-Einstein expressions while the temperature variation of Γ has

been fitted to a Bose-Einstein equation.

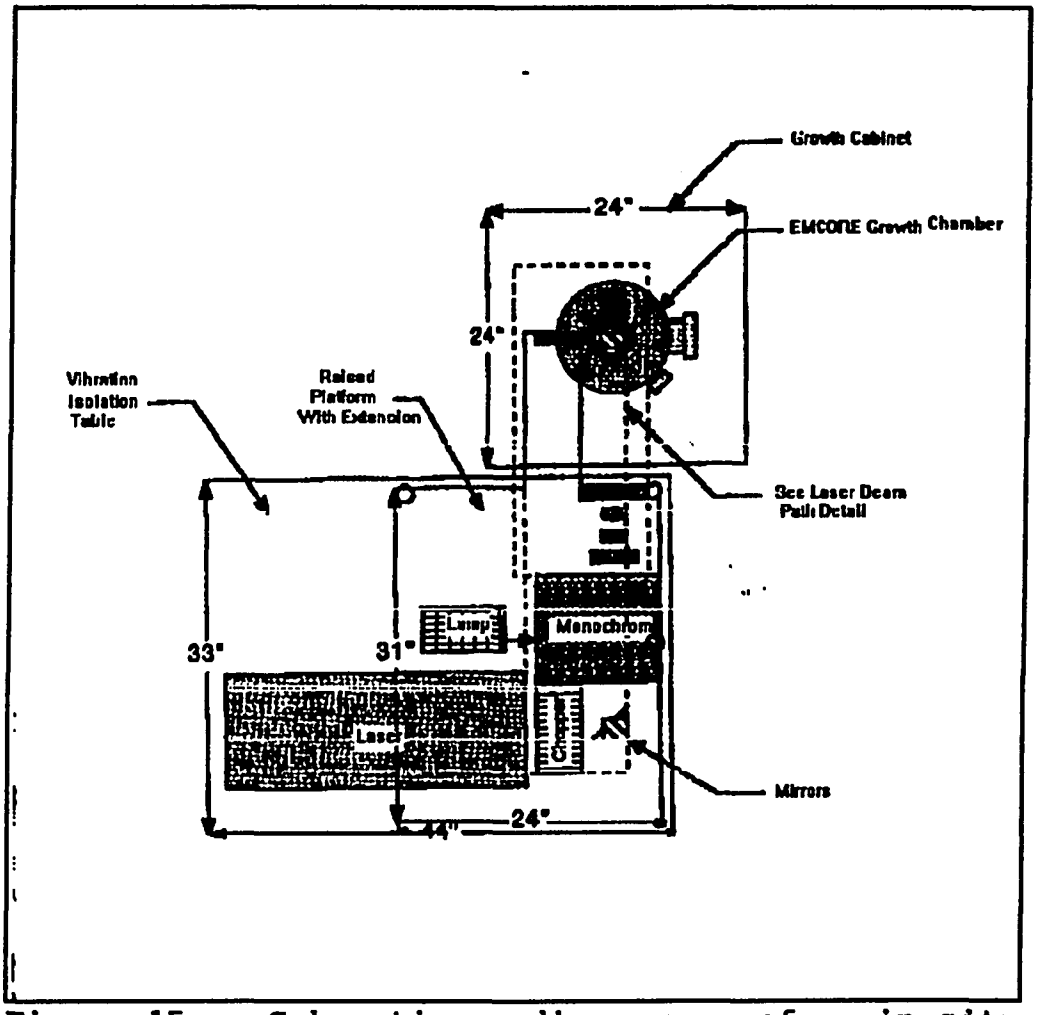

Figure 15 Schematic diagram of in-situ photoreflectance setup at EMCORE Co.

3.3 Application

3.3.1 In-Situ OMVPE Process Sensing of GaAs and AlGaAs [36]

Showin in Fig. 15 is an in-situ PR apparatus at OMVPE system at EMCORE Co, the light from a Xenon arc lamp (150W) was passed through a monochromator and focused on the sample by means of two lenses and a mirror. Optical access into the modified EMCORE Gs3200 vertical, cold-walled stainless-steel growth chamber was via a pyrex viewport and a perforated quartz gas diffuser in the reactor top plate. The surface field of the probe area was modulated by illuminating it with all lines of an air-cooled Argon-ion laser, and chopped at a frequency of 800 Hz by a optical chopper. The laser power was 650 mW at 650°C. The time required to obtain a complete in-situ PR spectra was 15 min, since the complete scan was repeated three to five times in order to reduce spurious features due to noise.

The reactor temperature is regulated by a PID controller, which receives feedback from a thermocouple located at a fixed point 1 mm below the rapidly rotating susceptor(500 rev/min). At 25°C reactor temperature is equal to the temperature of the susceptor. When the temperature is increased, the reactor temperature measured by the thermocouple

diverges negatively from the actual sample temperature. At a thermocouple temperature of 600°C, the susceptor temperature was 650°C by a Minolta optical pyrometer. The PR measurements were taken at 70 Torr with a palladium-diffused hydrogen flow of 18 slm. When the reactor temperatures were above 400°C, an arsine flow was on to prevent the degradation of the semiconductor surface.

The samples used in this study were undoped, (100) GaAs grown by the Liquid-encapsulated Czochralski method, and a multilayer MOCVD-grown GaAlAs/GaAs/GaAlAs heterostructure, in which the top layer was an AlGaAs deposition 1.4μm thick. For both samples, the measurements were made up to 690°C. The PR spectra for GaAs sample are shown in Fig. 16, for reactor temperatures between 25°C and 600°C. Each dot represents an average of over one hundred data points. The solid lines are least-squares fits to the FDGF, which modeled the data better for spectra taken at a reactor temperature below 350°C. Above this temperature, data are fit to the TDFF, as denoted by dashed lines in the figure. The values T_s are obtained from PR spectra of E_o(GaAs) at elevated

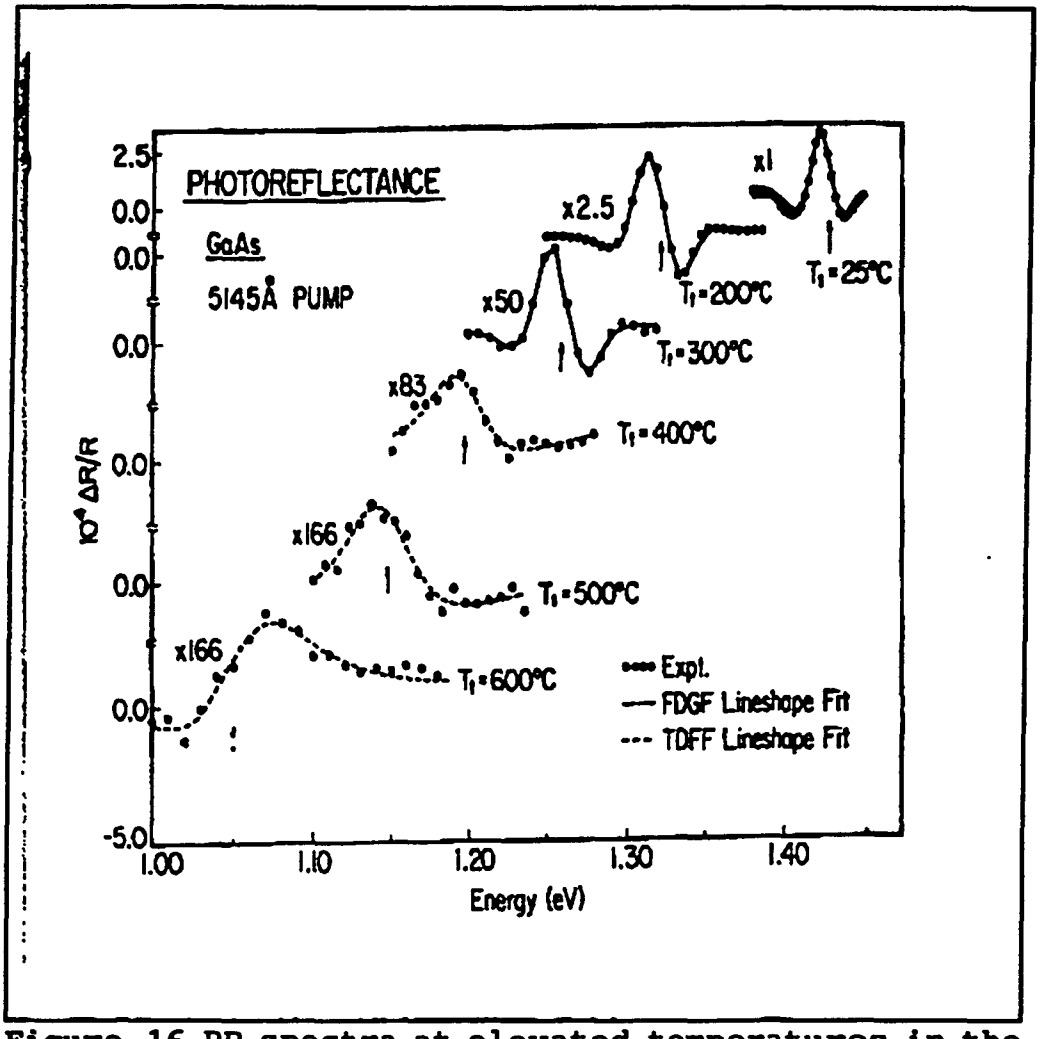

Figure 16 PR spectra at elevated temperatures in the in-situ experiments.

temperatures. T_t is the thermocouple temperature. The solid line is a least squares fit to FDGF while dashed line fit to TDFF. The obtained energies of $E_o(T)$ are indicated by arrows. There is a systematic difference between the thermocouple reading T_t and

Table V. Variation of E_o, the direct band gap of GaAs, with temperature in an MOCVD reactor. T_t is the thermocouple temperature while T_s is the temperature deduced from E_o and the data of the Section 2.2.1.

E_o (eV)	T_t (°C)	T_s (°C)
1.428±0.003	25	25
1.321±0.003	200	245±5
1.260±0.004	300	365±5
1.197±0.004	400	496±7
1.147±0.004	500	595±8
1.050±0.005	600	690±10

Table VI. Temperature Dependent of E_{o1}(GaAlAs) and E_{o2}(GaAlAs). T_t is the thermcouple temperature while T_s is the temperature deduced from E_o(GaAs) and the data of the Section 2.2.1.

E_{o1}(GaAlAs) (eV)	E_{o2}(GaAlAs) (eV)	T_t °C	T_s °C
1.652±0.002	1.690±0.002	25	25
1.546±0.003	1.579±0.003	200	245±5
1.505±0.005	1.505±0.005	300	365±5
1.470±0.006	1.431±0.004	400	495±7
1.425±0.008	1.373±0.005	500	595±8
1.384±0.040	1.329±0.006	600	690±10

actual substrate surface temperature, T_s for the GaAs sample. At the highest temperature T_t=600°C and E_o(GaAs)=1.049 Ev. This value of E_o corresponds to a surface temperature T_s=690°C from section 3.2.1 and Fig. 8. Listed in Table V are the values of E_o, T_t and T_s, the latter deduced from the value of E_o and the data of Section 3.2.1 and Fig. 8.

In the Fig. 17, the dotted line is the experimental data in the region of $E_o(Ga_{1-x}As_xAs)$ from the GaAlAs/GaAs/GaAlAs heterostructure sample. At 25°C there are two peaks corresponding to slightly different values of the Aluminum the barriers on either side of the GaAs region. The solid line is a least-square fit to the FDGF at 25°C, while above 25°C the solid lines are least-squares fit to the TDFF. The obtained values of E_{o1}(GaAlAs) and E_{02}(GaAlAs) together with T_t and T_s are listed in Table VI. From 25°C spectrum, we deduced that the x=0.16 for E_{o1} , and 0.19 for E_{02}. We also found that at T_t=200°C, the separation between two peaks has decreased, and that at T_t=300$_o$C only one peak is observed. Above the T_t=400°C the orders of the two peaks are reversed.

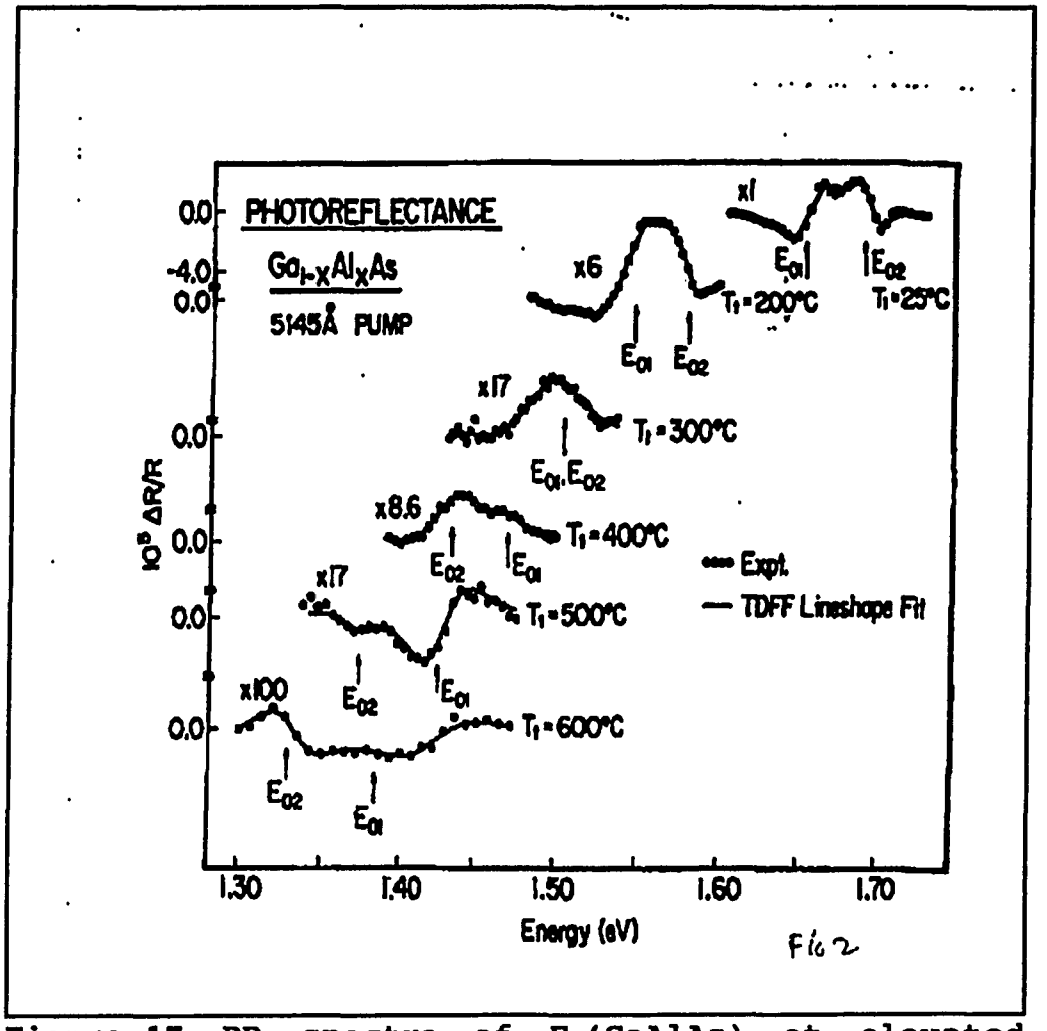

Figure 17 PR spectra of E_o(GaAlAs) at elevated temperatures in the in-situ experiments.

Plotted in Fig. 18 are the values of E_{o1}(GaAlAs), denoted by open circles, and E_{o2}(GaAlAs) indicated by the closed circles as functions of T_s. The temperature dependence of $E_o(Ga_{0.82}Al_{0.18}As)$ from Section 3.2.1 is displayed for comparison. It is evident that the E_{o2}(GaAlAs) follows quite well the

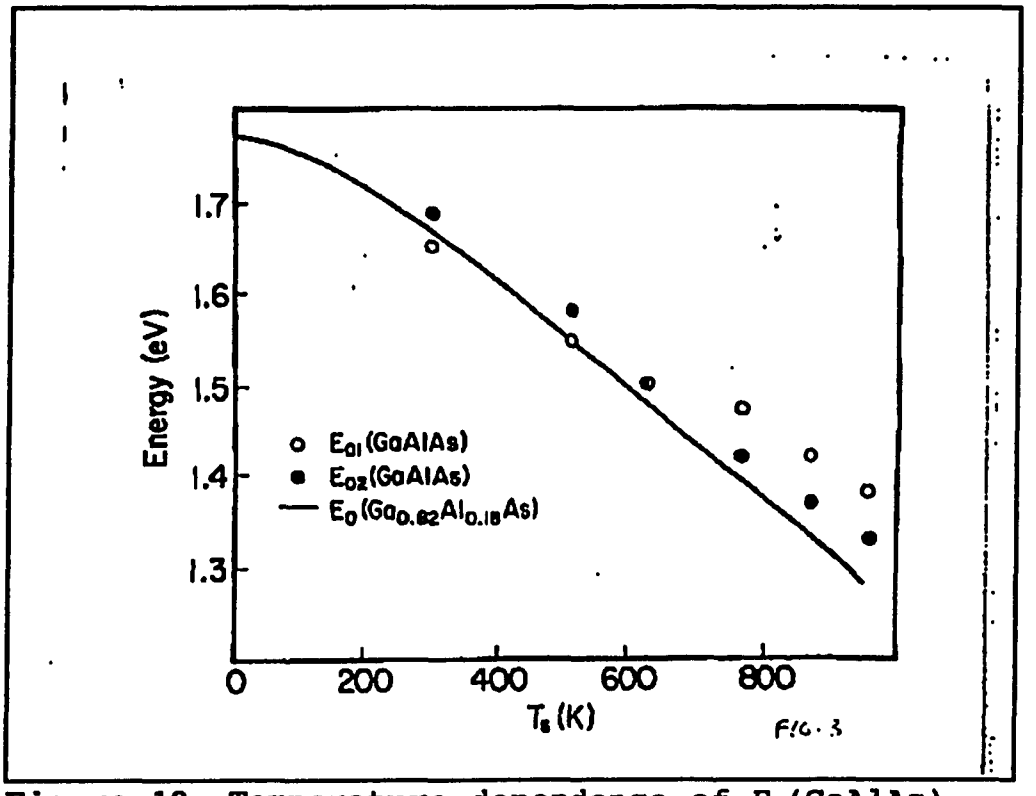

Figure 18. Temperature dependence of E_o(GaAlAs).

behavior of $E_0(Ga_{0.82}Al_{0.18}As)$. But E_{o1}(GaAlAs) displays an anomalous behavior which we do not understand at this time.

3.3.2 Real Time Measurements [28]

In order to be useful, a control/monitoring method must be capable of making measurements in real time. We have made a number of changes in hardware and software, in order to reduce data

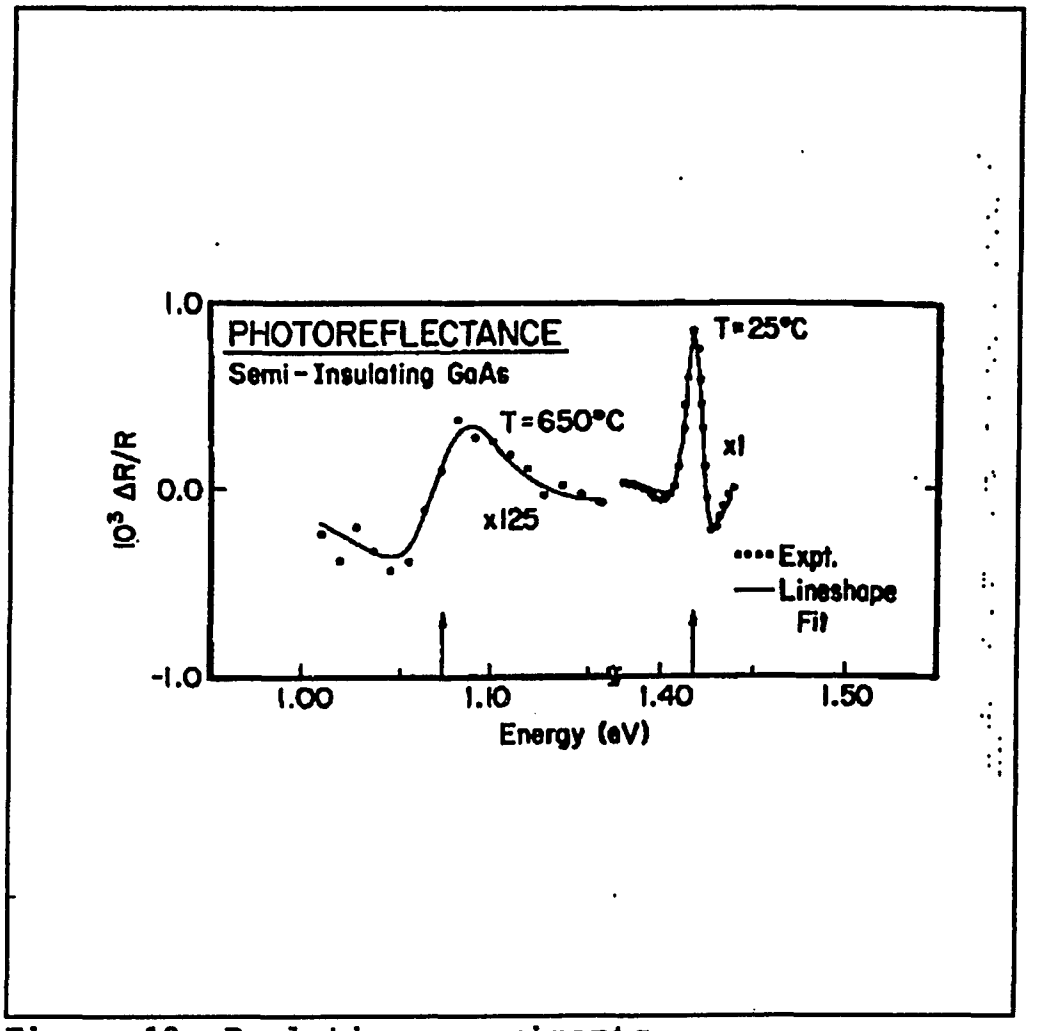

Figure 19. Real time experiments

acquisition time. Displayed in Fig. 19 by the dotted lines is the PR spectrum of E_o of GaAs at 25°C and 650°C. The data at 650°C was taken in 30 seconds. It was found that only around 15 points are necessary to fit the lineshape (there are 17 points in the Figure). Each point took about 2 seconds. The lineshape fit (solid line) is quite good. The

energies of E_o are denoted by arrows. It is possible that the data acquisition time can be further reduced to one second per point for a total of 15 seconds to determine E_o and hence the temperature. Since only a portion of the curve around the zero crossing needs to be scanned in order to evaluate shifts in E_o, variation in temperature can be deduced in a short time.

Chapter IV

MODULATION SPECTROSCOPY OF MICROSTRUCTURES

4.1 Theoretical Background of Microstructures

The idea of the semiconductor superlattice was originated by Easki and Tsu (1970) [26, 27, 75, 76]. Two kinds of superlattices were envisioned: compositional and doping. Compositional superlattices and MQW consist of alternating layers of two different types of semiconductors. The thickness of the individual layers is between a few angstroms and a few hundred angstroms. The composition variation modulates the electronic potential on a length scale shorter than an electron mean free path. Doping superlattices consist of alternating n- and p-type layers of a single semiconductor. Electric fields that are generated by the charged dopants modulate the electronic potential. The first attempt to grow superlattice used the chemical vapor depostion technique in the $GaAs/GaAs_{1-x}P_x$ material systems. The relatively large lattice constant mismatture caused difficulties in these early growth experiments. Subsequently, the

GaAs/$Ga_{1-x}Al_xAs$ materials system was considered. The lattice constant mismatch (0.08% between GaAs and $Ga_{1-x}Al_xAs$) is very small in this system. Observations of negative differential resistance were the first evidence of quantum confinement effects in a superlattice. Since then, the GaAs/$Ga_{1-x}Al_xAs$ system has been extensively studied by both electrical transport and optical techniques. It is by far the most thoroughly invesigated superlattice.

The band gap of GaAs is smaller than that of $Ga_{1-x}Al_xAs$. In a GaAs/$Ga_{1-x}Al_xAs$ heterojunction, the conduction band edge in GaAs lies at a lower energy than that of $Ga_{1-x}Al_xAs$. Thus the GaAs acta as a quantum well and the $Ga_{1-x}Al_xAs$ as a potential barrier both for electrons and for holes. Becaused of the very close match of lattice constants in this materials system, the constituent materials are not significantly strained. Therefore the heavy- and light-hole band edges of the constituent materials remain essentially degenerate.

In this thesis, we focus on compositional layer structures such as GaAlAs/GaAs [42,43], InGaAs/GaAs [44] and GaSb/AlSb [45] systems. For the

composition layer structures there are two kinds of systems: lattice matched, and lattice mismatched systems. The GaAlAs/GaAs is a typical lattice matched system, in which the difference of lattice constants between the GaAs and GaAlAs is only 0.08%. The lattice mismatched system, such as InGaAs/GaAs or GaSb/AlSb, creates coherent strains in the individual layers with essentially no misfit defect or dislocation generation. This freedom from the need for precise lattice matching widens the choice of compatible materials and greatly increases the ability to control the electronic and optical properties of such structures. The strain changes the band gaps of constituent materials and splits the degeneracy of the heavy and light hole bands [77, 78, 79]. In Fig. 20, we show a schematic diagram of the band-edge lineup for type-I for three lattice-constant conditions: both lattice constants of materials A and B are equal; the lattice constant of A greater than that of material B (The strain in A is compressive, the heavy-hole band is shifted relatively closer to the conduction band than the

light -hole band); and then the lattice constant of material A less than that of material B (The strain in A is tensile and the strain shifts the light-hole band closer to the conduction band than the heavy-hole band.

In order to understand the electronic properties of the composition layer SL, we treat the SL as simply a series of semiconductor layers, with each layer contributing

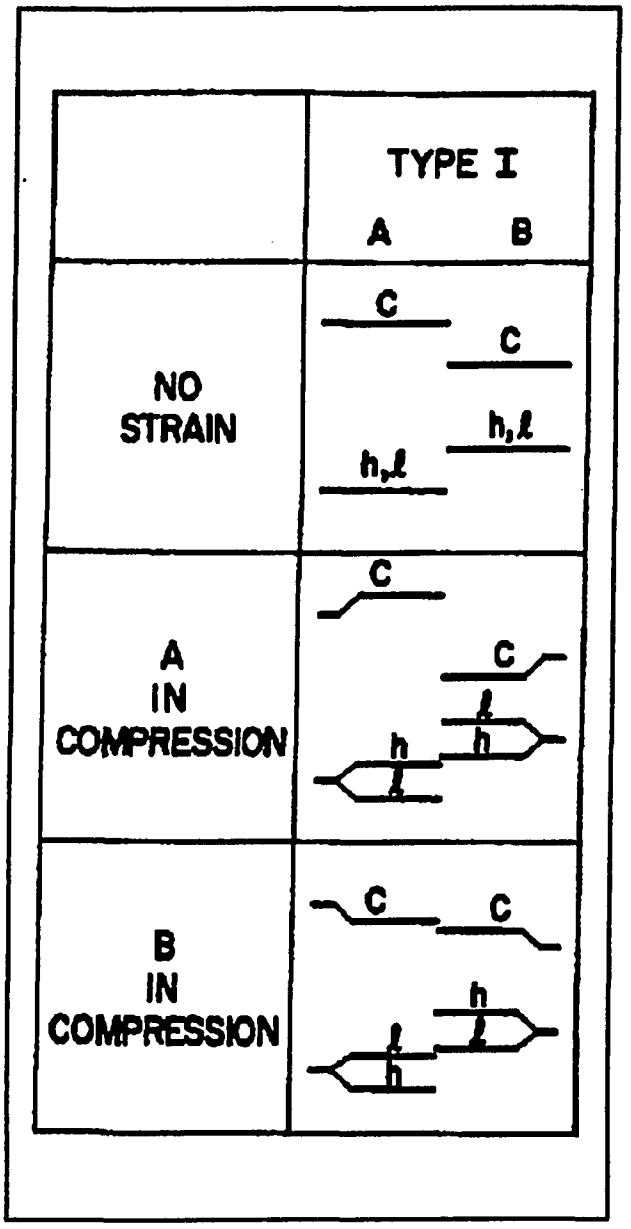

Figure 20 Schematic illustration of the band-edge lineup in type-I superlattice. Band lineups for three strain conditions are shown.

its characteristic properties. The periodic variation of the layers gives rise to periodic alternation in the electrical potential. Inside each potential well, only discrete energy levels or minibands are available for conduction (valence) band electrons (holes) (see Fig. 21).

Assume the two alternating components of the MQWs have energy band gaps E_g^I and E_g^{II}, with layer thickness d^I and d^{II} (for example I=GaAs and II=GaAlAs), respectively. The energy gap difference

$$\Delta V_o = E_g^{II} - E_g^I \tag{67}$$

is divided into ΔE_c and ΔE_v which both appears as a discontinuity in the conduction band edge $E_c(z)$ and valence band edge $E_v(z)$, respectively.
The energy level (miniband) can be calculated quite easily in the envelope function approximation, either using the modified boundary continuous conditions, or the Bastard model [80, 81, 82] for describing the electron and hole states of the two parent materials. The most important single property of a semiconductor heterojunction is the band

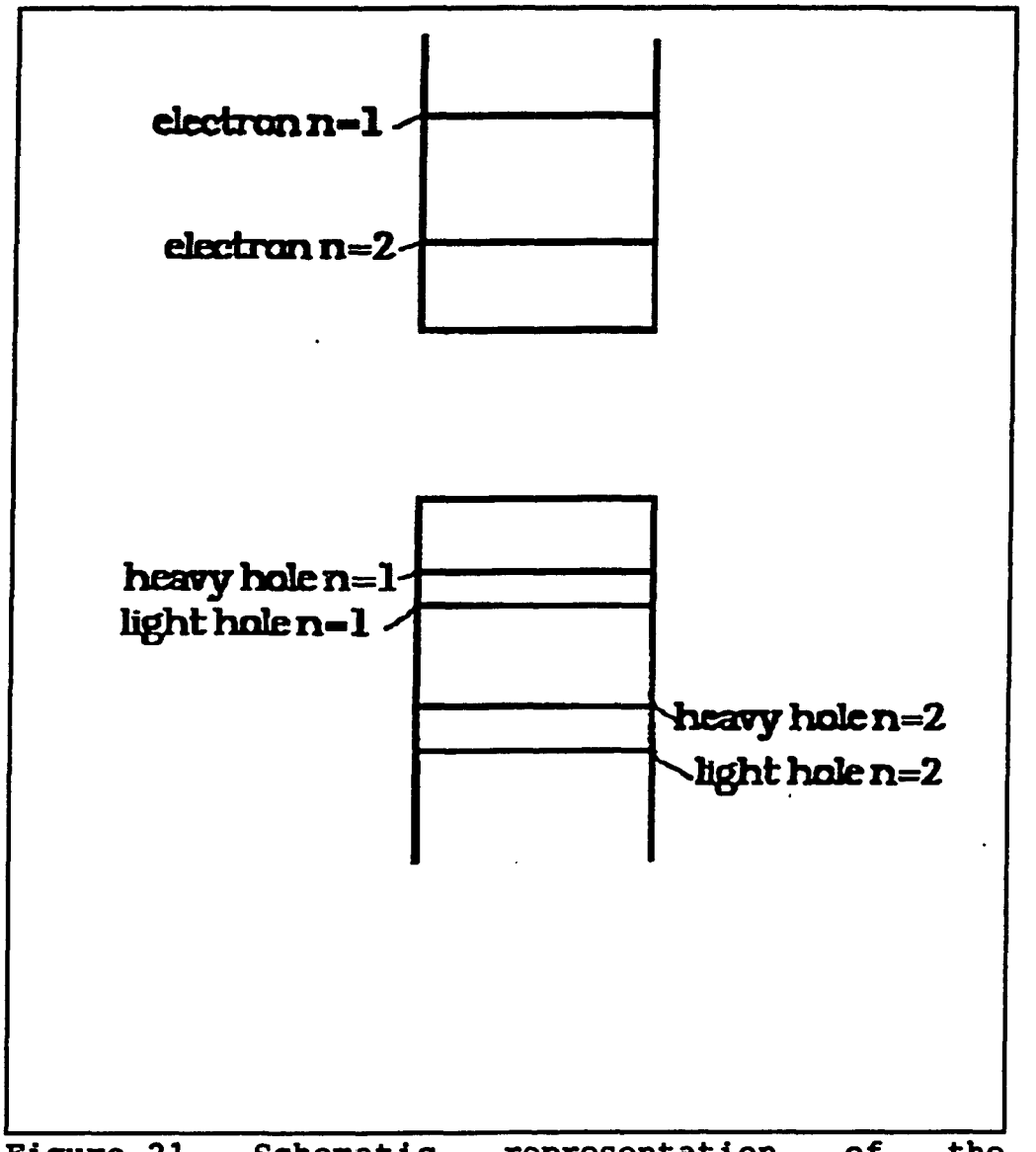

Figure 21 Schematic representation of the conduction, heavy hole and light hole states in a quantum well.

"lineup", i. e., the relative position in energy of the band gaps in the two semiconductors. This lineup determines the conduction-and valence-band discontinuities, and hence the effective barrier for

electron or hole transport across the interface. This parameter represents the fraction of the band gap difference, i. e.

$$Q_c=\Delta E_c/\Delta V_o \qquad (68)$$

This quantity fixes the relative portion of the band structure of the well and barrier layer. In this study, we can indirectly deduce the band offset parameter from PR measurements. To our knowledge, this is one of the best methods to determine the band offset parameter for the heterostructures.

4.1.1 Modified Kronig-Penny model

It can be shown that the total wave function of well and barriers can be written as:

$$\Phi(r)=\Sigma A_j \psi_j(r) F_j(r) \qquad (69)$$

where $\psi_j(r)$ is a host wave function, and $F_j(r)$ is an envelope function. The envelope function $F_j(r)$ satisfies the following Schrodinger equation:

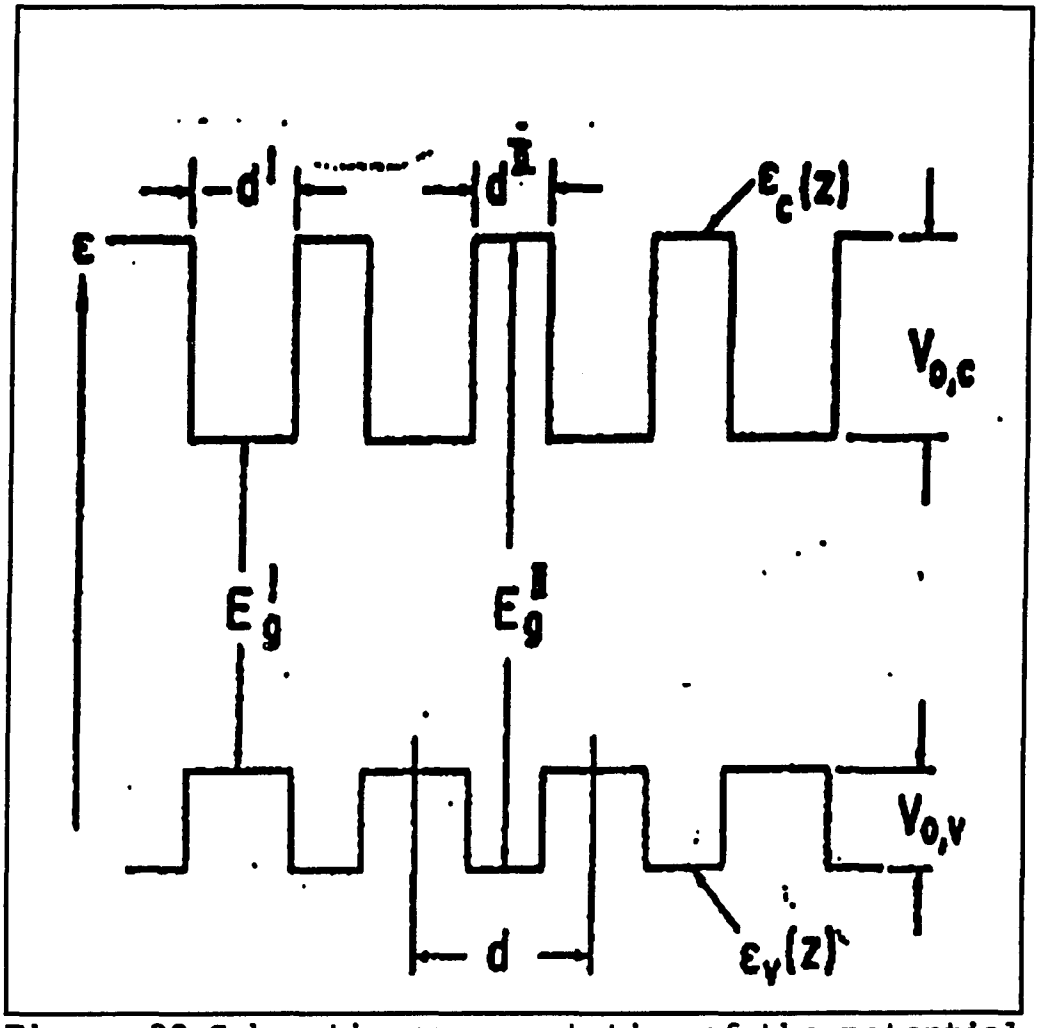

Figure 22 Schematic representation of the potential profile of a compositional superlattice.

$$[\ -(\hbar^2/2m^*)\nabla^2 + V_p\ ]F(r)=EF(r) \qquad (70)$$

where m^* is an effective mass. For the multiple quantum wells $V_p = V(z)$, equation (70) becomes a one dimensional periodic problem. The simplest situation

is that we treat the MQW potential as a one-dimensional square wave, as shown in Fig. 22 (Kronig-Penney model). The calculation of this model can be found in standard quantum mechanics textbooks [76]. The difference between the modified Kronig-Penney Model and the textbook model is that the boundary contining condition at the interface is modified. Instead of using $df_{c,v}(z)/dz$ continuous at the interface, we assume that $[1/m^*(z)][df_{c,v}(z)/dz]$ is continuous at the interface, where $m^*(z)$ is the effective mass along the growth direction z. This boundary condition insures the continuity of the probability of currents. F(z) satisfies the Bloch equation $F(z+md)=\exp(iqmd)F(z)$, where $d=d_I+d_{II}$. The modified Kronig-penney equation is:

$$\cos(qd)=\cos(k_I d_I)\cos(k_{II} d_{II})-1/2(x+1/x)\sin(k_I d_I)x \sin(k_{II} d_{II}) \qquad (71)$$

This is for unconfined states or miniband. For confined states (miniband)

$$\cos(qd)=\cos(k_I d_I)\mathrm{ch}(\beta d_{II})-1/2(\xi+1/\xi)\sin(k_I d_I)X \mathrm{sh}(\beta d_{II}) \qquad (72)$$

$$x=k_I m^*_{II}/k_{II} m^*_I \tag{73}$$

$$\xi=k_I m^*_{II}/\beta m^*_I \tag{74}$$

and,

$$k_I^2=(2m^*_I E/\hbar^2)-k\perp^2 \tag{75}$$

$$k_{II}^2=[2m^*_{II}(\Delta E_{c,v}-E)/\hbar^2]-k\perp^2 \tag{76}$$

$$\beta^2=[2m^*_{II}(E-\Delta E_{c,v})/\hbar^2] \tag{77}$$

$k\perp^2=k_x^2+k_y^2$, i. e. the momentum perpendicular to the superlattices direction and q is the wave vector in the subband, and $\Delta E_{c,v}$. The superlattice(or MQW) potential V_p removes the four-fold degeneracy of the top of the valence band on the band structure of the diamond and zincblende type material. It makes the z direction inequivalent to x, y. The top of the valence band consists of heavy hole (m_{HH}) and light hole (m_{Lh}) contributions. The degeneracy is a consequence of the cubic symmetry of these materials.

4.1.2 Bastard Model [81, 82]

Calculation of the Bastard model begins with the 6X6 Kane matrix [83] describing the K.P interaction with Γ_6 and Γ_8 subspace [81]. By decoupling the heavy hole (M_j=+3/2) from the light hole (electron and light hole M_j=+1/2), the Kane matrix can be transformed into two identical 2X2 differential systems (for describing coupling between light hole and electron) and two 1X1 systems (for describing heavy hole). The 1X1 equation leads to the same solution as the modified Kronig-Penney Model, in which the boundary condition is same as of the Modified Kronig-Penney Model. However the 2X2 matrix equations introduces the change of boundary condition, it becomes $[E_g+E-E_v]^{-1}$ d/dz$[F_s(z)$ continuous at the interface where E_g is the band gap of the semiconductor material, and $F_s(z)$ is the electron envelope function. For the light hole, the boundary condition becomes $[E-\Delta E_c]^{-1}$ d/dz$[F_p(z)$ continuous at the interface, where $F_p(z)$ is the light hole envelope function. By including the new boundary condition, a small modification to the

Kronig-Penney equation (70) is introduced, i. e. we replace x by

$$x=k_I(E+E_g^{II}-\Delta E_v)/K_{II}(E+E_g^{I}) \quad \text{for electron} \tag{78}$$

$$X=K_I(E-\Delta E_c)/K_{II}E \quad \text{for light hole} \tag{79}$$

for the unconfined states, and for the confined states

$$\xi=k_I(E+E_g^{II}-\Delta E_v)/\beta(E+E_g^{I}) \quad \text{for electron} \tag{80}$$

$$\Xi=K_I(E-\Delta E_c)/\beta E \quad \text{for light hole} \tag{81}$$

The advantage of this method is that it has almost no cost in terms of the computational effect and it gives quite satisfactory results. The mixing of the conduction band and light hole is considered, and the non-parabolicity of the band is included in a natural way. The disadvantage of the envelope

function approximation is that it allows no mixing of two or more bulk states with widely separated wave vectors and no mixing of bulk heavy and light holes in the superlattice wave function.

In the case of very thin layers, the envelope function tends to break down; it can be calculated using Linear Combination of Atomic Orbital (LCAO) methods, which have been performed by Schulman, et al. [84, 85]. When the layer thickness is larger than 6-8 monolayers, the results are similar to the envelope function approximation.

4.1.3 Coupling Between Wells And Miniband Dispersion

Two important effects can occur if we let the barrier thickness decrease to the point where states from adjoining wells interact. First, for just a pair of wells the interaction will lead to two new states that are split away from each other. Second, if this is allowed to occur for a large number of interacting wells, then a miniband structure is formed in a manner similar to the formation of a

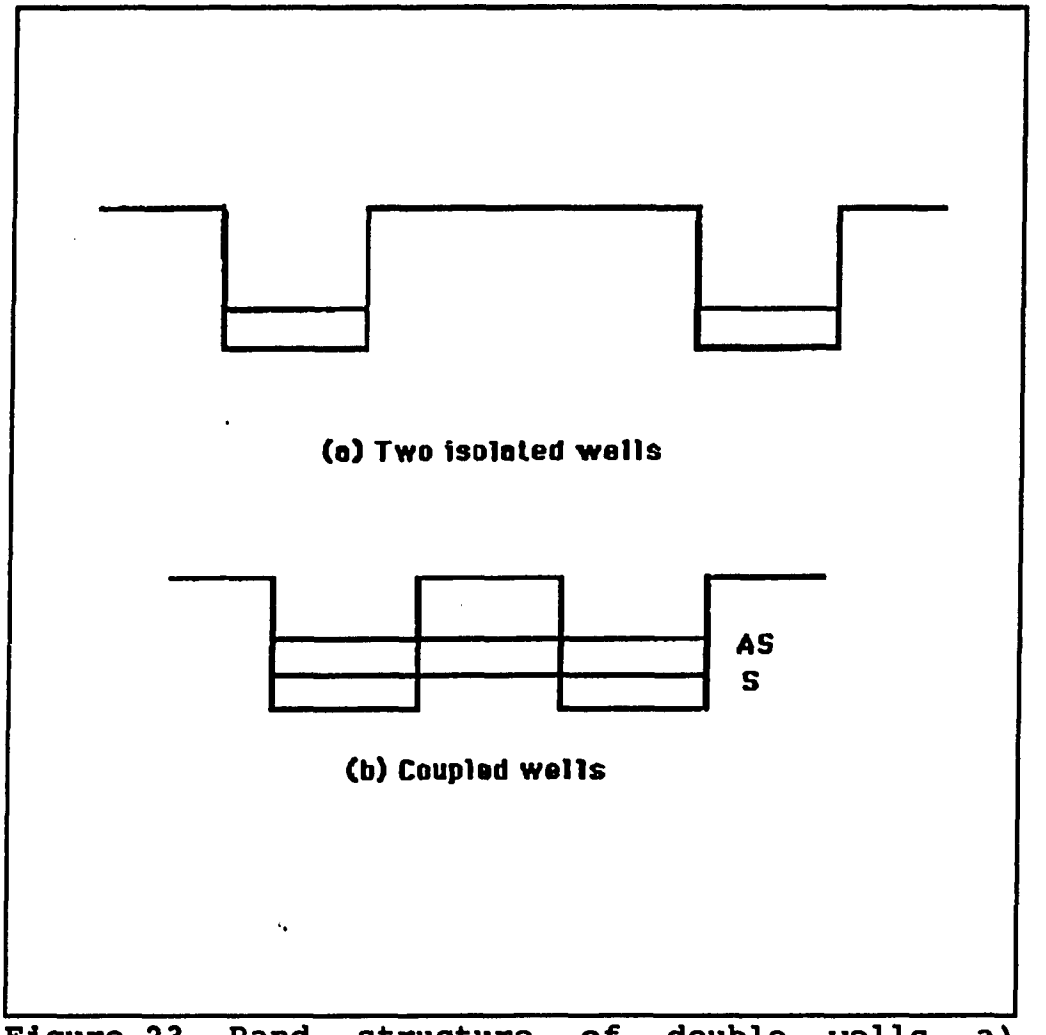

Figure 23 Band structure of double wells a) Uncoupled wells; and b) coupled wells.

semiconductor by bringing together many atoms to form semiconductor bands. Shown in Fig. 23a is an isolated double-wells structure in which the thickness of the barrier is very large, and the wave functions F_1 ,F_2 do not interact with each other. In Fig. 23b, as the barrier thickness is decreased, the

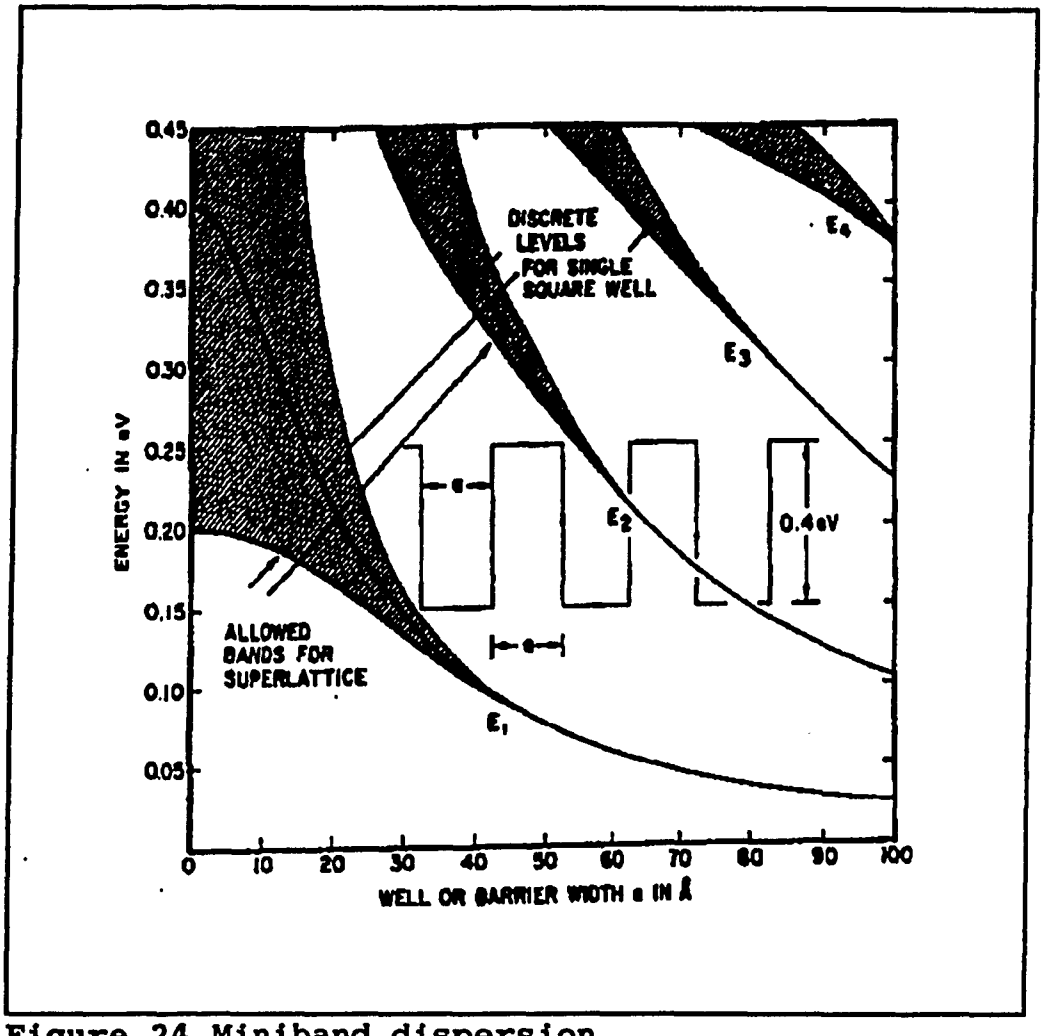

Figure 24 Miniband dispersion.

exponential decaying wave function is in the next well, the interaction of the wavefunction overlapping leads to the degenerate well levels splitting into both symmetric and antisymmetric.

Introducing more wells leads to the creation of a continuous band of states. By Equation (10), the

allowed discrete energy bands are given as usual by $-1 < \cos qd < 1$. Shown in Fig. 24, allowed energy bands E_1, E_2, E_3 and E_4 (hatched) calculated as a function of well or barrier width ($L_z=L_B=a$) in a superlattice with a barrier potential V=0.4 eV. The confined and unconfined energies (minibands), below and above the barrier potential, respectively are shown in the figure.

4.1.4 Interband Transition

The intensities of interband transitions can be obtained from quantum well wave functions, which are products of envelope functions representing the well with bulk like wave functions from the plane of the well. The momentum matrix element P_{sl} related to optical transition can be written as

$$\begin{aligned} P_{sl} &= \langle \psi_{0c}(r)^* F_{c,n1}(z) | \; ih\nabla \; | \; \psi_{0v}(r)^* F_{v,n2}(z) \rangle \\ &= M_{cv} \langle f_{c,n1}(z) f_{v,n2}(z) \rangle \\ &= M_{cv} I_{cv,n1,n2} \end{aligned} \tag{82}$$

where $M_{cv}(k)$ was defined in Eq. (8) of Chapter 1, the overlap integral is defined as: $I_{cv,n1,n2}$

$=<f_{c,n1}(z)f_{v,n2}(z)>$ and $\Phi_{s1}(r)=\psi_{0c}(r)f_{c,n1}(z)$ is the total wave function, a product of the bulk Bloch function $\psi_{0c,v}(r)$ and the envelope function $f_{c,n1}(z)$. For an infinitely deep well, and parabolic conduction/valence bands were assumed, we would obtain so called "allowed" selection rules for interband transitions, i. e. m=n, where m, n are quantum numbers of the conduction and valence bands, respectively. The selection rule is a consequence of the nodal property of the wave functions at the well/barrier interface. For finite wells, the situation is somewhat more complex. The wave function of deeply confined states do not penetrate into the barrier, i. e. there is a node at the well/barrier interface; thus the allowed selection rule is applicable. This selection rule may be broken due to nonparabolicity of the valence states as well as due to the influence of electric field (internal, external), etc.. However, for states near the top of the barrier (also above it) there may be considerable penetration of the wave function into the barrier region and additional nodes may appear in the barrier. The amount of penetration into the

barrier region is dependent upon the position of the state with respect to the top of the barrier. Therefore, the overlap integral between the electron and hole states for "forbidden" transitions need not be zero and thus P_{el} does not equal zero. The forbidden transitions were observed in the optical experiment [86, 87]. Also from P_{el}, the allowed transitions originating from a light hole state will be three times weaker than a corresponding one from a heavy hole state.

4.1.5 The Lineshape of Multiple Quantum Wells

The role of the modulating field and the nature of the electric modulation lineshapes in microstructures are different from those in the bulk material, as developed in Chapter I. In order to understand modulation mechanisms of microstructures, we begin with the dielectric function. The zero field dielectric function for multiple quantum wells can be expressed as:

$$\epsilon(E,\Gamma)=1+$$

$$(e^2\hbar^2)/(\pi^2 m^2 E^2 L_z)\Sigma_n \int d^3k |e \cdot M_{cv}(k) I_{cv,n}|^2 [1/(E_{cv,n}-E-i\Gamma)] \quad (83)$$

where n is the principle quantum number of the confined states and L_z is the width of the confined region and $I_{cv,n}$ is the overlap integral between the electron and hole envelope functions. Under the application of a small electric field F along the confining direction z, the perturbation produces three effects in the system: 1) the electric field redistributes charges with electron and hole localized at opposite ends of the confining region [88, 89], which is in terms of the overlap integral $I_{cv,n}$. The overlap integral $I_{cv,n}$ is changed by a fixed amount $\delta I_{cv,n}$ and without time dependence; 2) The electric field does not accelerate particles. The energy does not change continuously in time. It changes only by a fixed amount $\delta E_{cv,n}$ due to the stark effects. The new energy is given by $E_{cv,n}+\delta E_{cv,n}$; 3) The electric field can modulate the life time of the state and it will also change a fixed amount $\delta\Gamma_{cv,n}$ because of the electric field. The new broadening parameter can be written as: $\Gamma=\Gamma_{cv,n}+\delta\Gamma_{cv,n}$.

Therefore the change of the dielectric function induced by the electric field can be written as:

$$\Delta\epsilon=[(\partial\epsilon)/(\partial I_{cv,n})(\partial I_{cv,n}/\partial F)+(\partial\epsilon)/(\partial E_{cv,n})(\partial E_{cv,n}/\partial F) +(\partial\epsilon)/(\partial\Gamma)(\partial\Gamma/\partial F)]\ \Delta F \qquad (84)$$

Thus indicates that for an isolated confined system, electromodulation leads to the first derivative like optical features of two dimensional critical points. But for interacting MQW system, the situation is complicated. In this case, there is a dispersion in the miniband as well as a new translation symmetry. The electron and hole wave functions are not localized in a single layer, they can freely move in the layers. If the electric field is small, which does not destroy the miniband, electron and holes will be accelerated, and the situation is similar to the case of the band-to-band transition of bulk material in Chapter I. The electromodulation gives rise to the third derivative functional form. It has been shown both theoretically and experimentally that at a moderate field, the electron and hole wave functions begin to localize to several layers. At

high fields there is a complete localization into a single layer. This leads to first derivative functional form.

It should be pointed out that the coulomb interaction between photoexcited electron and hole, exciton, plays an important role in the optical properties of semiconductors. They are even more important in the case of microstructures, where the electron and hole are confined in real space, since quantum wells tend to be < 500 Å in width, while the exciton Bohr radius is about 200 Å for bulk GaAs. Because of this consideration, the excitonic effect must be included whenever quantum states are formed for both electron and holes. It also well known that exciton exist in quantum wells even at elevated temperatures or in larger electric fields [85].

Previous discussion indicates that the electromodulation spectrum of excitonic transition should be described by the first derivative of lorentzian lineshape. Glembocki and etc. [17, 90] found that at elevated temperatures the spectrum of excitonic transitions is well represented by the first derivative of Gaussian lineshape because of

temperature dependent inhomogeneous broadening of excitonic absorption. Toyozawa [91] has shown that this type of broadening can be caused by either strong exciton interactions at low temperatures, weak exciton-phonon coupling at elevated temperatures or by random distributions of impurities and defects. These effects cause the absorption profile of excitons to be Gaussian rather than Lorentzian. In deriving the formula of lifetime broadening, as stated in Chapter 2, due to the electron-phonon interaction from the rigid-ion model, the other scattering mechanisms (exciton, impurity and defect) were not considered. Thus, the electron-phonon interaction leads to Lorentzian lineshape broadening .

4.2 Experiments

4.2.1 GaAs/GaAlAs system: Confined and Unconfined States Including Miniband Dispersion [42]

In this section we report a systematic study of PR at 300K of four samples of GaAs/$Ga_{0.82}Al_{0.18}As$ MQWs

with different L_B all having the same well thickness L_z [42]. We have observed the evidence for coupling between multiple wells(miniband dispersion) in several confined transitions. The coupling effects were also obseved in several unconfined transitions. Excellent agreement is found between experiment and a Bastard model calculation.

The MQWs and $Ga_{1-x}Al_xAS$ epilayer used in this study were fabricated in Varian Gen II Molecular Beam Epitaxy system at the United Technology Research Center. These structures were grown on GaAs buffer layers (not intentionally doped) of 0.8 μm thickness on semi-insulating GaAs substrate. The MQWs all had L_z=Å (25 monolayer of 2.83Å) but LB of 71Å, 99Å, 150Å, and 201Å. The number of periods were 75, 62, 48 and 39, respectively, in order to keep the MQW thickness at 1.05 μm for all four samples.

Shown in Fig. 25 is the 300K PR spectrum of a thick $Ga_{1-x}Al_xAs$/GaAs epitaxial layer. The feature at about 1.41 eV corresponds to the direct band gap of GaAs [E_o(GaAs)] and originates in the GaAs buffer/substrate. The sharp peak denoted A is probably an exciton. The PR peak at about 1.65 eV

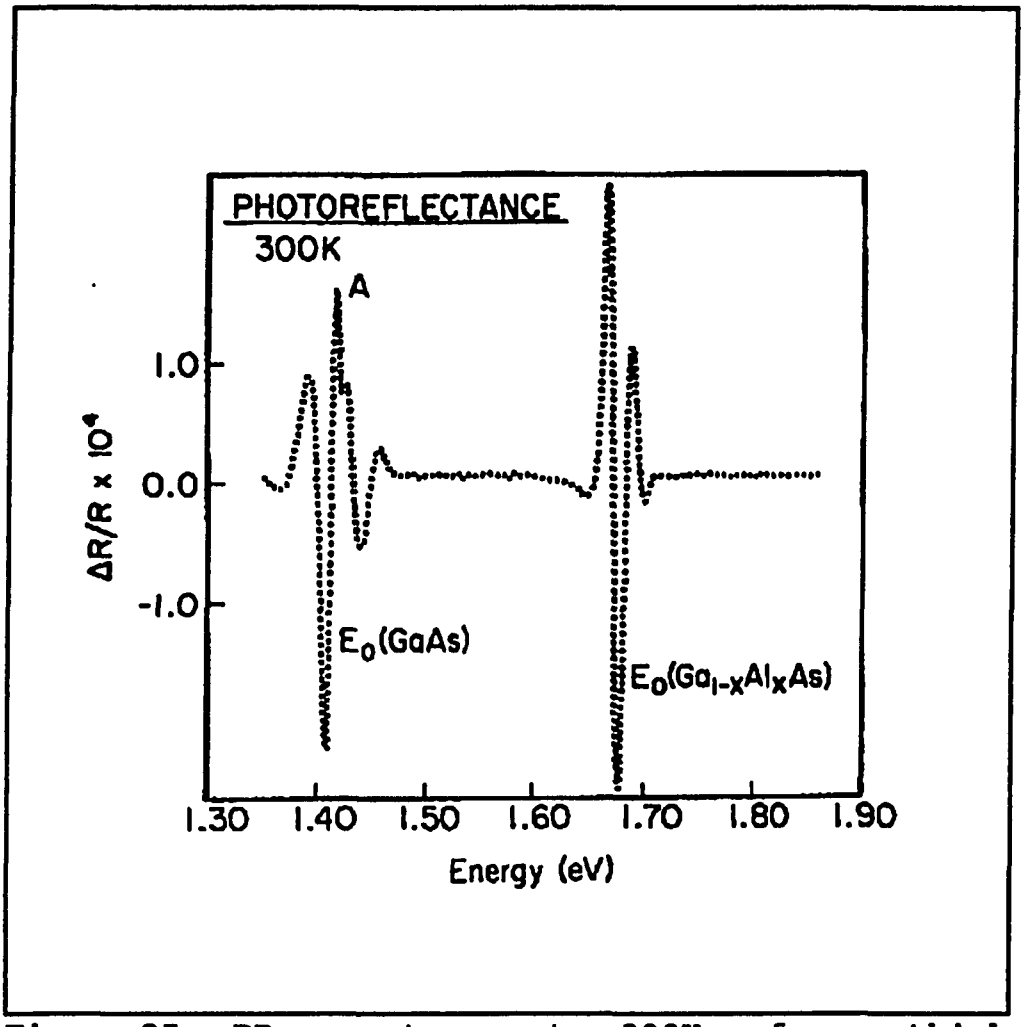

Figure 25 PR spectrum at 300K of a thick $Ga_{0.82}Al_{0.18}As$/GaAs epilayer.

originates from the direct band gap of the $Ga_{1-x}Al_xAs$ epilayer [$E_o(Ga_{0.82}Al_{0.18}As$]. It was not possible to fit the lineshape of either of these features with a third-derivative functional form of electromodulation or first-derivative function form of Gaussian since both appear to exhibit

Franz-Keldysh oscillations. The energy positions can be obtained from a three point fit method yielding $E_o(GaAs)=1.417\pm0.005$ eV and $E_o(Ga_{0.82}Al_{0.18}As)=1.673 \pm0.005$ eV. The Al concentration, x, can be estimated from $dE_o(Ga_{1-x}Al_xAs)/dx=1.455$ for $x\leq 0.4$ [92]. In our case $x=0.18\pm0.005$, in reasonably good agreement with the value of x=0.20 deduced from the growth condition. From this measurement, the barrier height $V_o[=E_o(Ga_{0.82}Al_{0.18}As)-E_o(GaAs)]$ is used with the MQW study.

In Fig. 26, we plot the PR spectra (dotted line) at 300K of four samples. The arrow at the bottom of the figure represents $E_o(Ga_{0.82}Al_{0.18}As)$. All transitions above this energy can be clearly identified as UT. In attempting to fit the lineshape of the spectra of Fig. 26, it was found that the first derivative of a Gaussian lineshape form gave the best overall agreement. However, above about 1.52 eV, the first derivative of a gaussian or third-derivative functional form [90, 93] yield comparable results. A least squares fit to Gaussian derivative is shown by the solid lines of Fig. 26. Indicated by arrows for the four samples are the

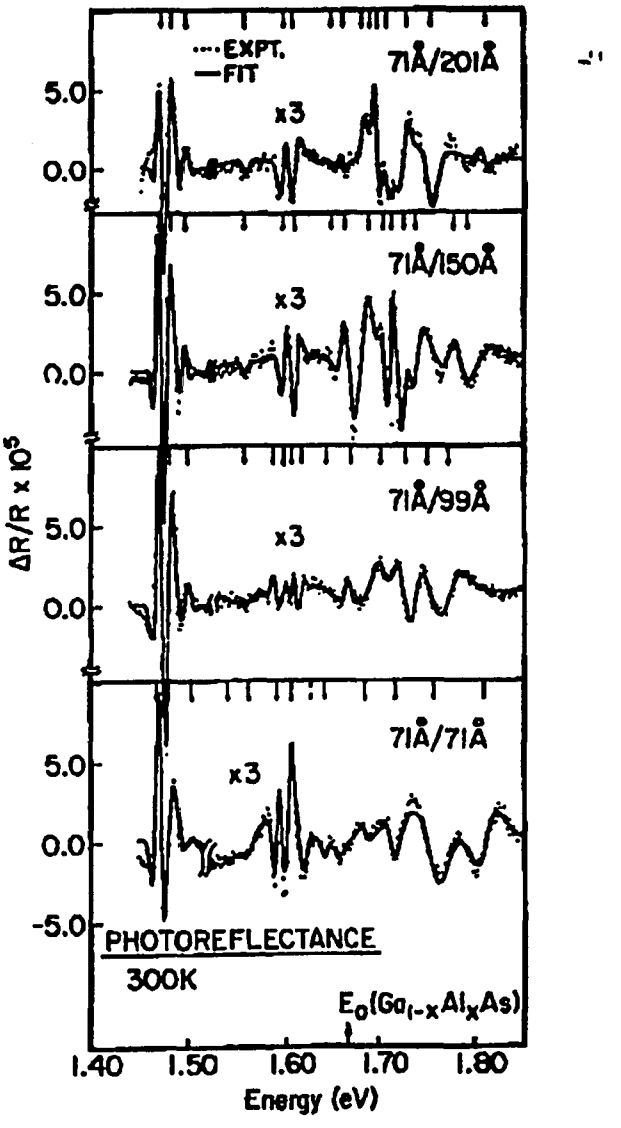

Figure 26 PR spectra of four GaAlAs/GaAs MQWs having the same well widths but different thicknesses at 300K.

energies of the various transitions as evaluated

from the lineshape fit. These values are listed in Table VII. The notation mnH/L denotes transition between the m^{th} conduction to n^{th} valence subband of heavy (H)- or light (L)-hole character while the notation (Γ, π) indicates that the states at Γ and π are essentially degenerate, i. e., no miniband dispersion.

Comparing with the theoretical calculation of transition energies and matrix elements (for UT), we can identify the origins of the large number of features observed in the PR spectra. Listed in Table VII are the results of this calculation for the four samples. The best agreement between experiment and theory was achieved for a conduction band offset of 0.65 and the listed values of L_z and L_B.

Table VII. Experimental and theoretical values of the various confined and unconfined quantum transitions of several GaAs/$Ga_{0.82}Al_{0.18}As$ multiple quantum wells with different barrier layer thickness. The unconfined states occur ablove $E_o(Ga_{0.82}Al_{0.18}As)$=1.673 eV as indicated by the dashed line.

	L_z/L_B 71Å/201Å		L_z/L_B 71Å/150Å		L_z/L_B 71Å/99Å		L_z/L_B 71Å/71Å	
Transition	Expt.	Theory	Expt.	Theory	Expt.	Theory.	Expt.	Theory
11H(Γ,π)	1.469	1.467[a]	1.469	1.447[a]	1.469	1.466[a]	1.467	1.465[a]
11L(Γ,π)	1.479	1.481[b]	1.480	1.481[b]	1.479	1.480[b]	1.479	1.478[b]
12H(Γ,π)	1.494	1.502[c]	1.495	1.502[c]	1.497	1.501[c]	1.502	1.501[c]
13H(Γ)	1.555	1.547[c]	1.555	1.546[c]	1.555	1.546[c]	1.540	1.544[c]
13H(π)	1.555	1.548[c]	1.555	1.549[c]	1.555	1.551[c]	1.560	1.556[c]
21L(π)	1.595	1.590[d]	1.595	1.589[d]	1.587	1.586[d]	1.589	1.584[d]
21H(Γ)	1.595	1.591[d]	1.595	1.592[d]	1.599	1.597[d]	1.604	1.605[d]
22L(π)	1.644	1.649[d]	1.647	1.648[d]	1.638	1.644[d]	1.642	1.639[d]
22L(Γ)	1.658	1.655[d]	1.662	1.658[d]	1.666	1.667[d]	1.685	1.689[e]
33H(Γ)	1.680	1.684[e]	1.682	1.690[e]	1.704	1.704[e]	1.718	1.722[e]
33L(Γ)	1.689	1.693[e]	1.705	1.704[e]	1.728	1.731[e]	1.759	1.766[e]
34H(π)	1.696	1.696[e]	1.713	1.713[e]	1.748	1.755[e]	1.809	1.812[e]
43H(π)	1.706	1.712[e]	1.727	1.734[e]	1.778	1.776[e]		
33L(π)	1.706	1.712[e]	1.740	1.741[e]				
45H(Γ)	1.728	1.743[e]	1.779	1.788[e]				
54H(Γ)	1.754	1.757[e]	1.793	1.799[e]				
56H(π)	1.806	1.809[e]						

(a) Exciton binding energy of 8 meV from Ref. 74
(b) Exciton binding energy of 10 meV from Ref. 74
(c) Exciton binding energy of 7 meV from Ref. 74
(d) Exciton binding energy of 6 meV from Ref. 74
(e) Exciton binding energy of 4 meV from Ref. 74

4.2.2 Strained layer system I: GaSb/AlSb

The strained layer GaSb/AlSb multiple quantum structures have generated much interest due to their potential for application in fiber optical technology and having a variety of effects from lattice mismatch [45], quantum confinements [94] and deep potential wells in the conduction band [95, 96, 97, 98, 99]. In this system, there will be a stress-induced shift as well as heavy hole and light band splitting which are related to the lattice mismatch. Also, since there are very deep potential wells in the conduction band, a number of new quantizations induced phenomena have been observed. The band gap of GaSb corresponds to wavelength range (1.5 μm) of the best performance of optical fibers.

For this system, there is little work done on the optical properties related to the electronic states. Cebullla et al had reported absorption and excitation spectroscopy on a series of multiple quantum wells (MQW's) with different well widths [99]. Low temperature absorption measurements on MQW's also have been performed by Voison et al [95]. Electroreflectance results at 30K on a single

quantum well have been presented [100]. Light scattering has been employed to evaluate the band offsets [101]. Also, the simultaneous recombination of two electrons and two holes has been observed due to quantization-induced changes of the wave-function symmetry [97]. Recently Rockwell et al [102, 103] have studied the pressure dependence of the excitonic transition in GaSb/AlSb MQW by using PR and PL. The pressure coefficients (α) of the excitonic transitions arising from the conduction band (CB) to heavy hole (HH) and light hole (LH) subband were evaluated.

In order to gain information about this system, we have studied the photoreflectance (PR) spectra at 77K of two (100) GaSb/AlSb MQW's having well (L_z) and barrier (L_B) width of 260Å/280Å (sample A) and 130Å/140Å (Sample B), which were fabricated by MBE. The sample specification was as follows: the structures were grown on 0.3 μm thick AlSb buffer on (100) GaAs substrate. The MQW's of both materials consisted of a total of 10 periods. The well and barrier widths for sample A and B were determined by high resolution transmission electron microscopy.

The former sample had a 50Å GaSb cap while the latter had a cap of 40Å of GaSb on top of 380 Å of AlSb. The PR pump beam was the 6328Å line of 1 mW He-Ne laser. Measurements were made at 77K. In the energy range 0.7-1.3 eV a cooled InAs detector was employed while above this region a Si photodiode detector was used.

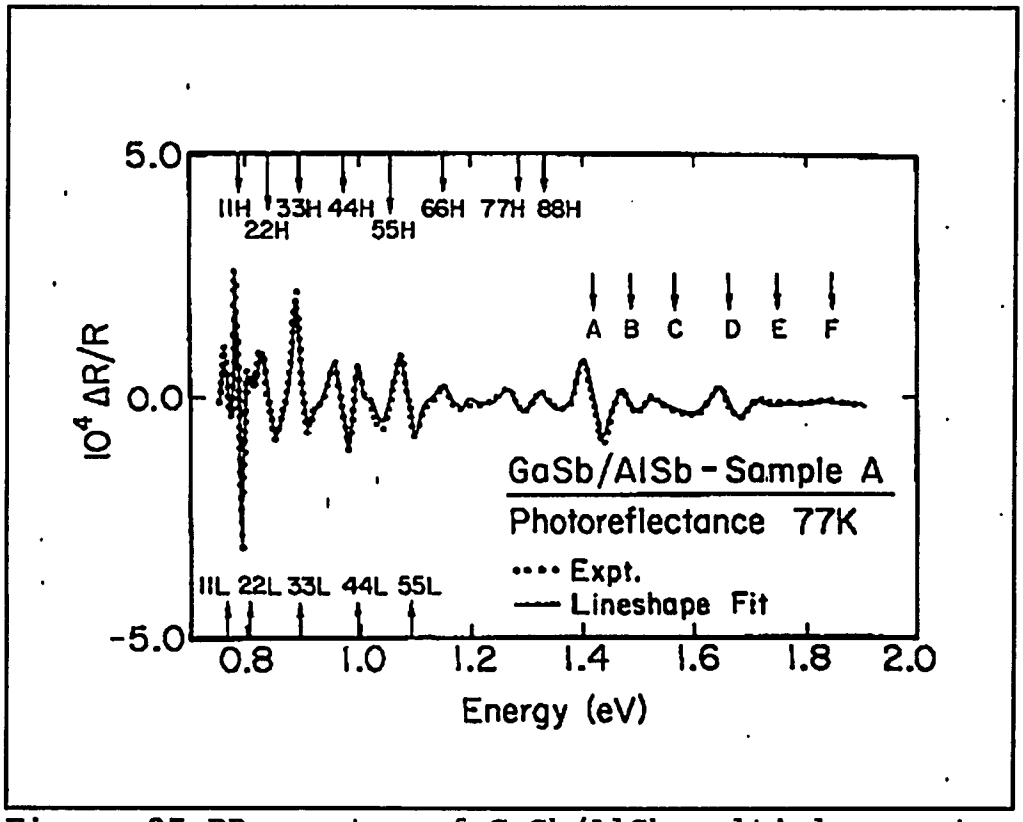

Figure 27 PR spectra of GaSb/AlSb multiple quantum wells at 77K

Shown by the dotted lines in Fig. 27 and 28 are the experimental PR spectra in the range 0.7-2.0 eV

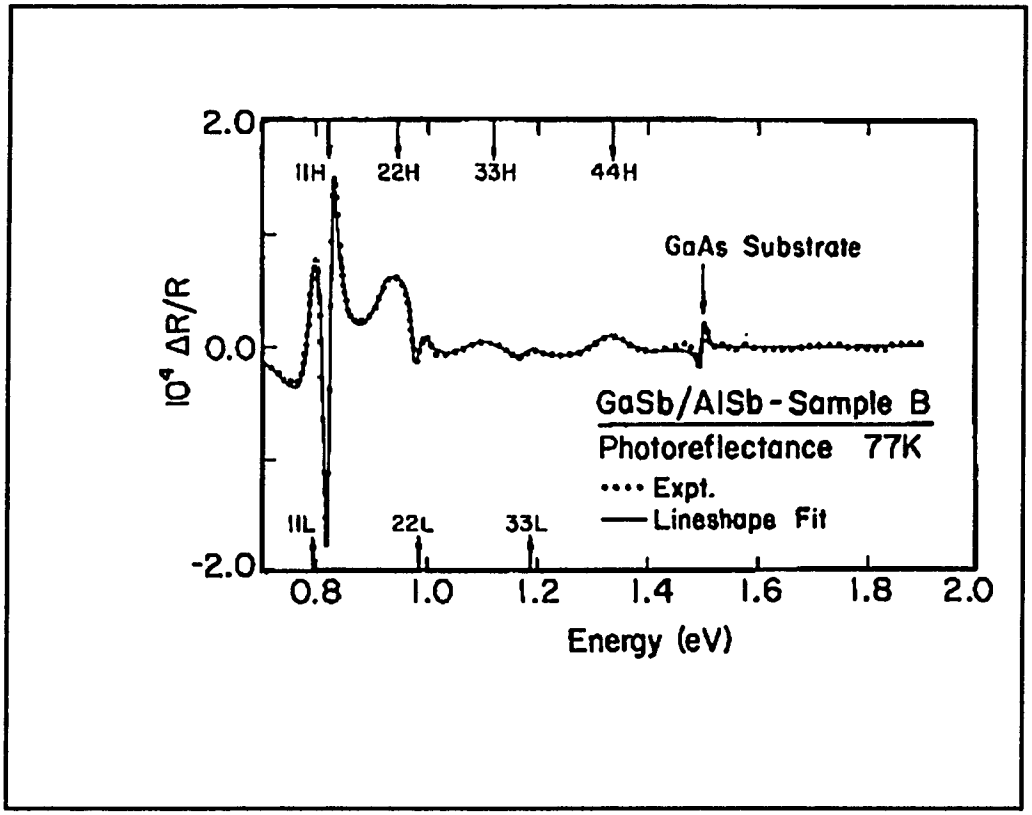

Figure 28 PR spectra of GaSb/AlSb multiple quantum wells at 77k (sample B).

of samples A and B, respectively. The solid lines in both figures are least-square fits to a lineshape function which is related to the first-derivative of a Gaussian profile. The obtained values of the transition energies are indicated by arrows. The notation mnH/L indicates transitions from mth conduction to the nth valence subband of Heavy (H)- or light (L)-hole character. Symmetry allowed transitions have m=n. Note that in Fig. 27 the

lowest lying feature (11L) is above a factor three smaller than the second peak (11H). This is opposite to the result obtained on the GaAs/GaAlAs system [17, 90, 104], in which the heavy-hole is the ground valence state, i.e., 11H lies below 11L. The 11L-11H splitting can be used to evaluate the strain distribution. The structure marked "GaAs substrate" in Fig. 28 corresponds to the direct gap of GaAs at 77K and originates from the GaAs substrate. No corresponding feature was observed in sample A. The interpretation of our results is based on the following considerations. The GaSb layers are under biaxial tensile stress due to the lattice mismatch of 0.65% between GaSb and AlSb. Since the elastic constants of GaSb and AlSb are essentially the same, the both GaSb and AlSb are strained in order to match their lattice parameter $a_\perp$:

$$a_\perp=(a_1L_z+a_2L_B)/(L_z+L_B) \qquad (85)$$

where a_1(6.0959Å) and a_2(6.1355Å) are the lattice constants of GaSb and AlSb, respectively. The biaxial tensile strain in the plane of GaSb is given

by:

$$\epsilon=(a_{\perp}-a_1)/a_1 \qquad (86)$$

The AlSb layer are under equal compressive biaxial stress.

The modification of the conduction (C) to heavy (HH)- and light (LH)- hole energy gaps of GaSb is given by:[77, 99]

$$E_o^{c,HH}=E_g+\delta E_H-\delta E_S \qquad (87a)$$

$$E_o^{c,Lh}=E_g+\delta E_H+\delta E_S-2(\delta E_s)^2/\Delta_o+ \qquad (87b)$$

where E_g is the energy gap of GaSb in the absence of stress and

$$\delta E_H=2a[(C_{11}-C_{12})/C_{11}]\epsilon \qquad (88a)$$

$$\delta E_S=b[(C_{11}+2C_{12})/C_{11}]\epsilon \qquad (89b)$$

The parameters a and b are the interband hydrostatic pressure and uniaxial deformation potential, respectively, and C_{ij} are elastic-stiffness

constants. The light hole valence band has a nonlinear strain dependence because of the strain-induced coupling with the spin-orbital split band [73]. Alternatively, δE_H and δE_S can be also expressed in terms of the stress T and elastic compliance constants S_{11}, S_{12}:

$$\delta E_H = 2a(S_{11}+2S_{12})T \tag{90a}$$

$$\delta E_S = b(S_{11}-S_{12})T \tag{90b}$$

where

$$T = \epsilon/(S_{11}+S_{12}) \tag{91}$$

Because of small strain and large valence band spin-orbit splitting (Δ_o) in our materials [77], the fourth term in Eq (87b) is very small and it can be neglected. For our case, in the GaSb layer, due to the tensile stress, a shrinkage of the GaSb band gap is due to the hydrostatic component and a splitting of the valence band, such that the valence band ground state is the light-hole level. This

strain-induced upward shift of light-hole level combined with the opposite shift of the heavy-hole band can lead to a mass reversal for wide quantum wells and thick barriers. In the AlSb layer where the biaxial stress is compressive, the band gap is increased and the heavy-hole state remains the ground state in the valence band.

Using the above strain consideration and a

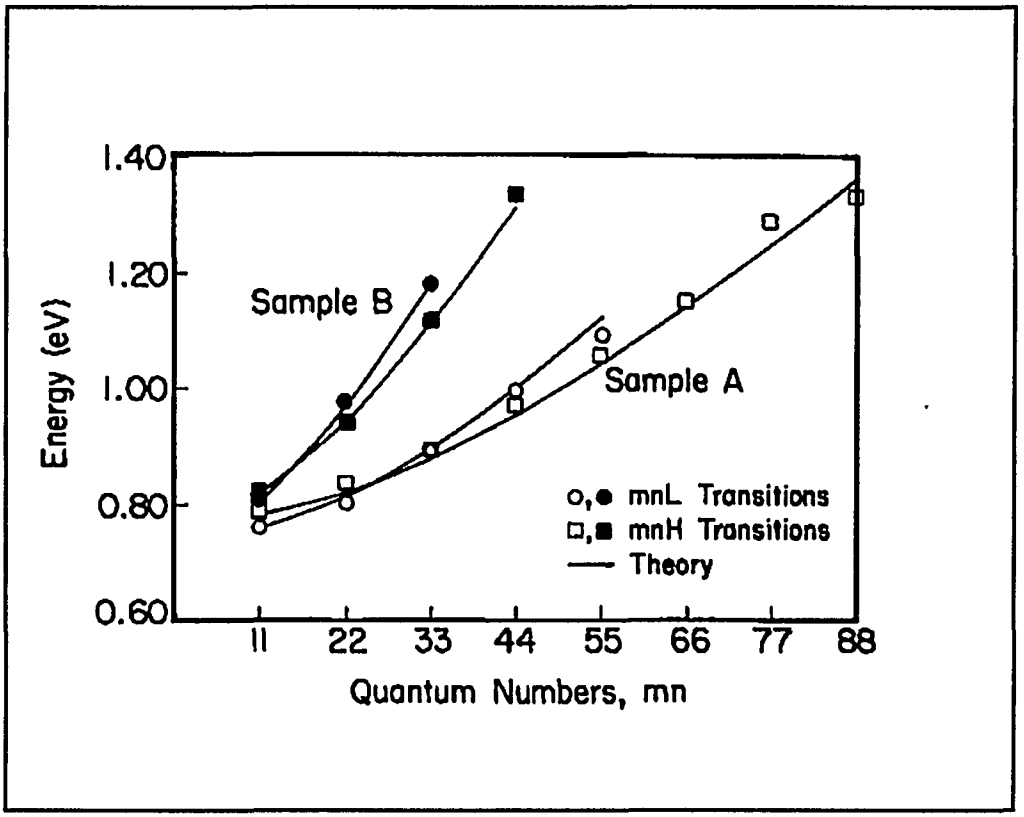

Figure 29 Energy transition of GaSb/AlSb multiple quantum wells.

three-band envelope function model [78,101], we have calculated the energies of the quantum transitions in GaSb wells for our two samples [102]. On our calculation we have used E_g(GaSb)=0.795eV, E_g(AlSb)=2.3eV, Δ_o(GaSb)=0.752eV, parameters such as S_{11}, S_{12}, a, b, m_{hh}^*, m_{lh}^* for two materials were the same as those used in Ref. 91. The three-band model was used since the band gap and spin-orbital splitting are comparable. This procedure thus accounts for nonparabolic effects due to the interaction of the conduction band with the light-hole and spin-orbit valence bands. In making a comparison with experiment, 6 meV of exciton binding energies have to be considered [99, 105]. In Fig. 29 we have plotted the experimental values of the various quantum transitions (minus the exciton binding energy) in Figs. 27 (except for A-F) and 28. Also shown are the results of our theoretical calculation (solid lines) for the two samples. The overall agreement is very good below 1.4 eV, thus confirming our assignment of these spectral features to the symmetry allowed mnh/L transitions (m=n). The best overall fit is obtained for an elastically

distributed strain and a conduction band offset parameter Q_c=0.85±0.08 (before strain). This corresponds to a zero-strain conduction band offset of 1309±100 meV. That the strains are distributed elastically between layers, despite a thick AlSb buffer, is probably due to the large and comparable values of L_z and L_B.

Above 1.4 eV for sample A (feature A-F) the good agreement between theory and experiment cannot be maintained. The situation is more complicated in this energy region, because a) the hole state is no longer confined, b) additional Γ-derived nonparabolic interaction may occur and c) of the proximity of the X conduction band minimum of AlSb barriers. In order to evaluate features due to unconfined transitions it is necessary consider intensity effects (matrix element overlap) [107]. We have performed such a calculation and find the A-F features cannot be attributed to unconfined hole transitions. Nonparobolic behavior not included in our theory may occur because of conduction band states above the lowest lying Γ_6 conduction barrier. For example, the spin-orbit split Γ_7, Γ_8 second

conduction band is about 3.2 eV above the Γ_8 state. [108]. In order to evaluate the nonparabolic influence of these higher lying states, we have performed a 30X30 (including spin-orbit splitting) full-zone K.P calculation. We found that in the energy range of our experiment theses additional bands produce negligible nonparabolic effects. The proximity of the X conduction band minimum of the AlSb barriers could produce a nonparabolicity not included in our Γ-derived calculations. Such an effect would decrease the energy separation of our intersubband transitions, which is consistent with the experimental observation above 1.4 eV (features A-F).

The evaluation of band offset in this system is consistent with a number of recent experiments [99, 101, 109] but cannot be reconciled with the small valence band discontinuity (~40-70 meV) reported in some earlier work [110, 111]. Tersoff [112] reported a zero dipole theory for evaluating the band lineup at ideal semiconductor interfaces. This theory gives a conduction band offset of 0.65 eV for GaSb/AlSb heterostructure. The self-consistent

heterojunction offset calculation of Van de Walle and Martin [113] yields 0.62 eV, while the linear muffin tin orbital approach of Cardona and Christensen produces 0.66 eV. [114]

In conclusion we have measured the PR spectra at 77K from two GaSb/AlSb MQW's. Excellent agreement between experiment and theory has been obtained in the energy range 0.7-1.4 eV where the hole states are confined and the electron levels are below the X conduction band minimum AlSb. We have evaluated a zero-strain conduction band offset of 0.85±0.08 and determined that the strain is distributed elastically between the wells and barriers. Deviations in the agreement above 1.4 eV provide some evidence for the mixing of Γ-X states.

4.2.3 Strained System II: $In_xGa_{1-x}As/GaAs$ [44]

In recent years there has been considerable interest in strained layer $In_xGa_{1-x}As/GaAs$ heterostructures.[44, 78, 115, 116, 117, 118, 119, 120]. This is a potentially attractive material system from a device prospective since the narrow

band gap of $In_xGa_{1-x}As$ makes it useful as an infrared detector fabrication as a superlattice or quantum well. In addition, the low effective electron mass in $In_xGa_{1-x}As$ can be exploited in high-frequency transistor applications. Accordingly this material system has received a great deal of attention both theoretically and experimentally.

Despite detailed investigations, however, one of the most fundamental questions, the relative alignment of the conduction and valence bands along the growth axis, still remains unanswered. A related issue is whether the system is fully type I or mixed. In the mixed case, the light holes exhibit type-II behavior, the behavior of heavy hole remain type-I. Knowledge of the band alignment is vital if the transport and optical properties are to be accurately calculated. Unfortunately the valence (or conduction)-band offset cannot be observed directly, but is usually inferred from optical measurements such as X-ray photoelectron spectroscopy [121], absorption and photoluminescence [78, 122, 123, 124, 125], photoreflectance [44, 126, 127], modulated transmission spectroscopy [128], Raman

scattering[125], photocurrent [129, 130] and photoluminescence under hydrostatic pressure [131]. By applying a suitable band-structure theory to calculate the energies, the valence-band offset is obtained by fitting the energy difference to the observed spectrum, treating the offset as an adjustable parameter. Based on this approach, Marzin et al. [78] estimated the conduction-band offset to be about 0.7 for x=0.15, where the offset is defined as the fraction of the electron-heavy hole band difference appearing across the conduction band edge. Taking into account the effects of strain, this offset leads naturally to the conclusion that the electron-heavy hole (e-hh) exciton is direct (type I) and the electron-light-hole (e-lh) exciton indirect (type II) in real space. This result was confirmed by Ji et al [132] using a similar model to fit their data for x varying from 0.13 to 0.193. A number of subsequent studies [126, 127, 133, 134, 135, 136, 137, 128], many of them being PR [44], PL [137], and Photomodulated transmission [128] experiments, place the value of conduction band offset (Q_c) between 0.6 and 0.8. In contrast, three

groups [119, 126, 127, 136] found Q_c=0.4 which would lead to type-I behavior for both light- and heavy-holes. This discrepancy might be explained by a dependency of Q_c on In composition x as recently proposed by Joyce et al.[120]. Recent data by Yu et al [130] using photocurrent spectroscopy agree with this suggested trend. In order to explain the abobe discrepancy, recently Jogai and Yu [138] numerically solved the complete K P Hamiltonian with strain to obtain the energies and wave functions of this system. They show that the theory accurately reproduces the spectra of a wide range of published samples for valence-band offsets ranging from 0.3 to 0.6. It is also found that the transition energies are relatively insensitive to the valence-band offset over a wide range of offsets. The electron-light-hole exciton energy is fitted more closely at the lower offset values and suggests a conduction-band offset close to 0.6. At this offset, the light holes exhibit type-II behavior, and are only slightly localized in the GaAs layers.

In order to gain more information about this

interesting system we have studied the photoreflectance (PR) spectra at 300K and 77K of two [001] $In_xGa_{1-x}as/GaAs$ ($x\approx 0.12$) MQW's. Our MQW's samples have nominal well (L_z) and barrier (L_B) widths of (50Å/100Å) (sample A) and (30Å/100Å) (sample B), and are grown by metal-organic vapor-phase epitaxy on [001] GaAs substrate [93]. A 600Å GaAs buffer was grown on the substrate before the MQW fabrication. Sample A is lightly doped with Mg ($p \approx 1016\ cm^{-3}$) while sample B is undoped.

When grown on a GaAs buffer the $In_xGa_{1-x}As$ layers sustain a biaxial in-plane compression and a corresponding extension along the [001] growth direction. In general, since the GaAs buffer layer is much thicker than the $In_xGa_{1-x}As$ layers, the biaxial strain ϵ is given by [77]

$$\epsilon=(a_{1,2}-a_{1,1})/a_{1,1} \qquad (92)$$

where $a_{1,1}$ and $a_{1,2}$ are the lattice constants of the InGaAs and GaAs, respectively. The former is obtained by a linear interpolation between the

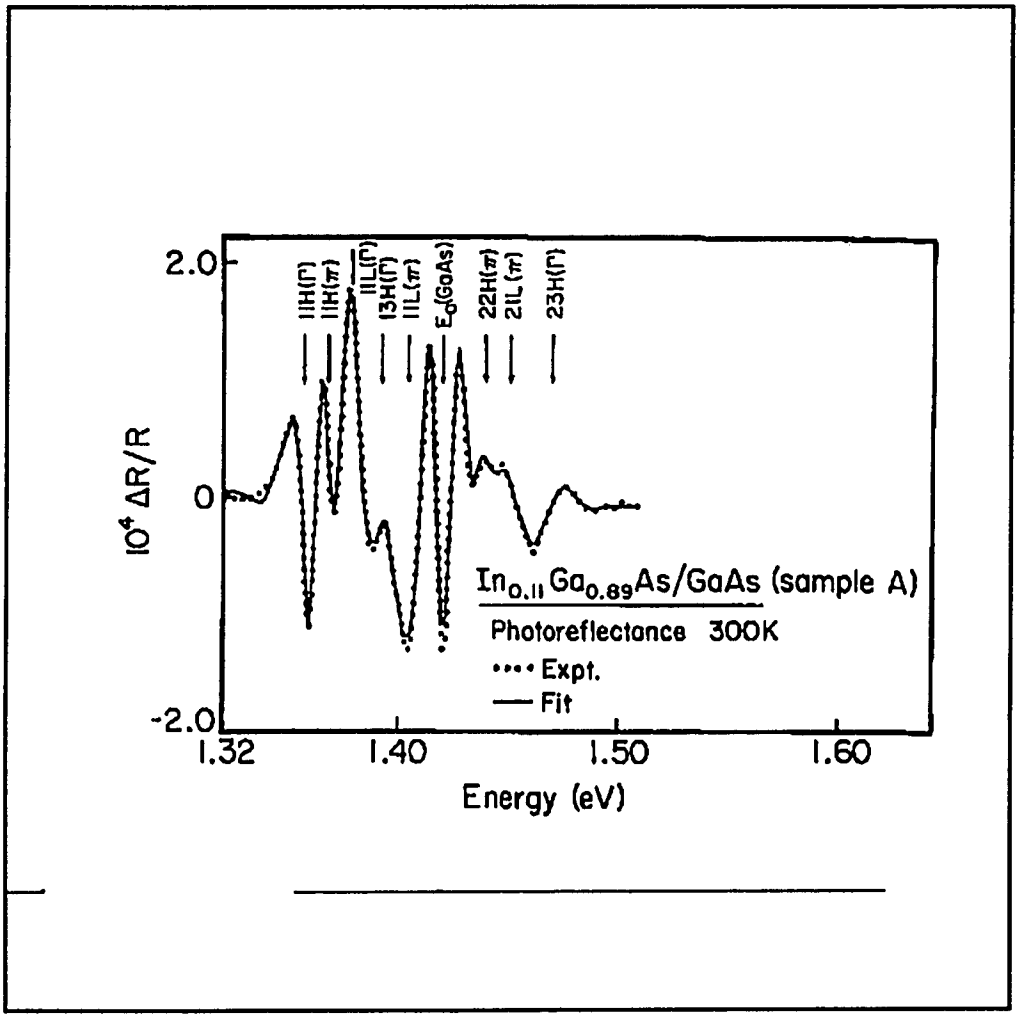

Figure 30 PR spectrum (dotted lines) of an $In_{0.11}Ga_{0.89}As/GaAs$ coupled multiple quantum well (sample A) at 300K. The solid line is a lineshape fit as discussed in the text.

lattice constants of InAs and GaAs.

This strain alters the band structure of the $In_xGa_{1-x}As/GaAs$ MQW. The strain-dependent conduction (C) to heavy-(HH) and light-(LH) energy gaps are given by Eq.(85).

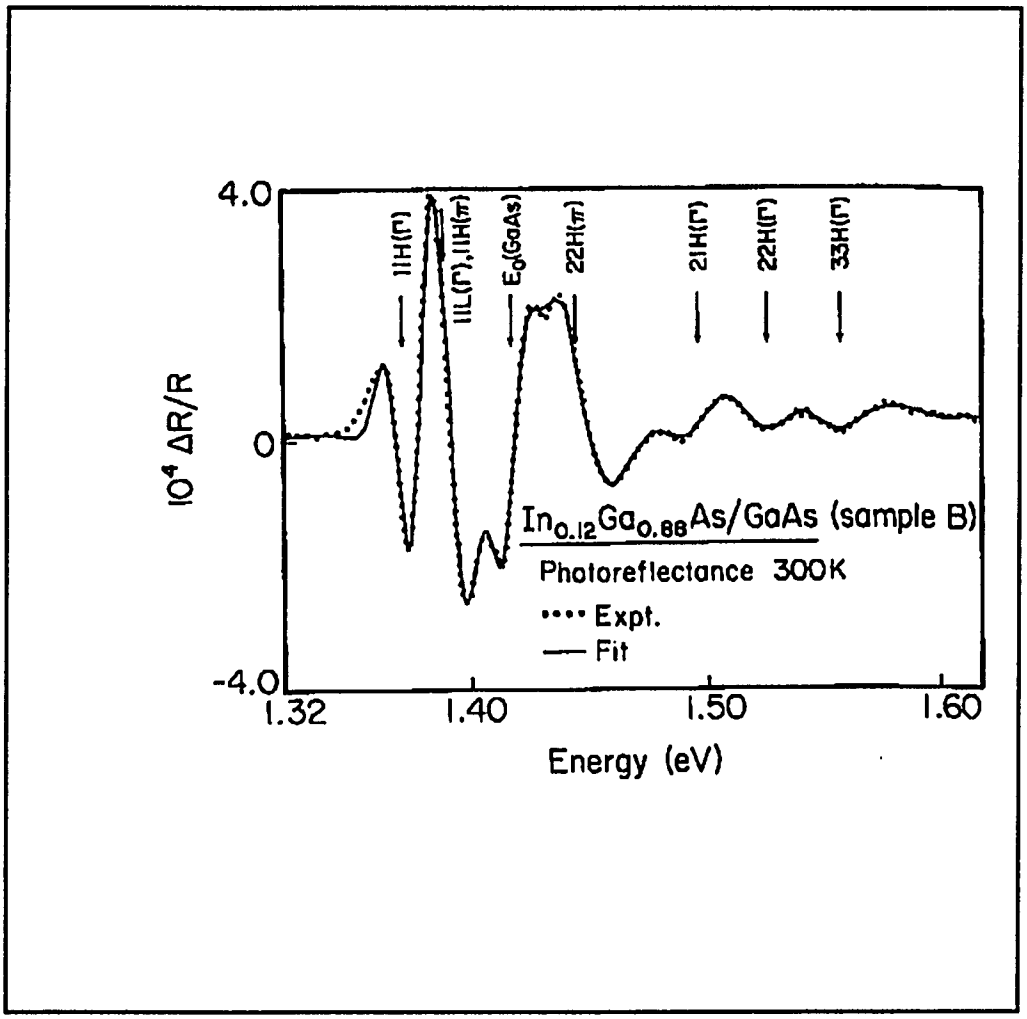

Figure 31 PR spectrum (dotted lines) of an $In_{0.12}Ga_{0.88}As/GaAs$ coupled multiple quantum well (Sample B) at 300K. The solid line is a lineshape fit as discussed in the text.

Since for our case $\epsilon<0$, the effect of the lattice-mismatch strain is to (1) increase the energy gap of the InGaAs (hydrostatic-pressure component), and (2) split the degeneracy of the valence-band edge at the center of the Brillouin

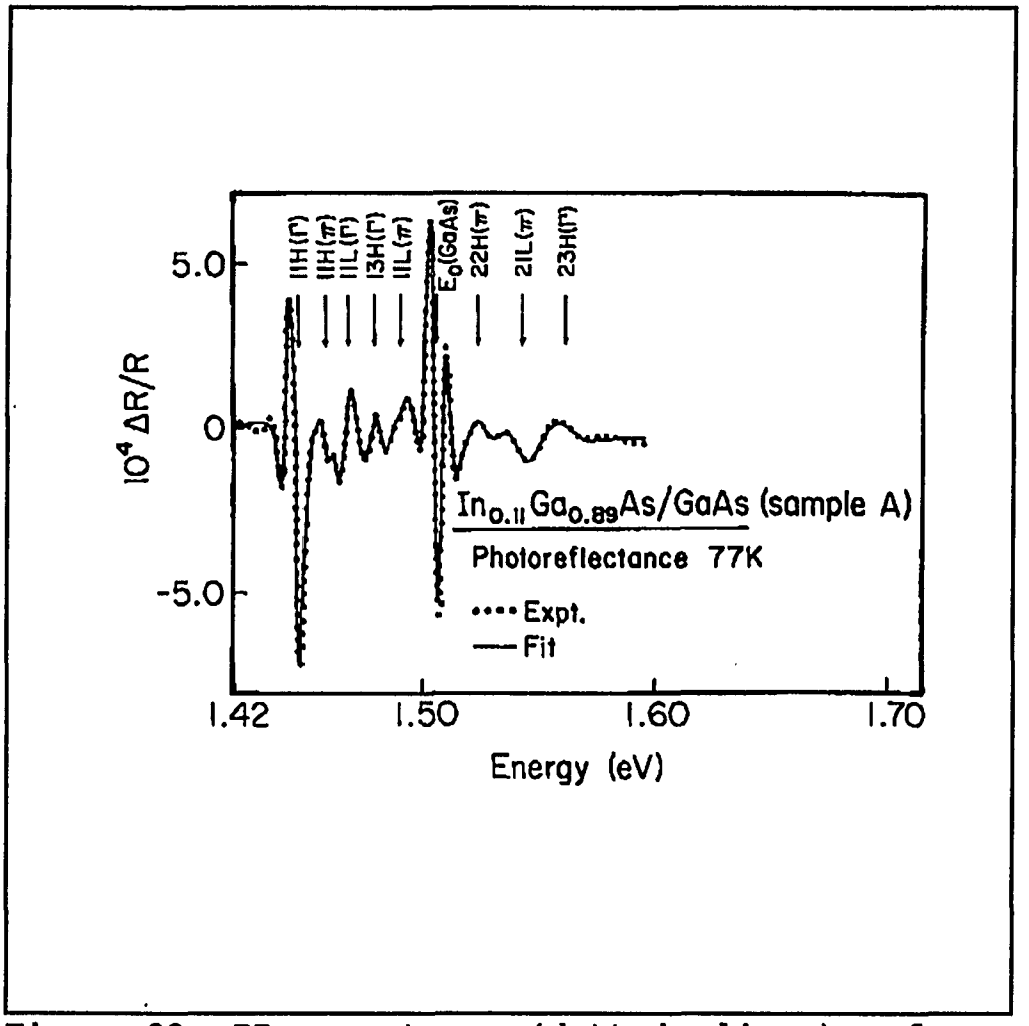

Figure 32 PR spectrum (dotted lines) of an $In_{0.11}Ga_{0.89}As/GaAs$ coupled multiple quantum well (Sample B) at 77K. The solid line is a lineshape as discussed in the text.

zone so that the heavy-hole band moves up and light-hole band moves down, relative to the unstressed valence band. Thus in such a system the relative positions of band in the InGaAs wells and GaAs barrier can lead to two possible configurations

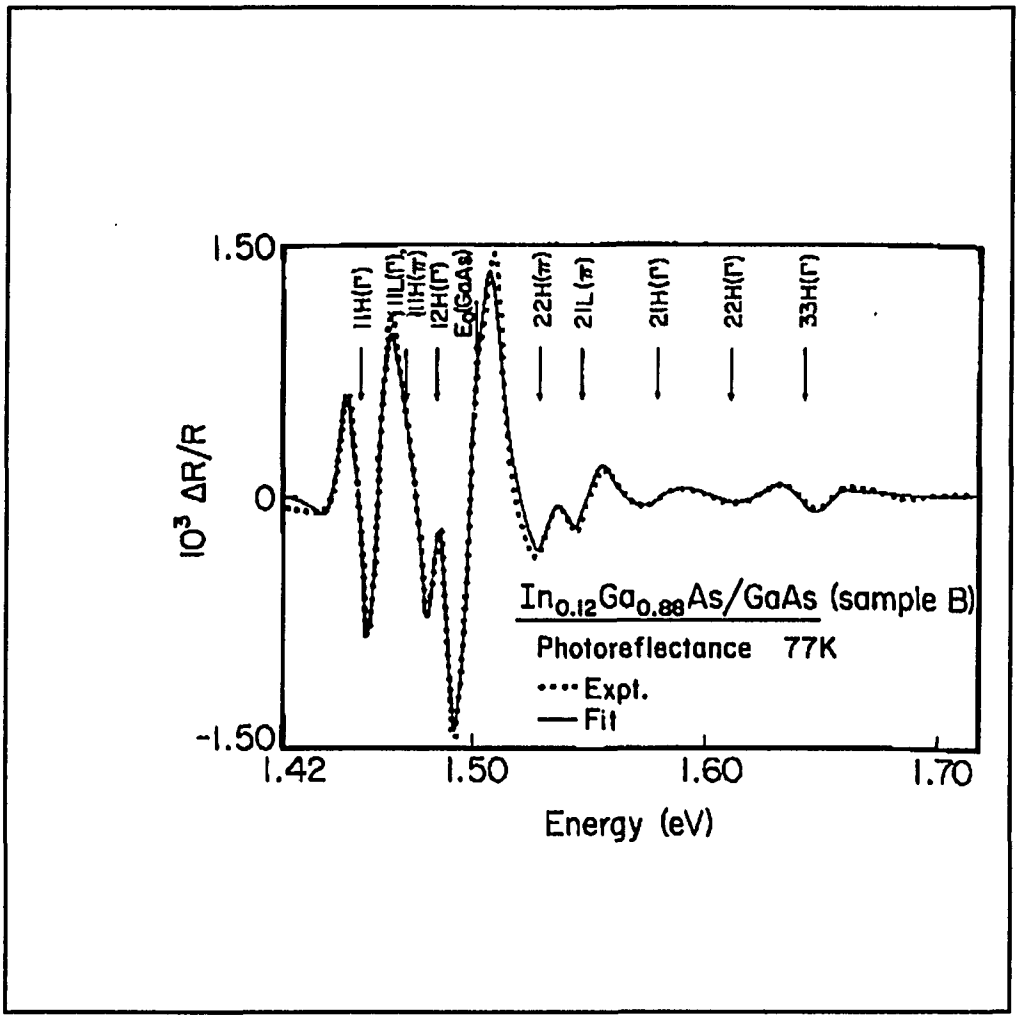

Figure 33 PR spectrum (dotted lines) of an $In_{0.12}Ga_{0.88}As/GaAs$ coupled multiple quantum well (sample B) at 77K. The solid line is a lineshape fit as in the text.

of the superlattice potential as shown in Fig. 34. In the configuration on the left-hand side the electron and both the heavy and light holes are confined in the InGaAs wells (type-I superlattice). However, in the configuration on the right-hand side

the electrons and heavy holes are in the $In_xGa_{1-x}As$ region (type-I) while the light holes are in the GaAs layers (type-II).

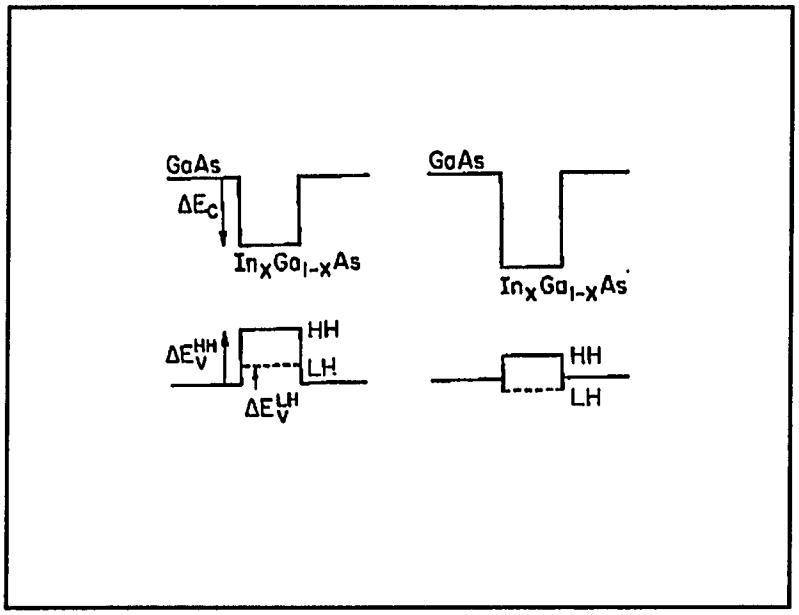

Figure 34 Possible energy-band configuration in a strained layer $In_xGa_{1-x}As/GaAs$ quantum well.

In order to calculate the subband energies of the MQW structures, we used the envelope function model [82] discussed before and strain-induced shifts and splitting given above. The values of the various strain-related parameters used in the calculation are listed in table VIII. Linear interpolation was used for InGaAs values. The values of the energy gaps and masses are as follows:

$$E_o(In_xGa_{1-x}As)=E_o(GaAs)-1.53x+0.45x^2 \qquad (91)$$

at 300K from Ref. 63,

$$E_o(In_xGa_{1-x}As)=E_o(GaAs)-1.47x+0.375x^2 \qquad (92)$$

at 77K from Ref. 139,

$$\Delta_o=0.341-0.09x+0.14x^2 \qquad (93)$$

from Ref. 140,

$$m^*_c=(0.0665-0.044x)m_o \qquad (94)$$

from Ref. 141,

$$m^*_{LH}=(0.094-0.062x)m_o \qquad (95)$$

from Ref. 142 and

$$m^*_{HH}=(0.45-0.07x)m_o \qquad (96)$$

from Ref. 142, where m_o is the free-electron mass. The band alignment was used as an adjustable parameter. Also, since our barriers are relatively

thin (≈100Å), coupling effects (miniband dispersion) were taken into account. The temperature or stress dependence of the masses in the [100] direction were neglected. In addition to energy considerations, we have employed intensity effects (i. e., wave-function overlap) to correlate the spectral features with intersubband transition. Listed in Tables IX and X are the theoretical values of transition energies for samples A and B, respectively.

Shown by the dotted lines in Figs. 30 and 31 are the experimental PR spectra at 300K of sample A and B, respectively. The dotted lines in Figs. 32 and 33 indicate the experimental PR spectra at 77K from sample A and B, respectively. The solid lines in these figures are a least-squares fit of a lineshape function to the experimental data. The obtained energies of the various transitions are indicated by arrows at the top of the figures. The feature denoted E_o(GaAs) corresponds to the direct band gap of unstrained GaAs and originate in the GaAs buffer-substrate region of the sample. Similar observations have been made in previous PR studies

of this system [117, 122]. The energy of this feature at 300 and 77K is used in Eqs. 91 and 92, respectively, to calculate $E_o(In_xGa_{1-x}As)$.

Due to a combination of relatively small confinement energies and barrier widths of these samples, there is significant coupling between wells even for the fundamental heavy-hole to conduction-subband transition. We know that this coupling leads to different transition energies at the mini-Brillouin zone center (Γ) and edge (π) along the growth direction (miniband dispersion).

The energies of other structures for sample A and B, which originate in MQW structure, are listed in Table VIII and IX, respectively. In order to minimize any possible exciton-binding-energy as well as temperature effects, we also have listed the energies relative to the lowest-lying feature, which we identify as 11H (Γ). The notation mnh (or L) indicates transitions from the m^{th} conduction to n^{th} valence subband of heavy-(H) or light-(L) hole character. The designation Γ or π denotes transitions at the minizone center or edge, respectively .

For both samples there is almost no temperature dependence of the intersubband energies relative to 11H(Γ). This means that the temperature dependence of the effective mass plays a minor role. The transition E_o(GaAs) can clearly be identified as unconfined and occur below the blank lines in Tables VIII and IX. For sample A the best overall agreement was obtained for x=0.11±0.01, L_z=52±3 Å, L_B=105±5 Å and conduction band offset of 0.7±0.05. For sample B, the best fit was found for x=0.12±0.01, L_z=32±3Å, L_B=95±5Å and conduction band offset of 0.70±0.05.

As we see in Tables IX and X, for the 11H(Γ) transition, there is about a 4-5 meV difference, which may be due to exciton effects. For uncoupling states, the exciton binding energy should be about 10 meV for $In_xGa_{1-x}As$ with such narrow wells [82, 141]. The coupling effect may reduce this value. Therefore 4~5 meV is quite reasonable for the exciton binding energy in such strongly coupled states.

We now turn our attention to the 11L(π) transitions. It can be demonstrated, from both

symmetry arguments as well as a detailed matrix-element (wave function overlap) calculation, that if the light holes are confined in the GaAs region, 11L(π) should be a very weak feature. This transition corresponds to the antisymmetric component of the splitting caused by the coupling, while 11L(Γ) is related to the symmetric component. It can also shown that even for type-II configuration 11L(Γ) is still fairly strong. These considerations are certainly consistent with our observation for sample B, in which we do not observe 11L(π), which should occur above 60 meV above 11H(Γ). Note that there is no feature in this energy range in Fig. 31 or 33. For sample A we apparently do observe 11L(π), but it is difficult to determine its amplitude since it occurs on the low-energy side of E_o(GaAs). It has been demonstrated that there are often considerable interference effects on the low energy shoulders of features originating from the barrier and/or substrate[143, 144]. This complicates the evaluation of the amplitude of 11L(π) for sample A. However, the situation of the sample B is clear. The fact that we can clearly observe 11L(Γ) for

sample A demonstrates that "spatially indirect" transitions can be observed in modulated reflectivity, as first pointed out in Refs. 117 and, 122.

For strained-layer systems, a convenient quantity is the average valence-band edge E_v^{av} given by

$$E_v^{av}=1/3(E_v^{HH}+E_v^{LH}+E_v^{SO}) \qquad (97)$$

where E_v^{SO} is the spin-orbit-split valence band. The parameter E_v^{av} is useful because it is independent of the uniaxial component of the strain. Thus we can define

$$\Delta E_v^{av}=E_v^{av}(In_xGa_{1-x}As)-E_v^{av}(GaAs) \qquad (98)$$

based on our result of $Q_c=0.7\pm0.05$ for samples with $x\approx 0.12$, we find that a linear extrapolation to $x=1$ yields $\Delta E_v^{av}=0.1\pm0.1$ eV for the InAs/GaAs interface. Menendez et al. report $\Delta E_v^{av}=0.49\pm0.10$ eV extrapolated to the InAs/GaAs system [79]. A similar value for the band lineup also has been deduced from

measurements on $In_xGa_{1-x}As/GaAs$ bipolar structures [145]. There have been several theoretical calculations of the band lineup of this system. Using a self-consistent calculation, including strain effect, Van de Walle finds $\Delta E_v^{av}=0.37$ eV for the [001] InAs/GaAs interface [142]. Tersoff's midgap theory yields 0.0 eV, while Cardona and Christensen [114] find $\Delta E_v^{av}=-0.15$ eV. These values should be corrected for the hydrostatic-pressure component of the strain. However, this effect should be quite small [114]. As pointed out in Ref. 146 the above value is based on a preliminary calculation for the [001] interface. The author notes that a full study should really include a determination of the stable structure by minimization of the total energy with respect to the atomic positions near the interface. Van de Walls has assumed that the InAs and GaAs bond lengths at the interface are equal and given by the average of the bond lengths in each material (one of which is strained). It turns out that the band lineups are fairly sensitive to the choice of this parameter; changing the position of the As atom by 0.1 Å in the [001] direction can

Table VIII. The material parameters used in calculating the stress-dependent band gaps in $In_xGa_{1-x}As$

Material	a_0 (Å)	a (eV)	b (eV)	C_{111} 10^{11}dyn/cm^2	C_{12} 10^{11}dyn/cm^2
GaAs	5.6533[a]	-9.8[b]	-1.76[b]	11.88[b]	5.32[a]
InAs	6.0584[c]	-5.8[b]	-1.80[b]	8.33[c]	4.53[c]

a) Reference 102
b) Reference 66, Landolot-Bornstein, New Series Group III
c) Reference 63

Table IX. Experimental and theoretical values at 300 and 77K of the energies of the various features of an $In_{0.11}Ga_{0.89}As/GaAs$ coupled multiple quantum well (sample A). To minimize exciton and temperature effects, the energies relative to the lowest-lying transition, 11H(Γ), also are listed. The first five features are unconfined. The best theoretical results are obtained for L_z=52±3Å, L_B=105±5Å, and a heavy-hole valence-band offset of 0.30±0.05.

Spectral features	Experiment				Theory			
	300K		77K		300K		77K	
	E (meV)	E-E[11H(Γ)] (meV)	E (meV)	E-E[11H(Γ)] (meV)	E (meV)	E-E[11H(Γ)] (meV)	E (meV)	E-E[11H(Γ)] (meV)
11H(Γ)	1358±2	0	1448±1	0	1363	0	1453	0
11H(π)	1368±2	10±4	1459±1	11±2	1371	8	1461	8
11L(Γ)	1379±3	21±5	1469±2	21±3	1388	25	1478	25
13H(Γ)	1392±3	34±5	1481±2	33±3	1393	30	1483	30
11L(π)	1405±5	47±7	1493±4	45±5	1407	44	1497	44
22H(π)	1439±3	81±5	1527±2	79±3	1438	75	1528	75
21L(π)	1455±4	97±6	1546±3	98±4	1454	91	1544	91
23H(Γ)	1476±4	118±6	1563±3	117±4	1490	127	1580	127

Table X. Experimental and theoretical values at 300 and 77K of the energies of the various features of an $In_{0.12}Ga_{0.88}As/GaAs$ coupled multiple quantum well (sample B). To minimize exciton and temperature effects, the energies relative to the lowest-lying transition, 11H(Γ), also are listed. The first five features are unconfined. The best theoretical results are obtained for L_z=32±3Å, L_B=95±5Å, and a heavy-hole valence-band offset of 0.30±0.05.

Spectral features	Experiment				Theory			
	300K		77K		300K		77K	
	E (meV)	E-E[11H(Γ)] (meV)	E (meV)	E-E[11H(Γ)] (meV)	E (meV)	E-E[11H(Γ)] (meV)	E (meV)	E-E[11H(Γ)] (meV)
11H(Γ)	1372±3	0	1453±2	0	1376	0	1457	0
11L(Γ)	1389±5	17±8	1473±4	20±6	1397	21	1478	21
11H(π)	1389±5	17±8	1473±4	20±6	1397	21	1478	21
12H(Γ)			1487±2	33±4	1409	33	1490	33
22H(π)	1446±6	74±9	1532±3	79±5	1458	82	1539	82
21L(π)			1551±3	98±5	1478	102	1559	102
21H(Γ)	1499±6	127±9	1582±4	129±6	1507	131	1588	131
22H(Γ)	1528±3	156±6	1616±5	163±7	1540	164	1621	164
33H(Γ)	1560±6	188±9	1646±4	193±6	1566	190	1647	190

shift the lineups by as much as 0.3 eV.

In conclusion we have performed PR on two [001] $In_xGa_{1-x}As/GaAs$ strained-layer, coupled MQW's. We have observed a number of features corresponding to miniband dispersion of both confined and unconfined states. Comparison of the experimental intersubband energies with an envelope-function calculation yields $x=0.11\pm0.01$, $L_z=52\pm3$ Å, and $L_B=105\pm5$Å for sample A and $x=0.12\pm0.01$, $L_z=32\pm3$Å and $L_B=95\pm5$ Å for sample B. This agrees well with those deduced from the growth conditions. For both samples we find a heavy-hole valence-band-offset parameter of 0.36 ± 0.05.

Chapter V. EVOLUTION OF THE SURFACE VOLTAGE OF AIR EXPOSED MBE-GROWN (100) GaAs [156]

At the surface and interface of GaAs it is well known that the Fermi level (V_f) is pinned in the energy gap by surface states. The position of V_f at the surface cannot simply be derived from its bulk value but has to be measured separately for every surface, each of which may differ by crystallographic orientation or environment [147]. Recent work has elucidated the role of orientation-dependent chemistry on the Schottky barrier formation at metal/GaAs interfaces [148]. Most studies of V_f have involved soft X-ray photoemission (PES). However as pointed out by Hecht, surface photovoltage (V_s) effects in PES are significant [149, 150, 151]. Thus V_s may be important in other optical probes of V_F.

In order to explore the role of environment and V_s on the evaluation of V_f we have used photoreflectance (PR) to study the surface barrier height on (100) MBE-grown n-and p-GaAs both in-situ in the MBE growth chamber and after exposure to air.

Measurements were performed as a function of temperature (77K<T<450K) and light intensity of both the pump (I_{pu}) and probe (I_{pr}) beams. The n- and p-samples had a well controlled electric field (F) created by fabricating an undoped layer of thickness L on a buried 1μm (a) Si-doped (n-2x10^{18} cm^{-3}) buffer on an n^{+} substrate or (b) Be-doped (p-4x10^{18} cm^{-3}) buffer on a p+ substrate, respectively [147]. The pump beam was the 6328 A line of a He-Ne laser.

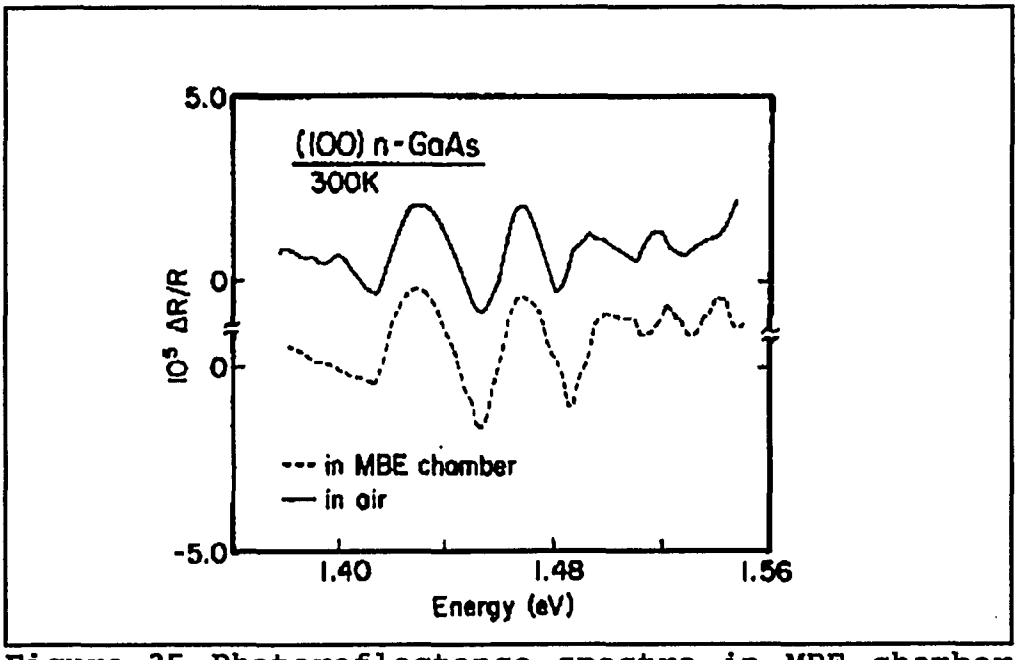

Figure 35 Photoreflectance spectra in MBE chamber and after exposure to air

Shown by the solid and dashed lines in Fig. 35 are the PR spectra of the n-sample (L-228nm) at 300K in the ultra-high vacuum (UHV) MBE chamber and

immediately after exposure to air, respectively, with $I_{pu}=10\mu W/cm^2$ and $I_{pr}=2\mu W/cm^2$. Similar results were obtained for the p-sample. The field F can be determined from the observed Franz-Keldysh oscillations (FKO) from the equation (50). This plot is shown in Fig. 36. The measured barrier height V_m $(=V_F-V_s)$ is given by $V_m = FL+[\epsilon F^2/2qn(p)]+(kT/q)$, where ϵ is the static dielectric constant of GaAs and n(p) are the carrier concentrations in the buffer layers.

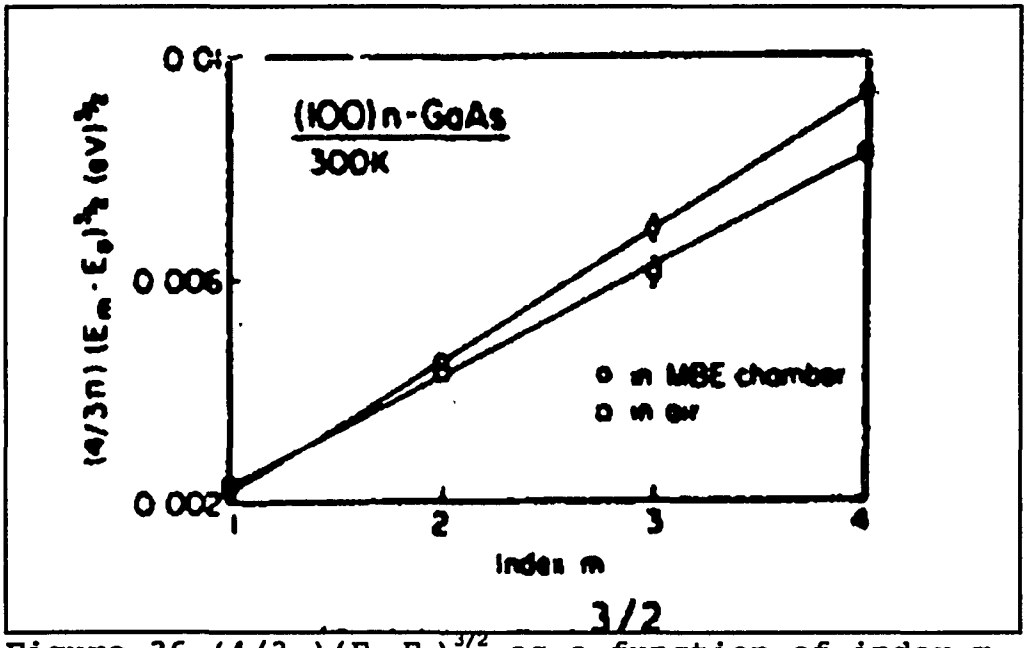

Figure 36 $(4/3)(E_m-E_o)^{3/2}$ as a function of index m.

From above analysis we find for the n-and p-samples in UHV and in air the following values of V_m relative to the conduction and valence bands,

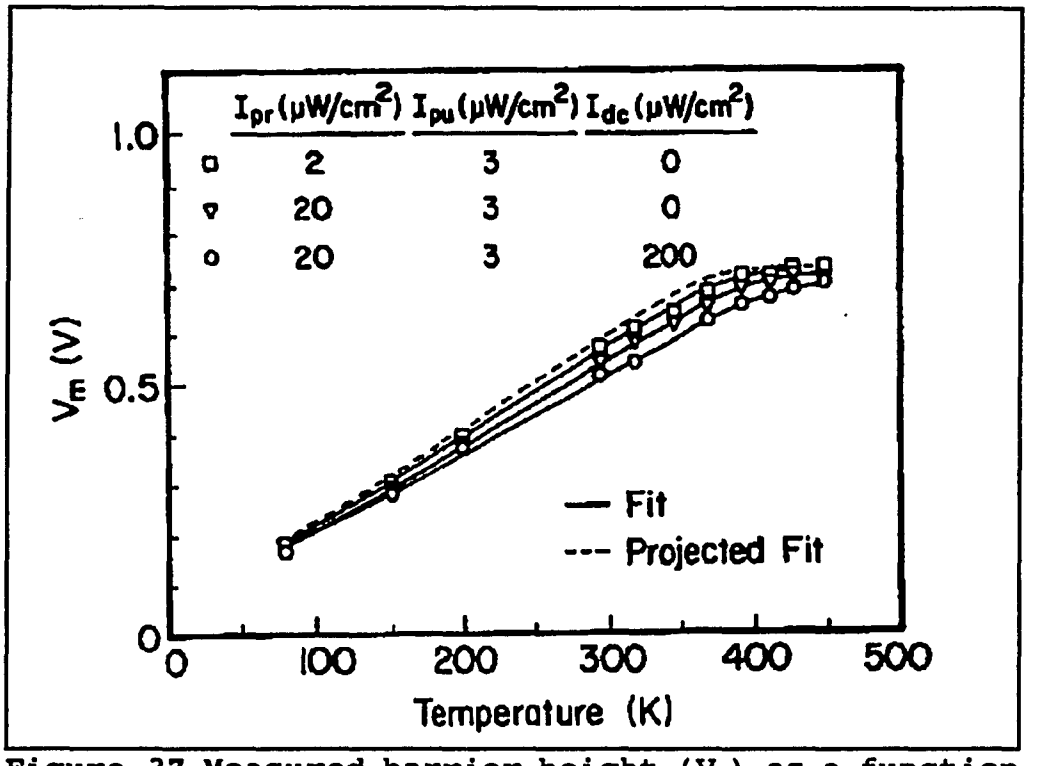

Figure 37 Measured barrier height (V_m) as a function of temperature and light intensity.

respectively: V^n_m((UHV)=0.69±.025V V^n_m(air)=0.57±0.025V, V^p_m(UHV)=0.74±0.035V and V^p_m(air)=0.66±0.035V. There is a significant difference in surface potential between the UHV and air-exposed surfaces. First we see that [V^n_m(UHV)+ V^p_m(UHV)]= 1.43eV, (the band gap energy for GaAs) and is greater than the sum of the n and p surface potentials for air exposed surfaces(=1.23eV). Therefore, the air-exposed surface is more "flat band" and hence less "pinned" than the UHV surface.

We can understand this difference from the following considerations. In Ref. 148 it was shown that surface state density and hence "pinning intensity" is correlated with the degree of misorientation for (100) surfaces. This in turn correlates with atomic step density. Furthermore, Ref. 148 showed that there is increased chemical reactivity at these atomic steps. If so, we might expect enhanced selective oxidation at atomic steps during air exposure. Therefore to explain the results of this work we surmise that in the UHV condition there is a maximum in surface state density due to "unpassivated" atomic steps. Air exposure causes preferential oxidation and hence passivation at the atomic steps. This in turn reduces the surface state density and hence the pinning density.

On an n-sample (L-110nm) that had been exposed to air for several days we explored the effects of temperature and light intensity. Shown in Fig. 37 are V_m for 77<K<450K for $I_{pu}=3\mu W/cm^2$ and $I_{pr}=2$ and $20\mu W/cm^2$. Up to about 350K the variation of V_m with T is approximately linear and then saturates at higher temperatures; for larger I_{pr} this saturates

shifts to higher T. The solid lines are least-squares fits to [149]:

$$V_m = V_F - V_s \qquad (99)$$

Where

$$V_s = (nkT/q)\ln\{[J_{PC}/J_0(T)]\exp(qV_F/kT)+1\} \qquad (100)$$

where n is an ideality factor, J_{pc} is an adjustable parameter which represents the induced photocurrent created within the depletion and buffer (diffusion) regions and $J_o(T)$ is the saturation current which depends on the dominant current flow mechanism. For our sample configuration and temperature range, thermionic emission and diffusion are the main contribution to $J_o(T)$. One can write [155] $J_o(T)=A^{**}T^2/(1+BT^{3/2})$, with $A^{**}=8.0$ A/cm^2-k^2 (modified Richardson constant) and $B=3.3X10^{-4}K-3/2$.

As can be seen from Eq.(99), at sufficiently high temperatures V_s becomes negligible and V_m approaches V_F. In his low temperature analysis Hecht [149] omitted the unity term in the brackets of

Eq.(99) and hence his expression for V_s does not become zero at elevated temperatures. Our analysis yields n=0.91, $J_{pc}=(1.2\pm0.6)\times10^{-4}/cm^2$ (for the lower light level) and V_F= 0.73±0.02V, the latter in good agreement with other measurements.[152, 153, 154]

Shen et al have recently explored the influence of light intensity on the determination of V_F at 300K in similar n-GaAs and n-GaAlAs structures[154]. They did not study temperature effects or make a detailed comparison with theory such as Eq.(99).

In conclusion, from the FKO oscillations observed in the PR spectra of n-and p-GaAs samples with well controlled F we have investigated the effects of environment on the determination of V_F The details of the dependence of V_m on T and light intensity can be explained by an extension of the Hecht theory [149].

Chapter VI

SUMMARY AND CONCLUSIONS

This thesis is an investigation of semiconductors and semiconductor microstructures by using electromodulation spectroscopy. Samples used in this study are $Ga_{1-x}Al_xAs/GaAs$, $In_xGa_{1-x}As$ and GaSb/AlSb MQWs, semi-insulating GaAs and InP bulk materials, and heterostructures including $Ga_{0.82}Al_{0.18}As$ and $In_xGa_{1-x}As$ (x=0.06 and 0.15).

We have demonstrated that photoreflectance can be used to measure the direct gap E_o of III-V semiconductor materials in a wide temperature range, up to 600°C. We have demonstrated that while both electron-optic and electron-acoustic phonon interactions contribute to the energy shifts of the band gap (E_o) of InP and $In_xGa_{1-x}As$ (x=0.06 and 0.15), the temperature dependence of the broadening parameter $\Gamma(E_o)$ is due mainly to electron-optical phonon interaction. This finding is consistent with the theory developed by Cardona et al.

We also made considerable progress in developing PR as an in-situ monitoring/control

method for semiconductor growth. Measurements have been performed in an actual metalorganic chemical vapor deposition (MOCVD) reactor. We found a systematic difference between the temperature of the GaAs substrate and a thermocouple not in contact with the sample. Also, it is now possible to evaluate Aluminum composition in GaAlAs during actual growth. Another major step forward has been the substantial reduction in data acquisition time to 30 seconds, so that real-time measurements are now feasible.

We have studied alternating composition layers of MQW, both lattice-matched systems($Ga_{1-x}Al_xAs$/GaAs MQW) and lattice-mismatched or strained systems ($In_xGa_{1-x}As$/GaAs and GaSb/AlSb MQW). The rich spectra that were observed consisted of both confined transitions (CT) and unconfined transition(UT). Both CT and UT exhibited coupling effects between wells(miniband dispersion). It helps us not only to examine existing theories such as Bastard Model theory, but also to experimentally determine: 1) the important parameter of the band alignment of the heterostructures; 2) alloy composition of the

epilayers; and 3) the width of wells and barriers.

In Conclusion, this study can be summarized as follows:

1). Modulation spectroscopy, especially photoreflectance, is a powerful tool to investigate and characterize the semiconductor microstructures.

2). Temperature dependence of Energy gap (E_o) and broadening parameter ($\Gamma(E_o)$) yields information about electron-phonon interaction and exciton effect. The parameters which describe the temperature behavior of energy gaps were evaluated.

3). We have found that both electron-optical and electron-acoustic phonon interactions contribute to the energy shifts of the band gap (E_o) of InP and $In_xGa_{1-x}As$ (x=0.06 and 0.15).

4). We have also found that mainly the electron-optical phonon interaction contributes to the broadening of the energy gaps.

5). The direct gap (E_o) of GaAs, $Ga_{0.82}Al_{0.18}As$, InP and $In_xGa_{1-x}As$ (x=0.06 and 0.15) can be evaluated to ±5 meV at 600°C. Thus, the

temperature of the GaAs and InP substrate material could be determined to ±10°C.

6). Considerable progress in developing PR as a in-situ tool to monitor thin film growth was made. PR measurements have been performed at a real MOCVD reactor. Also, the acquisition time was reduced to 30 seconds for GaAs at 650°C by reforming the software and hardware.

7). Photoreflectance spectra from a series of $Ga_{0.82}Al_{0.18}As$ multiple quantum wells (MQW) exhibit coupling effects between wells in several confined as well as unconfined transitions.

8). From the PR spectra of strained layer, coupled MQW, $In_xGa_{1-x}As/GaAs$, the conduction band offset parameter was evaluated to be 0.7±0.05.

9). Investigation of the GaAs/AlSb MQW enables us to determine that the conduction band offset parameter is 0.85±0.08

10. Form the FKO observed in the PR spectra of n- and p-GaAs samples with well controlled F we have investigated the effects of environment on the determination of V_f.

Bibliography

1. See for example, K. Onabe, Y. Tashiro, and Y. Ide, Surf. Sci. 174, 401(1986).

2. S. Yamada, T. Fukui and A. Sugimura, Surf. Sci, 174, 444(1986).

3. A. C. Wright and J. O. Williams, Mat. Letts.,3, 80(1985); R. D. Dupuis, R. C. Millier and P. M. Petroff., Mat. Letts., 3, 398(1985).

4. R. Dingle., Wiegman, W. and C. H. Henry, Phys. Rev. Lett. 33, 827(1974).

5. C. Weisbuch, R. C. Miller, R. Dingle, A. C. Gossard and W. Wiegmann, Solid State Commun. 37, 219(1981).

6. R. C. Miller, D. A. Kleinman and A. C. Gossard, Phys. Rev. B29, 7085(1984).

7. A. Pinczuk and J. M. Worlock, Surf. Sci. 113, 69(1982).

8. P. Lautenschlager, M. Carriga and S. Logothetidis and M. Cardona, Phys. Rev. B35, 9174(1987) and references therin.

9. P. Lautenschlager, M. Carriga and M. Cardona, Phys. Rev. B36, 4813(1987) and references therin.

10. H. Shen, P. Parayanthal, Y. F. Liu and F. H. Pollak, Rev. Sci. Instrum. 58, 1429(1987).

11. D.E. Aspnes in Handbook on Semiconductors, ed. by T.S. Moss (North-Holland, New York, 1980) Vol. 2, P.109. and F. Bassni and G. P. Parravicini, Electric State and Optical Transition in Solid (Ammerica Press, 1975).

12. M. Cardona in Modulation Spectroscopy (Academic, New York, 1969) and references therin.

13. H. Shen, S. H. Pan, F. H. Pollak, M. Dutta and T. R. Aucoin, Phys. Rev. B36, 9384(1987).

14. H. Shen, F. H. Pollak and J. M. Woodall, J. Vac. Sci. Technol., B7, 804(1989).

15. H. Shen, Z. Hang, S. H. Pan, F. H. Pollak and J. M. Woodall, Appl. Phys. Letts. 52, 2058(1988); H. Shen, Z. Hang, S. H. Pan, F. H. Pollak, T. F. Kuech, J. M. Woodall and R. N. Sacks, Proceedings of the 9th International Conference on the Physics of Semiconductors, Warsaw, 1989, ed. by W. Zawadzki (Institute of Physics, Polish Academy of Science, Warsaw, 1989) p1087.

16. F. H. Pollak and O. J. Glembocki in Proceedings of the Society of Photo-Optical Instrumentation Engineers (SPIE, Bellingham, 1988), 946, 2(1988).

17. O. J. Glembocki and B. V. Shannbrook, Superlattices and Microstructures, 5, 603(1989).

18. F. H. Pollak and H. Shen, to be published in J. Crystal Growth.

19. O. J. Glembocki and B. V. Shannbrook, N. Bottka, W. T. Beard and J. Comas, Appl. Phys. Lett. 46, 970(1985); Also in Proceedings of the Society of Photo-Optical Instrumentation Engineers (SPIE, Bellingham, 1985) 24, 86(1985).

20. R. N. Bhattacharya, H. Shen, P. Parayanthal, F. H. Pollak, T. Coutts and H. Aharoni, Phys. Rev. B37, 4044(1988); also Proceedings of the Society of Photo-Optical Instrumentation Engineers (SPIE, Bellingham, 1987) 794, 81(1987); also, Solar Cells 21, 371(1987).

21. R. Glosser and N. Bottka, Proceedings of the Society of Photo-Optical Instrumentation Engineers (SPIE, Bellingham, 1987) 794, 88(1987);

22. H. Shen, F. H. Pollak and J. M. Woodall, J. Vac. Tech. B8(3), 413(1990).

23. X. Yin, F. H. Pollak, L. Pawlowicz, T. O'Neill, and M. Hafizi, Appl. Phys. Lett, 56, 1278(1990).

24. X. Yin, H. M. Chen, F. H. Pollak, Y. Chen, P. A. Montano, J. M. Woodall, P. D. Kirncher and D. Pettit, Proceedings of the 20th International Conference on the Physics of Semiconductors, Greece, 1990.

25. H. Shen and etc. to be published in Appl. Phys. Lett.

26. See, for example, H. Shen, S.H. Pan, Z. Hang, J. Leng, F.H. Pollak, J.M. Woodall and R.N. Sacks, Appl. Phys. Letts. 53, 1080 (1988).

27. Z. Hang, H. Shen and F. H. Pollak, Solid State Comm. 73 ,5(1990).

28. Z. Hang, H. Shen, and F. H. Pollak, to be published in proceeding of the Socity of Phot-Optical Instrumentation Engineers (SPIE), 1285(1990).

29. Z. Hang, D. Yan, and F. H. Pollak, submitted to Phys. Rev B.

30. P. Lautenschlager, P. B. Allen and M. Cardona, Phys. Rev. B33, 5501(1986).

31. P. B. Allen and M. Cardona, Phys. Rev. B23, 1495(1981).

32. Sudha Goaplan, P. Lautenschlager and M. Cardona, Phys. Rev. B35, 5577(1987).

33. P. B. Allen and M. Cardona, Phys. Rev. B27, 4760(1983).

34. P. Lautenschlager, P. B. Allen and M. Cardona, Phys. Rev. B31, 2163(1985).

35. A. Manoogian and J. C. Woolley, Can. J. Phys. 62, 285(1984).

36. K. Capuder, P. E. Norris, H. Shen, Z. Hang and F. H. Pollak, J. of Electr. Mat. 19, 295(1990).

37. F. H. Pollak, to be published in Superlattice and Microstructures.

38. L. Esaki in Proceedings of the 17th International Conference on the Physics of Semiconductors, Berkely, 1984. ed by J. O. Chodi and W. A. Harrison (Springer Verlay, NY 1985) p473.

39. L. Esaki in Recent Topics in Semiconductor Physics, ed by H. Kamimurs and Toyozawa, World Scientific, Singapor, 1983, p1.

40. K. Ploog and G. H. Dohler, Advances in Physics, 32, 285(1983).

41. R. Dingle, Advances in Solid State Physics, Vol. XV, ed by H. J. Quiesser(Braunschweig: Pergamon-Vierwag, 1975) p21, ibid Festkorperprobleme 15, 21(1975).

42. H. Shen, S. H. Pan, Z. Hang, F. H. Pollak, and R. N. Sacks, Solid State Comm, 65, 929(1988).

43. S. H. Pan, H. Shen, Z. Hang, F. H. Pollak, T. F. Kuech J. C. Lee, T. E. Schesinger and M. A. Shahid, Superlattices and Microstructures, 4, 609(1988).

44. S. H. Pan, H. Shen, Z. Hang, F. H. Pollak, W. Zhuang, Q. Xu, A. P. Roth, R. A. Masut, C. Lacelle and D. Morris, Phys. Rev. B38, 3375,(1988). and also in the Proceedings of the Society of Photo-Optical Instrumentation Engineers (SPIE, Bellingham, 1989) 943.

45. H. Shen, Z. Hang, Jing Leng, F. Pollak, L. L. Chang, W. I. Wang and L. Esaki, Superlattices and Microstructures, 5, 591(1989).

46. F. H. Pollak, in Proceeding of the Society of Photo Optical Instrumentation Engineers (SPIE, Bellingham, 1981) 276, 142 (1981 and references therein).

47. Y. Hamakawa and T. Nishino in Optical Properties of Solid: New Developments, ed by B. O. Seraphin (North Holland, N. Y. 1976) p 225.

48. B. O. Seraphin and N. Bottka, Phys. Rev 145, 628(1966).

49. J. Gallaway, Phys. Rev. 130, 549(1963); and K. Tharmalingham, Phys. Rev. 130, 2204(1963).

50. D. E. Aspenes, Phys. Rev. 147, 554(1966) and J. Callaway, Phys. Rev 134, A998(1964).

51. K. S. Viswanathan and J. Callaway, Phys. Rev. 143, 564(1963).

52. F. H. Aymerich and F. Handler, and D. F. Blossey, Phys. Rev. 166, 921(1968).

53. D. E. Aspenes, Phys. Rev. 153, 927(1967).

54. H. Shen, Ph. D. Thesis, 1986, City University of New York, and H. Shen and F. H. Pollak, Phys. Rev. B42, 7097(1990).

55. N. Bottka, D. K. Gaskill, R. S. Sillman, R. Henrry and R. Glosser, J. Electron Mat. 17, 161(1988).

56. H. Shen, S. H. Pan, Z. Hang, Jing, F. H. Pollak, J. M. Woodall and R. N. Sacks, Appl. Phys. Lett., 53, 1080(1988).

57. T. F. Kuech, D. J. Wolford, R. Pototemski, J. A. Bradley, K. H. Kelleher, D. Yan, J. P. Farrel, P. M. S. Lesser and F. H. Pollak, Appl. Phys. Letts., 51, 505(1987).

58. Y. P. Varshni. Physica, 34, 149(1967).

59. N. F. Mott and H. Jones, The theory of

properties of metals and alloys. Dover Publication, New York, NY. 8(1958).

60. Z. Hang, H. Shen, and F. H. Pollak, J. Appl. Phys. 64, 3233(1988).

61. for example, S. M. Sze, in Physics of Semiconductor Devices, 2nd ed (John Wiley & Son, New York, 1981).

62. H. Mork and H. Unlu, in Semiconductors and Semimetals, ed by R. Dingle (Academic Press, New York, 1987) Vol 24, 135(1987).

63. S. Adachi, J. Appl. Phys, 58, R1(1985).

64. J. W. Mayer and S. S. Lau in Electronic Material Science: For Integrated Circuits in Si and GaAs (Macmillan, NY, 1990) P425.

65. Z. Hang, H. Shen, F. H. Pollak, Dave Pettit and J. Woodall, private communication.

66. Because both samples have low In concertration, the exciton binding energy should be closed to that of GaAs. The binding energy of exciton of GaAs (5 meV) The parameter Γ for both samples at room temperature is about 15 meV.

67. J. Singh and K. K. Bajai, Appl. Phys. Lett., 48, 1077(1986).

68. J. M. Woodal, G. D. Pettit, T. N. Jackson and Langa, Phys. Rev. Lett., 51, 1783(1983).

69. F. H. Pollak and R. Tsu in the Proceedings of the Society of Photo-Optical Instrumentation Engineers (SPIE, Bellingham).

70. Landolt-Bornstein, Numerical Data and Functional Relationships in Science and Technologya, ed. by O. Madelung, M. Schulz and H. Weiss (springer, New York, 1982) Vol III.17a, and III/22.

71. D. S. Kim and P. Y. Yu, Phys. Rev. B43, 4158,

(1991).

72. D. S. Kim and P. Y. Yu, Phys. Rev. lett. 64, 946(1990).

73. J. Shah, R. C. C. Leite and J. F. Scott, Solid State Comm., 8, 1089(1970).

74. M. J. Rosker, F. W. Wise and C. L. Tang, Appl. Phys. Lett., 49, 1726(1986).

75. L. Easki in Synthetic Modulated Structures, ed by L. L. Chang and B. C. Giessen (Academic press, New York) p3.

76. D. L. Smith and C. Maihiot, Rev. of Modern Phys, Vol. 62, 173(1990).

77. F. H. Pollak, Surf. Sci. 37, 863(1973).

78. J. Y. Marzin, M. N. Charasse and B. Sermage, Phys. Rev. B31, 8298(1985).

79. J. Menendez, A. Pinczuk, O. J. Werder, S. K. Sputz, R. C. Miller, D. L. Sivco, and A. Y. Cho, Phys. Rev B36, 8165(1987).

80. E. Merzbacher, Quantum Mechanics, 2nd ed, John Wiley and Son, New York, 1970) pp100-105.

81. G. Bastard, Phys. Rev. B25, 7584(1982).

82. G. Bastard and J. A. Brum, IEEE J. of Quant. Elect. Vol QE-22, 1625(1986).

83. E. O. Kane, J. Phys. Chem, Solids, 1, 249(1957). Sputz, R. C. Miller, D. L. Sivco and A. Y. Cho, Phys. Rev. B36, 8165(1987).

84. J. N. Schulman, and T. C. McGill, Phys. Rev. B19, 6341(1979).

85. J. N. Schulman, and Y. C. Change, Phys. Rev. B24, 4445(1981).

86. H. Shen, P. Parayanthol, F. H. Pollak, Authur

L. Smirl, J. N. Schulman, R. A. Mcfarlane, and Irnee D'Haenens, Sold state Comm., 59, 557(1986).

87. H. Shen, P. Parayanthol, F. H. Pollak, Authur L. Smirl, J. N. Schulman, R. A. Mcfarlane, and Irnee D'Haenens, in the 18th International Coference on the Physics of Semiconductors Stockolm, 1986.

88. G. Bastard, E. E. Mendez, L. Chang and L. Esaki Phys. Rev. B28, 3241(1983).

89. D. A. B. Miller, D. S. Chemla, T. C. Damen, A. C. Gossard, W. Wiegmann, T. H. Wood and C. A. Burrus, Phys. Rev. B32, 1043(1985).

90. B. V. Shanabrrok, O. J. Glembocki and W. T. Beard, Phys. Rev. B35, 2540(1987); also Proc. 18th Int. Physics of Semiconductors, Stockholm, 1986, ed by O. Engstrom (World Scientific, Stockhom, 1987) p. 565.

91. Y. Toyozawa, Progress of Theoretical Physics, 20. 53(1958).

92. For $x<0.4$ a value of $dEo(Ga_{1-x}Al_xAs)/dx$ of 1.247 has been repoted by S. Adachi, J. Appl. Phys.56, R1 (1985) while a value of 1.455 has recently been published by T. F. Kuech, D. J. Wolford, R. Potemski, J. A. Bradley, K. H. Kelleher, D. Yan, J. P. Farrell, P. M. S. Lesser and F. H. Pollak, Appl. Phys. Letts, 51, 505(1987).

93. H. Shen, P. Parayanthal, F. H. Pollak, M. Tomkiwicz, T. J. Drumond and J. N. Schulman, Appl. Phys. Letts, 48, 653(1986).

94. D. Lefebvre, B. Gil, J. Allegre, H. Mathieu, Y. Chen and C. Raisin, Phys. Rev. B35, 1230(1987-II).

95. P. Voison, C. Delalande, M. Voos, L. L. Chang, A. Segmuller, C. A. Chang and L. Easki, Phys. Rev. B30, 2276 (1984).

96. G. Griffiths, K. Mohammed, S. Subbanna, H. Kroemer and J. L. Merz, Appl. Phys. Letts, 43, 1059(1983).

97. A. Forchel, U. Cebulla, G. Trankle, G. Griffiths, S. Subbanna and H. Kromer, Surface Science 174, 143(1986).

98. A. Forchel, U. Cebulla, G. Trankle, E. Lach, G. Griffiths, S. Subbanna and H. Kromer, Phys. Rev. Lett. 57, 3217(1986).

99. U. Cebulla, G. Trankle, U. Ziem, A. Forchel, G. Griffiths, H. Kroemer and S. Subbanna, Phys. Rev. B37, 6778(1988).

100. C. Raisin, L. Assabatere, C. Allibert, B. Girault, G. Abdel-Fattah and P. Voisin, Solid State Comm. 61, 17(1987).

101. J. Menendez, A. Pinczuk, D. J. Werder, J. P. Valladares, T. H. Chin and W. T. Tsang, Solid State Comm, 61, 703(1987).

102. B. Rockwell, H. R. Chandraskair, M. Chandraskair, F. H. Pollak, H. Shen, L. L. Chang, W. I. Wang and L. Esaki, Surface Science, 228, 322(1990).

103. B. Rockwell, H. R. Chandraskair, M. Chandraskair, F. H. Pollak, H. Shen, L. L. Chang, W. I. Wang and L. Esaki, Mat. Res. Soc. Symp. Proc., 160,

104. P. Parayanthal, H. Shen, F. H. Pollak, O. J. Glembocki, B. V. Shanabrook and W. T. Beard, Applied Physical Letts., 48, 1261(1986).

105. P. Lefebvre, B. Gil, J. Allegre, H. Mathieu, Y. Chen and C. Raisin, Phys. Rev. B35, 1230(1987).

106. J. R. Chelikowsky and M. L. Cohen, Physical Rev. B14, 556(1976).

107. M. Cardona and F. H. Pollak, Physical ReV. 142, 530(1966); C. W. Higginbotham, F. H. Pollak and

M. Cardona in Proceedings of the 9th International Conference on the Physics of Semiconductors, Moscow, 1968, ed by S. M. Ryvkin (Nauka Publishing House, Leningrad, 1968) Vol.1 p57.

108. L. D. L. Brown, M. Jaros and D. Ninno, Physical Rev. B36, 2953(1987).

109. G. J. Gualtieri, G. P. Schwartz, R. G. Nuzzo and W. H. Sunder, Applied Phys. Lett., 49, 1037(1986).

110. P. Voisin, C. Delalande, G. Bastard, M. Voos, L. L. Chang, A. Segmuller, C. A. Chang and L. Esaki, Supperlattice and Microstructures 1, 155(1985).

111. C. Raisin, L. Lassabatere, C. Allibert, B. Girault, G. Abdel-Fattah and P. Voisin, Solid State Comm., 61, 17(1987)

112. J. Tersoff, Phys. Rev. B30, 4874(1984) and Phys. Rev. Letts, 56, 2755(1986).

113. C. G. Van de Walle and R. M. Martin, Journal of Vacuum Science and Technology B4, 1055(1986).

114. M. Cardona and N. E. Christensen, Phys. Rev. B35, 6182(1987).

115. A. P. Roth, R. A. Masut, M. Sacilotti, P. J. D'Arcy, Y. Le Page, G. I. Sproule and D. F. Mitchell, Superlatt. Microstructure. 2, 507(1986).

116. N. G. Anderson, W. D. Laidig, R. M. Kolbas, and Y. C. Lo, J. Appl. Phys., 60, 2361(1986).

117. U. K. Reddy, G. Ji, R. Houdre, H. Unlu, D. Huang and H. Morkoc, Proc. Soc. Photo-Opt. Instrum. Eng. 794, 116(1987).

118. G. Ji, U. K. Reddy, D. Huang, T. S. Henderson and H. Morkoc, J. Vac. Sci. Technol. B5, 1346(1987).

119. J. Menendez, A. Pinczuk, D. J. Werder, S. K. Sputz, R. C. Miller, D. C. Sivco, and A. Y. Cho, Phys. Rev. B36, 8165(1987).

120. M. J. Joyce, M. J. Johnson, M. Gal, and B. F. Usher, Phys. Rev. B38, 10978(1988).

121. S. P. Kowalczyk, W. J. Schaffer, E. A. Kraut, and R. W. Grant, J. Vac. Sci. Technol. 20, 705(1982).

122. G. Ji, U. K. Reddy, D. Huang, T. S. Henderson and H. Morkoc, Superlattice and Microstructures: (to be published).

123. G. Ji, D. Huang, U. K. Reddy, T. S. Henderson, R. Houdre, and H. Morkoc, J. Appl. Phys. 62, 3366(1987).

124. F. Iikawa et al. Phys. Rev. B38, 8473(1988).

125. J. P. Rithmaier, R. Hoger, and H. Riechert, Appl. Phys. Lett., 56, 536(1990).

126. A. Ksendzov, H. Shen, F. H. Pollak and D. P. Bour, Surface Science, 228, 326 (1990).

127. A. Ksendzov, H. Shen, F. H. Pollak and D. P. Bour, Solid State Comm., 73, 11 (1990).

128. W. Shan, X. M. Fang, D. Li and S. Jiang, S. C. Shen and H. Q. Hou, W. Feng and J. M. Zhou, Appl. Phys. Lett., 57, 475(1990).

129. T. G. Anderson, Z. G. Chen, V. D. Kulakoowkii, A. Uddin, and J. T. Vallin, Phys. Rev. B37, 4032(1988).

130. P. W. Yu, G. D. Sanders, R. Evans, D. C. Reynolds, K. K. Bajaj, C. E. Stutz and R. L. Jones, Appl. Phys. Lett. 54, 2330(1989).

131. H. Q. Hou, L. J. Wang, R. M. Tang, and J. M. Zhou (unpublished). The PL measurement under hydrostatic pressure suggests a valence band offset Q_v=0.32.

132. G. Ji, U. K. Reddy, D. Huang, T. S. Henderson and H. Morkoc, J. Appl Phys. 62, 3366(1987).

133. G. J., W. Dobbelaere, D. Huang and H. Morkoc, Phys. Rev. B39, 3216(1989).

134. U. K. Reddy, G. Ji, T. Henderson, D. Huang, R. Houdre and H. Morkoc, J. Vac. Sci. Techno. B7, 1106(1989).

135. D. J. Arent, K. Deneffe, C. Van Hoof, J. Deboeck and E. Borghs, J. Appl. Phy. 66, 1379(1989).

136. H. Q. Hou, Y. Segawa, Y. Aoyagi and S. Namka, Solid State Comm., 74, 159(1990).

137. H. Q. Hou, L. J. Wang, R. M. Tang, and J. M. Zhou, Phys. Rev. Rev. B42, 2926(1990).

138. B. Jogai and P. W. Yu. Phys. Rev. B41, 12650(1990).

139. Y. L. Leu, F. A. Thiel, H. Scheiber, B. I. Miller, and J. Backmann, J. Electron. Matter, 8, 663(1979).

140. O. Berolo and J. C. Wooley, in Proceeding of the 11th International Conference on the Physics of Semiconductors, Warsaw, 1972(Polish Scientific, Warsaw, 1972), P1420.

141. K. K. Baijaj (private Communication)

142. S. Adachi, J. Appl. Phys. 53, 8775(1982).

143. H. Shen, S. H. Pan, F. H. Pollak, and R. N. Sacks, Phys. Rev. B37, 10919(1988).

144. X. L. Zhang, D. L. Heiman, B. Lax and F. H. Chambers, Appl. Phys. Lett., 52, 287(1988).

145. L. P. Ramberg, P. M. Enquist, Y. K. Chen, F. E. Najjar, L. F. Eastman, E. A. Fizerald, and K. L. Hananagh, J. Appl. Phys. 61, 1234(1987).

146. C. G. Van de Walle, Ph. D. thesis, Stanford University, 1986 (unpublished). 751(1990).

147. R. E. Viturro et al, J. Vac. Sci. Tochnol B7(4), 1007 (1989).

148 S. Chang, L. J. Brillson, Y. J. Kime, D. S. Rioux, P. D. Kirchner, G. D. Pettit and J. M. Woodall, Phys. Rev. Lett.64, 2551 (1990).

149. M. Hecht, Phys. Rev. B41, 7918 (1990); also, to be published in in J. Vac. Sci. Technol.

150. K. Jacobi, U. Myler and P. Althainz, Phys. Rev. B41, 10721 (1990).

151. S. Chang, I. M. Vitomirov, L. J. Brillson, D. F. Rioux, P. D. Kirchner, G. D. Pettit, J. M. Woodall and M. Hecht, Phys. Rev. B41, 12299 (1990).

152. C. Van Hoof, K. Deneffe, J. DeBoeck, D. J. Arent and G. Borghs, Appl. Phys Lett. 54, 608 (1989).

153. H. Hasegawa, H. Ishii, T. Sawada, T. Saitch, S. Konishi, Y. Lin and H. Ohno, J. Vac. Sci. Technol B6, 1184 (1988).

154. H. Shen, M. Dutta, L. Fotiadis, P. G. Newman, R. P. Moerkirk, W. H. Chang and R. N. Sacks, submitted to Appl. Phys. Lett.

155. X. Yin, H. M. Chen, F. H. Pollak, Y. Chan, P. A. Montano, J. M. Woodall, P. D. Kircher and G. D. Pettit, to be published in Appl. Phys. Lett. Jan. 19, 1991.

156. X. Yin, H. M. Chen, Z. Hang, F. H. Pollak and et al, published in 20th International Conference on the Physics of Semiconductors, 1990.